1-1-2016

Exploration Of Cancer Proliferative Signaling In Chemotherapy Drug Resistance And Mdig-Induced Tumorigenesis

Kai Wu
Wayne State University,

EXPLORATION OF CANCER PROLIFERATIVE SIGNALING IN CHEMOTHERAPY DRUG RESISTANCE AND MDIG-INDUCED TUMORIGENESIS

by

KAI WU

DISSERTATION

Submitted to the Graduate School

of Wayne State University,

Detroit, Michigan

in partial fulfillment of the requirements

for the degree of

DOCTOR OF PHILOSOPHY

2016

MAJOR: PHARMACEUTICAL SCIENCES

Approved By:

_____

Advisor Date

_____

_____

_____

_____

ACKNOWLEDGEMENTS

Firstly, I would like to express my deepest gratitude to my advisor Prof. Fei Chen for his professional instructions and kind support for my Ph.D study and research. He has also provided me many opportunities for diverse research projects as well as continuous guidance and encouragement through my entire program of study, which made my graduate program such a satisfying and rewarding one.

Besides my advisor, I would like to thank the other 3 members of my thesis committee: Prof. Anjaneyulu Kowluru, Prof. Douglas Ruden and Prof. Steven Firestine for their insightful comments, in-depth questions and invaluable intellectual input, which significantly contributed to my research projects.

My sincere thanks also go to my current and former lab mates. This thesis would not have been possible without their support and contributions. I am especially grateful to Ms. Yongju Lu for teaching me fundamentals of conducting scientific research with great patience and helping me design the complicated experiments. I am also thankful to Dr. Chitra Thakur, Dr. Bailing Chen, Dr. Ping Qiu and Dr. Qingshan Chang for sharing their research experience and leading-edge ideas with me, which greatly helped my research projects as well as my career development. I also thank my fellow lab mates, Ms. Lingzhi Li, Mr. Srinivas Kumar, Dr. Jia Liu, Dr. Jiaying Sun, Dr. Miaomiao Yu and Ms. Wei Wang for all their support and all the fun we have had in the past five years. I would also like to acknowledge Dr. Zhengping Yi and Dr. Xiangmin Zhang for help with mass spectrometry analysis in my research project. I would like to thank the Department of Pharmaceutical Sciences for providing me the opportunity to study in such a supportive research environment. Thanks are also due to the National Institutes of Health (under Grants ES017217 and ES020137 to F.C.) for the financial support that I otherwise would not have been able to develop my scientific discoveries.

Finally, I am deeply grateful to my family for their love and encouragement, which led me through the tough times in life and supported me in all my pursuits. Thank you.

TABLE OF CONTENTS

LIST OF TABLES

LIST OF FIGURES

CHAPTER 1 EXPLORE ABBERANT MDIG AND C-MYC SIGNALING CIRCUIT IN MULTIPLE MYELOMA

Introduction

Multiple myeloma (MM) is a malignant neoplasm of plasma cells localized within the bone marrow (BM) compartment and ranked second in prevalence of all hematopoietic malignancies. In 2014, there were around 24,000 and 110,000 new cases in U.S and worldwide, respectively. MM can occur de novo or from premalignant monoclonal gammopathy of undetermined significance (MGUS), which is characterized by abnormal proliferation of plasma cells and increased monoclonal immunoglobulins. In the past decade, large-scale genomics studies have determined genetic landscape of MM and identified abnormal genetic events present in various disease stages, from MGUS to smoldering multiple myeloma (SMM), active MM and relapsed MM.

Multiple "omics" technologies allow us to interrogate the alterations in MM cells from multiple aspects, including epigenetic regulatory machinery, global protein networks and kinase activities. Accumulating evidence has delineated a higher level complexity of MM pathogenesis that requires extensive interactions among oncogenic signaling pathways. The unique BM milieu is vital for the longevity of myeloma cells by providing various supportive BM cells and soluble factors. Among these driving forces, one of the most important factors is the interleukin-6 (IL-6) cytokine. After binding to its receptor (IL-6R) and recruiting a signal transducer, GP130 (also known as CD130 or IL-6ST), IL-6 can activate Janus Kinase (JAK)/signal transducer and activator of transcription (STAT), AKT and mitogen-activated protein kinase (MAPK) pathways to promote proliferation, survival and drug resistance of the MM cells.

A hallmark of MM pathogenesis is the mutation- or overexpression-induced C-MYC activation. C-MYC is a well-defined onco-protein involved in many types of human cancers.

As an essential transcription factor, C-MYC upregulates transcription of genes responsible for cell growth, proliferation and maintenance of cancer cell stemness. In MM, C-MYC overexpression can distinguish active MM from premalignant MGUS. In addition, activated C-MYC has been shown to sustain the survival of myeloma cells. More interestingly, a recent study indicates that crosstalk between the IL-6 pathway and C-MYC results in a significant acceleration of MM pathogenesis. However, the underlying mechanisms of this oncogenic interaction remain unclear.

As a C-MYC-induced protein, MDIG (mineral dust-induced gene, also known as mina53, MINA, or NO52) functions as a histidyl hydroxylase and potentially a lysine-specific demethylase, which regulates gene transcription through modifying the tri-methylated lysine 9 residue on histone 3 (H3K9me3). Consistent with this function, MDIG is found to be exclusively localized in the nucleus of various cell types. Some studies have demonstrated that MDIG exerts a strong immune-regulatory function by promoting differentiation of certain T helper (Th) cells, including Th1 and Th17 cells. Overexpression of MDIG has been observed in many types of human cancer, including lung cancer, colon cancer, gastric carcinoma, etc.. Meanwhile, MDIG has been shown to be able to promote cancer cell proliferation. Furthermore, MDIG overexpression has been observed in various B cell-derived malignancies among major human lymphoma subtypes, suggesting that MDIG may contribute to C-MYC-induced tumorigenesis in MM.

Some epidemiological studies have provided hints for potential risk factors and novel approaches to study the pathogenesis of MM. Several earlier studies suggested that environmental exposures to industrial or agricultural products, such as benzene, petroleum products, and pesticides, may contribute to the development of MM. More importantly, some recent cohort studies on the first responders, reconstruction workers and volunteers of the World Trade Center (WTC) after the terrorist attack on September 11, 2001, provided

evidence linking inhalation of the WTC dust to MM. However, there are no previous studies revealing the potential carcinogenic effect of WTC dust or how WTC dust causes malignant transformation of the mature plasma B cells.

In this chapter, we provide evidence revealing that WTC dust is potent in perturbing the intracellular signaling pathways by inducing MDIG in both normal B cells and MM cells and further demonstrating that overexpression of MDIG is significantly associated with the malignant transformation of MGUS to active MM, disease exacerbation and poor clinical outcomes. Biochemical studies unraveled that MDIG directly interacts with C-MYC and JAK1 proteins in MM cells, which contributes to the hyperactivation of the JAK1 and STAT3 signaling important for cell survival, proliferation and development of drug resistance of the MM cells. Taken together, our studies suggest that MDIG may serve as a key mediator for MM associated with WTC dust exposure and potential diagnosis/prognosis marker of MM.

Materials and methods

Cells and reagents—Human MM cell lines, NCI-H929 and MM1S, bronchial epithelial cell line BEAS-2B and normal B cell line C5B7 were purchased from American Type Culture Collection (ATCC, Manassas, VA, USA) and maintained in ATCC-recommended culture conditions. Inhibitor of C-MYC (10058-F4) and cycloheximide (CHX) were purchased from Sigma-Aldrich Co. (St. Louis, MO, USA). WTC dust was provided by Dr. Kenneth Reuhl at the Environmental and Occupational Health Sciences Institute of the Rutgers University.

siRNA transfection—Transfections were performed using Lipofectamine RNAiMAX™ (Invitrogen) according to manufacturer's protocol. Fifty nM of siRNAs were used for transfection followed by 48-hour incubation. Control siRNA, MDIG siRNAs and C-MYC siRNAs were all purchased from Qiagen (Valencia, CA, USA).

Immunohistochemistry (IHC)—Tissue microarray slides, T293 and BM483b, containing multiple myeloma samples and non-cancerous bone marrow tissue were

purchased from US Biomax, Inc (Rockville, MD). IHC staining was performed as previously described.30 Briefly, the slides were stained overnight at 4°C with mouse anti-human MDIG antibody (Invitrogen) at 1:50 dilution followed by biotinylated goat anti-mouse secondary antibody (Dako Denmark A/S, Glostrup, Denmark) at 1:200 dilution for 2 hours at room temperature. The slides were then incubated with ABC reagent and DAB (Vector Laboratories, Inc. Burlingame, CA), counter stained with hematoxylin and mounted with entellan. All images were captured using a Nikon Eclipse Ti-S Inverted microscope (Mager Scientific, Dexter, MI). Cut-offs between positive and negative cells were determined according to previously characterized MDIG-expressing breast cancer samples. Four random images were taken for each sample and both positive and negative cells were counted using ImageJ 1.48v (http://imagej.nih.gov/ij/). MDIG expression status of all samples was classified into four grades based on the percentage of positively-stained cells. Strongly positive: over 50%; moderately positive: between 50% and 25%; weakly positive: between 25% and 5%; negative: less than 5%.

Immunoblotting and Immunoprecipitation (IP)—Immunoblotting and IP analysis were performed as previously reported 40. NE-PER Nuclear Cytoplasmic Extraction KIT (Thermo Scientific Pierce, Rockford, IL, USA) was used to isolate nuclear proteins. Densitometric analysis of CHX-treated samples was completed using ImageJ 1.48v (http://imagej.nih.gov/ij/). When detecting C-MYC bands in IP samples, HRP-conjugated protein A (EMD Millipore, Temecula, CA, USA) was used to minimize the background noise caused by IgG heavy chain. Primary antibodies against phospho-AKT (Ser473), total AKT, phospho-STAT3 (Ser727), phospho-STAT3 (Tyr705), total STAT3, phospho-JAK1 (Tyr1022), total JAK1, GAPDH, actin and all secondary antibodies were purchased from Cell Signaling Technology (Danvers, MA, USA). Antibodies against GP130, IL-6R and methylated-lysine were purchased from Abcam (Cambridge, MA). Antibodies against C-MYC and lamin A/C

were purchased from Santa Cruz Biotechnology (Dallas, Texas, USA). MDIG (mouse) antibody was ordered from Invitrogen. Distinct antibodies used for IP include MDIG (rabbit) and C-MYC (mouse) from Abcam (Cambridge, MA, USA), C-MYC (rabbit) from Cell Signaling Technology (Danvers, MA, USA), JAK1 (rabbit) from Santa Cruz Biotechnology (Dallas, Texas, USA). All presented data are representatives of at least 3 independent experiments.

Confocal immunofluorescence (IF) analysis—For IF staining, 106 cells were centrifuged, fixed by 4% formaldehyde for 15 min, permeabilized by 0.3% Triton X-100 and blocked in PBS containing 5% normal goat serum and 0.1% Tween 20 for 1 hour at room temperature. Then they were incubated with primary antibodies, anti-JAK1 (rabbit, Santa Cruz Biotechnology) and anti-MDIG (mouse, Invitrogen) overnight at 4°C and with Invitrogen secondary antibodies, Alexa Fluor 488-linked antibody (goat anti-mouse) and Alexa Fluor 594-linked antibody (goat anti-rabbit) for 1 h at room temperature in dark. All antibodies were used at 1:100 dilutions. Prolong Gold™ antifade reagent with DAPI (Invitrogen) was used to preserve the samples. Co-localization of JAK1 and MDIG was detected by Zeiss LSM 780 confocal microscope (Carl Zeiss Microscopy, Jena, Germany). Pinhole size of 60 µm was used while thresholds for laser power, master gain and digital gain were determined by non-specific binding controls. DAPI, Alexa Fluor 488 and Alexa Fluor 594 were excited at 405 nm, 488 nm and 595 nm and corresponding fluorescence emissions were detected at 495 nm, 563 nm and 640 nm via 3 independent channels. All photos were processed using ZEN 2012 SP1 64 bit software (Carl Zeiss Microscopy, Jena, Germany).

PCR—Total RNAs were extracted using TRIzol™ Reagent (Life Technologies, Grand Island, NY, USA) and their integrity was assessed by 18S and 28S ribosomal RNAs. For reverse transcription PCR, AccessQuick™ RT-PCR system from Promega (Madison, WI) was used. The primers for MDIG are: 5′-TCA TGT CGG GCC TAA GAG AC-3′ and 5′-GGC ATT TGA TTC TGC AAA GG-3′, which amplifies a 1,510 bp DNA fragment covering the whole

coding region of the MDIG gene. Primers for GAPDH are: 5′-CTG AAC GGG AAG CTC ACT GGC ATG GCC TTC-3′ and 5′-CAT GAG GTC CAC CAC CCT GTT GCT GTA GCC-3′. For real-time PCR, one μg total RNAs were reverse-transcribed using High-Capacity cDNA Reverse Transcription Kit™ (Applied Biosystems, Waltham, MA, USA) and 1:20 diluted. Jak1 and ACTB Taqman Gene Expression Assays (Best Coverage™) were purchased from Applied Biosystems (Waltham, MA, USA). Samples were run in triplicates, quantified by ΔΔCt method with actin as reference gene and normalized to "Blank" group. Final results were shown as mean ± SD.

Mass spectrometry and proteomics analysis—Proteomics profiling of binding partners were performed as previously reported. Briefly, samples were subject to co-immunoprecipitation, 1D-SDS-PAGE separation, in-gel digestion, peptide purification and HPLC-ESI-MS/MS analysis. Protein identity was determined by MaxQuant™ software.

Biostatistics analysis— Protein interaction network analysis was completed using Gene Ontology database and visualized by Cytoscape™ 3.2. Binding proteins were first sorted according to their biological processes and further refined manually by merging repeating and redundant categories. Gene expression data were accessed through Multiple Myeloma Genomics Portal (https://www.broadinstitute.org/mmgp/home) for GSE6477 and through GEO for GSE39754 and GSE2658 before being processed and visualized using R project with ggplot2 package. Survival analysis in Figure 1.3E was performed using Kaplan-Meier method and the difference between 2 cohorts were determined using log-rank test. In Figure 1.3C and 1.3D, differences of mRNA levels between patient cohorts were calculated using one-way ANOVA and p-values were adjusted by Holm method. All other mRNA expression comparisons were performed using two-tailed t-test. Considering that expression levels of related genes are not always strictly linear to each other, we conducted "Force Rank" co-amplification analysis. A p-value less than 0.05 is considered statistically significant.

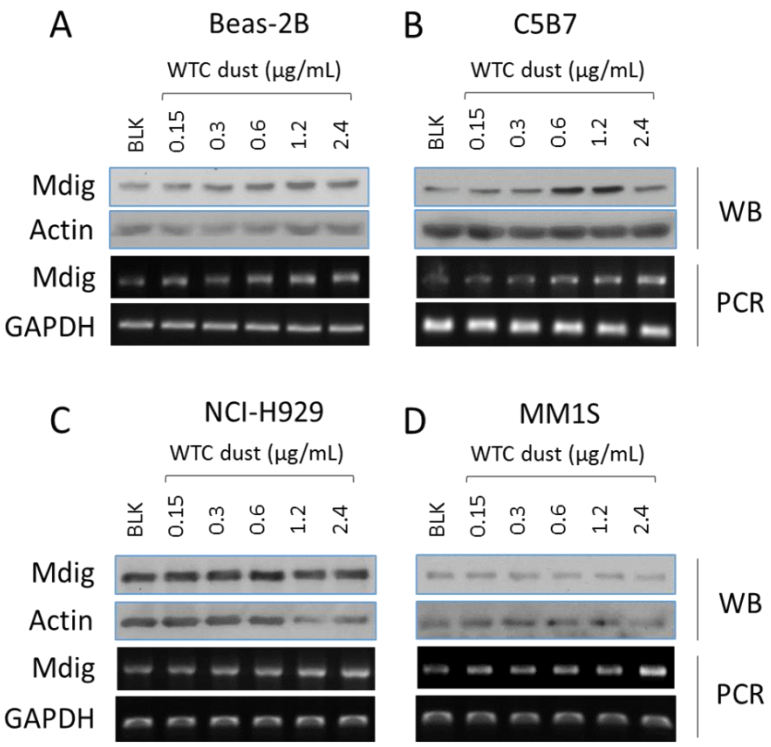

Figure 1.1 WTC dust induces MDIG in BEAS-2B cells (A), C5B7 cells (normal B cells, B), NCI-H929 cells (MM cell line, C), and MM1S cells (MM cell line, D). All of the cells were treated with the indicated concentrations of WTC dust for 6 h, followed by Western blotting (top two panels) and RT-PCR (bottom two panels). Each panel is representative of at least three independent experiments.

Results

WTC dust induces MDIG in bronchial epithelial cells, B cells and MM cells. The adverse effect of WTC dust on the respiratory system, including airway inflammation, impairment of the pulmonary function, airway hyperactivity, asthma, and sarcoid-like granulomatous pulmonary disease, had been well-established . Indeed, we noted that WTC dust is highly capable of inducing MDIG expression in the bronchial epithelial cell line, BEAS-2B cells, in concentrations ranged from 0.15 to 2.4 μg/ml (Fig.1.1A). Since concerns had been arisen about the potential for increased risk of MM among WTC responders, we also investigated the capability of WTC dust on the induction of MDIG in normal B cells using a B cell line C5B7. Similar to what we observed in BEAS-2B cells, we noted a dose-dependent induction of MDIG protein and mRNA by WTC dust in C5B7 cells (Fig.1.1B). In two MM cell lines NCI-H929 and MM1S, although we did not detect induction of MDIG protein, a pronounced induction of MDIG mRNA by WTC dust was observed (Figs.1.1C and 1.1D). These data, thus, clearly suggest that in addition to damage the

respiratory system through direct interaction, WTC dust or its components may also influence the intracellular signaling of the B cells and the MM cells.

Increased MDIG expression in the bone marrow (BM) of the MM patient. To determine whether MDIG expression is clinically relevant for MM, we evaluated MDIG protein levels in the BM specimens of MM patients through immunohistochemistry (IHC). In total of 16 cases of MM BM biopsies examined, 8 samples exhibited strong staining of MDIG proteins

A

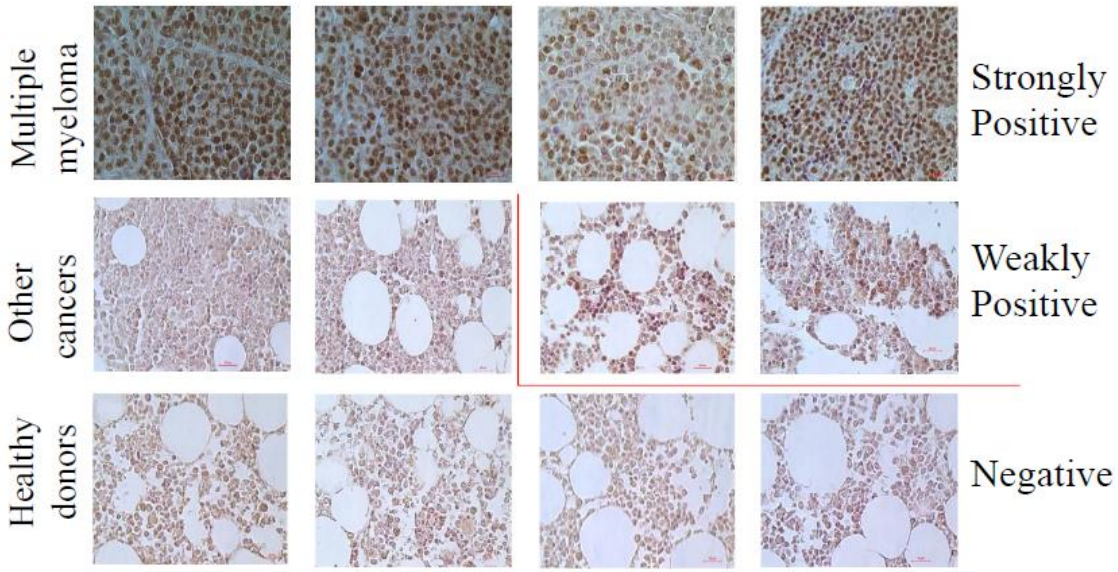

B

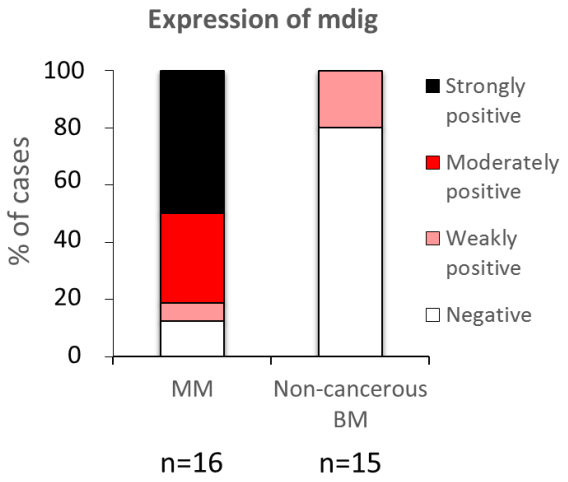

	MM		Non-MM	
	Counts	Ratio	Counts	Ratio
negative	2	12.50%	12	80.00%
weakly+	1	6.25%	3	20.00%
moderately+	5	31.25%	0	0.00%
strongly+	8	50.00%	0	0.00%
Total	16	100.00%	15	100.00%

Figure 1.2 Increased MDIG expression in human MM samples. (A) Representative IHC images of MDIG expression in bone marrow (BM) of MM patients (n=16), BM of non-hematological cancer patients (n = 11), and BM of healthy donors (n = 4). Magnification: 40×, scale bar: 50μm. Strongly positive: over 50%; moderately positive: between 50% and 25%; weakly positive: between 25% and 5%; negative: less than 5%. (B) Summary of the IHC results.

as judged by the criteria that more than 50% of cells are MDIG positive, 6 samples showed moderate or weak MDIG staining and 2 samples are MDIG negative (Figs.1.2A and 1.2B). We also checked another set of BM specimens collected from 4 healthy donors and 11 patients with other non-hematological cancers. MDIG protein was not detected in all 4 healthy donors' BM specimens and 8 out of 11 cases of non-hematological cancer patients. Three BM specimens from patients with non-hematological cancers showed weak positive of MDIG staining (Figs.1.2A and 1.2B).

Both MDIG and C-MYC are associated with disease aggressiveness of MM. There are several stages during disease development, including premalignant MGUS, asymptomatic smoldering MM (SMM), symptomatic MM, and relapsed MM. It has been well-accepted that C-MYC activation is a hallmark of MM pathogenesis, especially in the early malignant transformation from MGUS to active MM. C-MYC has also been implicated in the up-regulation of MDIG. Overexpression of MDIG has been observed in many types of human malignancies, but its potential role in C-MYC-related MM pathogenesis remains unknown. To determine whether MDIG contributes to C-MYC-induced MM pathogenesis, we examined expression levels of MDIG and C-MYC in MM patients. We noted that both C-MYC and MDIG mRNAs are significantly up-regulated in newly diagnosed MM patients when compared to healthy donors (Figs.1.3A and 1.3B). Further analysis of patients at continuous stages during MM development has demonstrated a robust elevation trend of both C-MYC and MDIG (Figs.1.3C and 1.3D). Statistically significant increases of MDIG mRNA, from MGUS to active MM and from SMM to relapsed MM were noted (Fig.1.3D), suggesting a positive correlation between MDIG expression and malignant transformation, disease progression and relapse of MM.

The involvement of MDIG in MM pathogenesis is further supported by survival analysis of 559 MM patients. High level of MDIG expression is significantly correlated with the poor

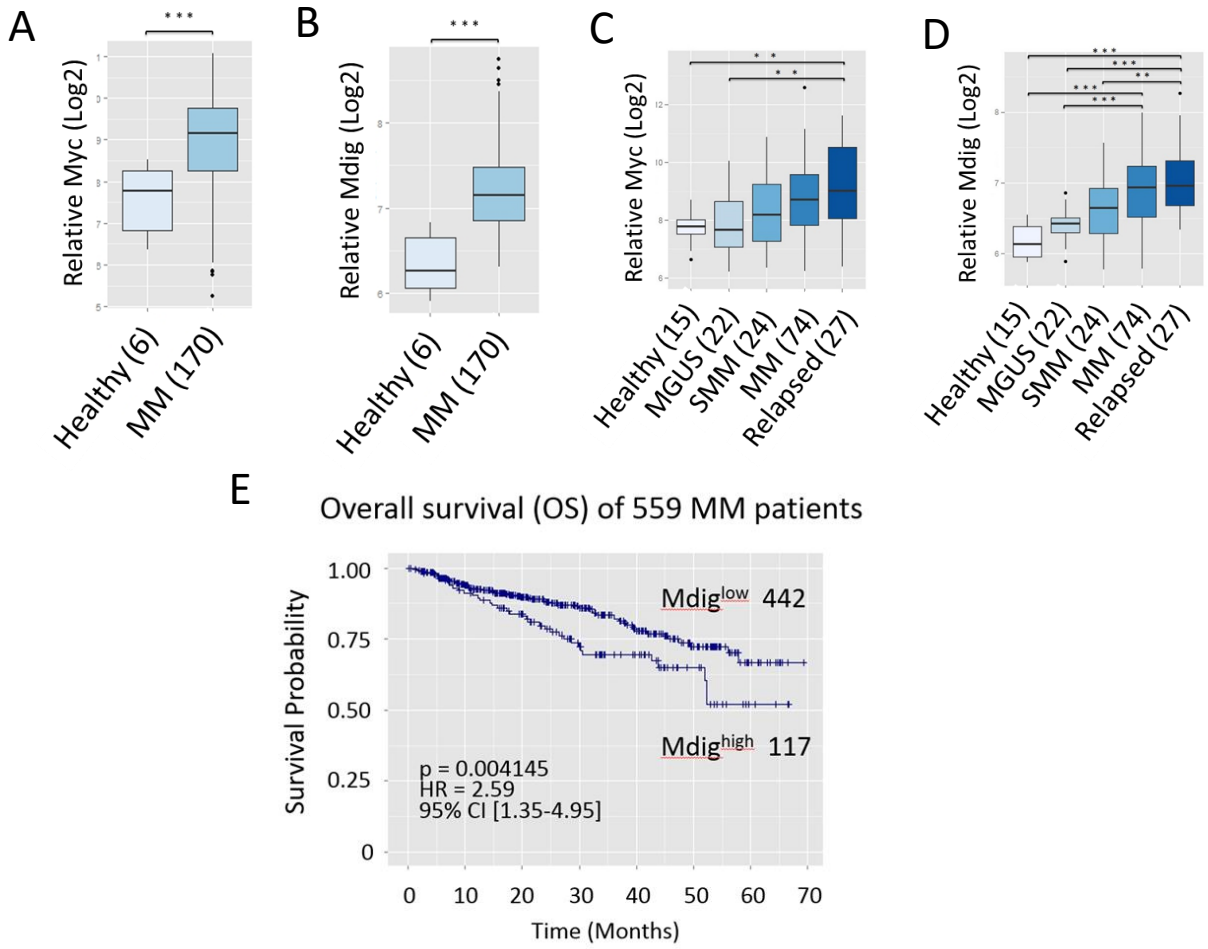

Figure 1.3 Overexpression of MDIG and C-MYC is associated with disease progression and poor prognosis of MM. (A) Box plot of relative level of C-MYC mRNA in newly diagnosed MM patients and healthy donors (GES39754, n = 176); (B) Box-plot of relative level of MDIG in newly diagnosed MM patients and healthy donors (GES39754, n = 176); (C) Expression level of C-MYC mRNA in CD138+ plasma cells from healthy donors and MM patients at various stages (GSE6477, n = 163); (D) Expression level of MDIG mRNA in CD138+ plasma cells from healthy donors and MM patients at various stages (GSE6477, n = 163). In the plots, boxes denote the inter-quartile range (25% to 75%), bars represent medians and whiskers indicate up to 1.5× the inter-quartile range which cover 95% of all samples. Outliers are indicated by the black dots. Sample sizes of each group are annotated in parentheses and expression levels are displayed in log2 scale. (***p<0.001, ** p<0.01). (E) Kaplan-Meier (KM) survival curve of 559 MM patients (GSE2658) stratified by their MDIG expression levels. Sample sizes of each group, log-rank p-value, hazard ratio and 95% confidence intervals are displayed in the figure. Tick marks on each arm represent censored samples.

overall survival of the MM patients, even though higher percentage of patients from "MDIG high" group (82%, 96/117) received intensive therapies than those from "MDIG low" group

(57.7%, 255/442) (Fig.1.3E). Taken together, all above data demonstrate a strong positive correlation of MDIG and C-MYC to the pathogenesis and aggressiveness of MM.

MDIG acts as a key interaction partner of C-MYC in MM cells. In order to decipher inter-regulation between MDIG and C-MYC in MM cells, proteomics study was performed on MM cell line NCI-H929 cells to screen their interaction partners, respectively. A total of 224 and 203 proteins were identified as significant binding partners of MDIG and C-MYC, respectively. Among these, 110 binding partners are shared by MDIG and C-MYC (Fig.1.4A). Strikingly, physical binding between MDIG and C-MYC was detected by mass-spectrometry in NCI-H929 cells (Fig.1.4B), which was further validated by co-IP assay in both NCI-H929 and MM1S cells (Fig.1.4C), implying that MDIG might be assembled into functional protein complexes together with C-MYC and directly participate in C-MYC-induced oncogenesis for the development of MM. Subsequent network analysis highlighted some major cellular events

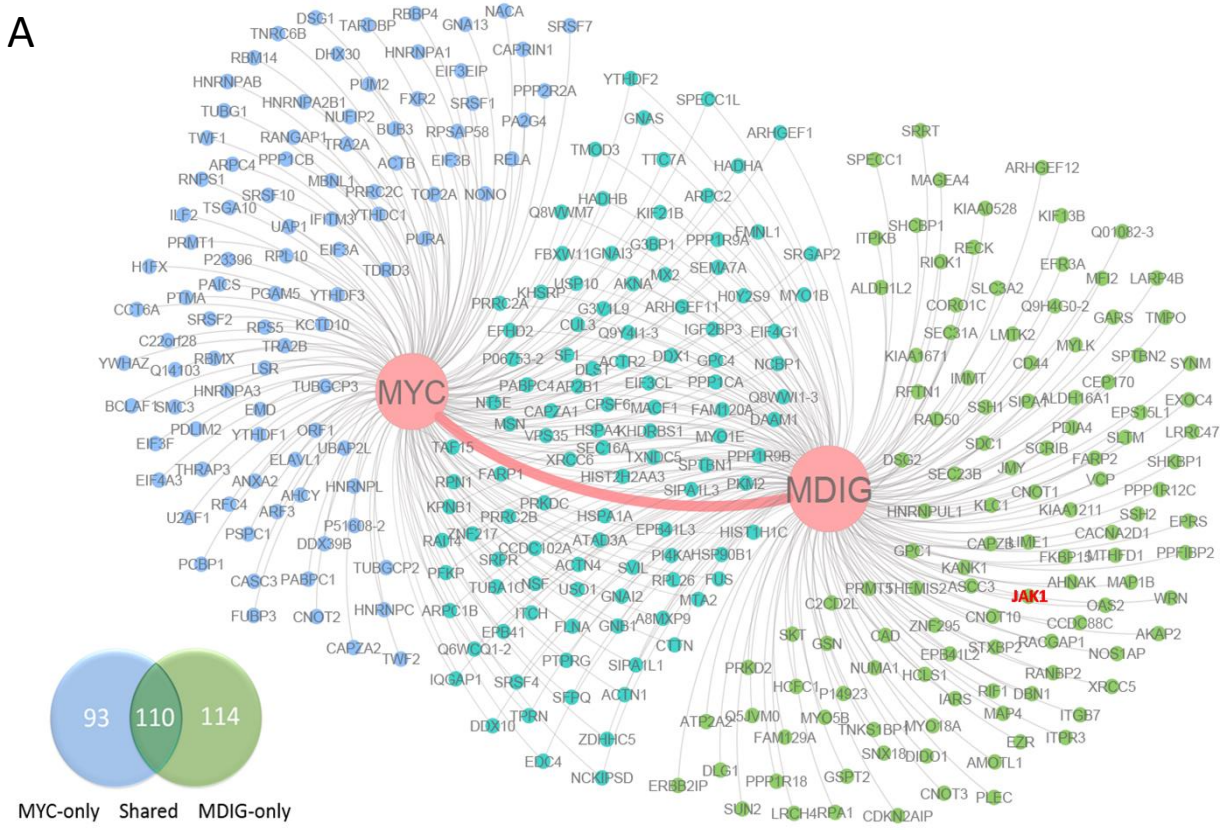

B

Sequence (MDIG)	Unique to MDIG
ATIQFHQPQR	yes
ELLSSDMKK	yes
EYSVEAEER	yes
LPPYSAGDGAELSTPGGK	yes
ETHMMGNEEETEFHGLR	yes
LYHPTVPLAR	yes

C

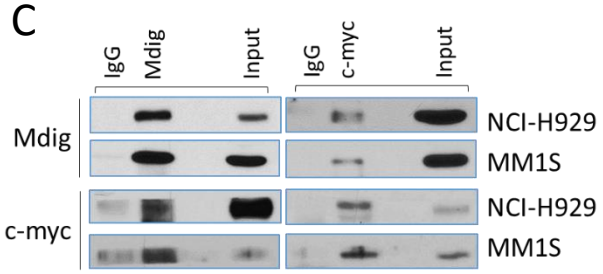

D

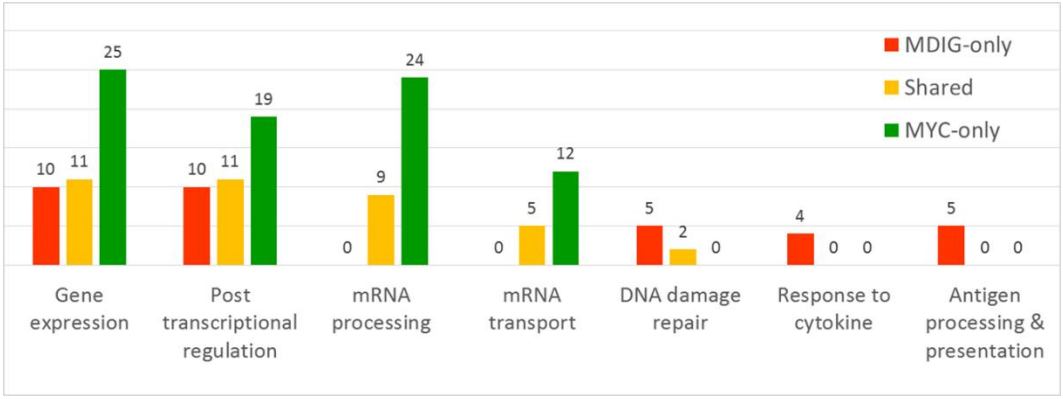

Figure 1.4 MDIG directly binds to and extensively cooperates with C-MYC. (A) Proteomic identification of the C-MYC-MDIG-centered protein interaction network following C-MYC and MDIG pull-downs. All determined proteins, excluding MDIG and C-MYC themselves, are categorized as Myc-only (blue), MDIG-only (green) and Shared (cyan) groups while total numbers of each group are listed in the Venn diagram; (B) A chart summarizes all the unique peptide sequences of MDIG detected by mass spectrometry in C-MYC pull-downs; (C) Co-immunoprecipitation (co-IP) assay shows direct physical binding of C-MYC and MDIG in NCI-H929 and MM1S cells; (D) Summaries of top biological processes that involve interaction partners of C-MYC and MDIG. All determined subjects are interrogated by Gene Ontology database and are sorted based on biological processes they participate in.

upon which C-MYC and MDIG are most likely to impose their impact (Fig.1.4D). Summary of sorted binding partners is available in Table 1.1. The shared binding partners are mainly clustered in 4 areas: gene expression, post-transcriptional regulation of gene expression, mRNA processing, mRNA transport. It is not surprising that C-MYC-only binding partners are actively involved in all 4 biological processes and MDIG-only binding partners involved in former 2 processes considering the well-established role of C-MYC as an essential transcription factor and MDIG as an important epigenetic regulator. Collectively, these data provide a strong rationale that MDIG is a core direct interaction partner of C-MYC and is most

likely to collaborate in gene expression-related functions in MM cells. Notably, MDIG-only binding partners are also enriched in proteins important for cellular responses to cytokine and

	MDIG-only	Shared	MYC-only
Gene expression	PRMT5, HNRNPUL1, CNOT1, CNOT3, TNKS1BP1, GARS, CNOT10, IARS, EPRS,GSPT2	EDC4, NCBP1, FUS, KHSRP, RPN1, SRPR, IGF2BP3, SRSF4, RPL26, EIF4G1, HSPA1A	RPL10, EIF4A3, SRSF1, PPP2R2A, U2AF1, CASC3, ELAVL1, PCBP1, HNRNPA1, HNRNPA3, RPS5, YWHAZ, HNRNPL, CNOT2, HNRNPA2B1, SRSF2, RNPS1, EIF3F, HNRNPC, PABPC1, RBMX, SRSF7, EIF3A, EIF3B, TNRC6B
Post transcriptional regulation	CNOT1, CNOT3, CCDC88C, FAM129A, CNOT10, IARS, LARP4B, EPRS, CDKN2AIP, HCFC1	KHDRBS1, YTHDF2, NCBP1, FBXW11, PRKDC, DDX1, FLNA, EIF3CL, IGF2BP3, EIF4G1, HSPA1A	RPS5, EIF4A3, SRSF1, PA2G4, CASC3, ELAVL1, PUM2, PURA, THRAP3, CAPRIN1, CNOT2, DSG1, EIF3F, HNRNPC, PABPC1, TARDBP, EIF3A, EIF3B, TNRC6B
mRNA processing	____	KHDRBS1, SFPQ, CPSF6, NCBP1, FUS, KHSRP, SRSF4, SF1, EIF4G1	HNRNPA3, MBNL1, NONO, EIF4A3, SRSF1, U2AF1, CASC3, HNRNPL, DDX39B, THRAP3, PCBP1, CNOT2, TRA2B, TRA2A, HNRNPA2B1, SRSF2, RNPS1, HNRNPC, PABPC1, TARDBP, HNRNPA1, RBMX, SRSF7, SRSF10
mRNA transport	____	NCBP1, MX2, KHSRP, IGF2BP3, SRSF4	DDX39B, RPSAP58, HNRNPA2B1, EIF4A3, SRSF1, SRSF2, RNPS1, U2AF1, CASC3, HNRNPA1, SRSF7, SRSF10
DNA damage repair	VCP, WRN, RAD50, XRCC5, RPA1	XRCC6, PRKDC	____
Response to cytokine	OAS2, EPRS, CD44, JAK1	____	____
Antigen processing & presentation	RACGAP1, RFTN1, KLC1, SEC31A, SPTBN2	____	____

Table 1.1 Summary of sorted binding partners.

antigen processing and presentation, which is in agreement with our previous findings suggesting that MDIG contributes to the function of the T helper 17 (Th17) cells. Most recently, we discovered that MDIG interacts with the DNA double strand break repair proteins in the non-homologous end-joining (NHEJ) pathway in human bronchial epithelial cells and lung cancer cells. In MM cells, we also identified at least 7 DNA repair proteins that interact with

MDIG, including XRCC5, XRCC6, RAD50, etc. (Fig.1.4D and Table1.1), indicating that MDIG may also be involved in handling cellular stress caused by ongoing DNA damages, a common feature in human MM. Full lists of the determined binding partners are available in Table S1.1 and S1.2.

MDIG binds JAK1 in MM cells. Among the most important signaling pathways, IL-6/JAK/STAT3 signaling has been viewed as an indispensable signal for the malignant transformation of plasma B cells and proliferation of the MM cells. Through cooperation with C-MYC, this signaling pathway drives formation of high malignant MM in mouse model. It is

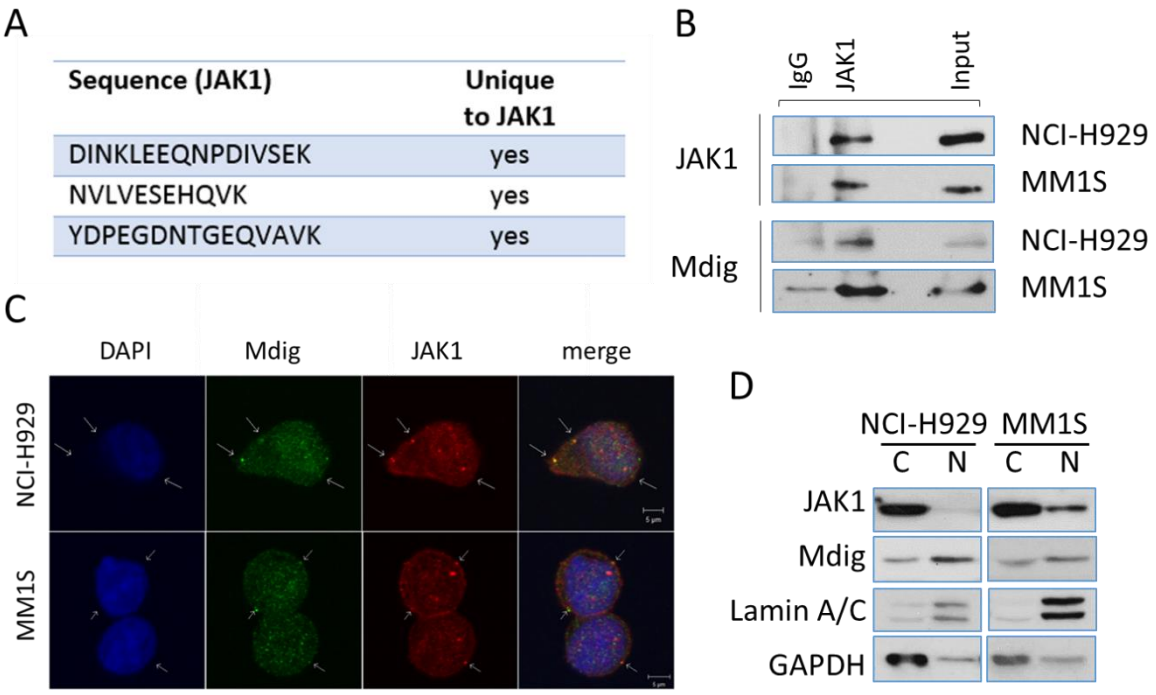

Figure 1.5 Direct interaction between MDIG and JAK1. (A) Proteomic identification of the unique peptide sequences of JAK1 detected by mass spectrometry in MDIG pull-downs; (B) Co-IP assay demonstrates the physical binding between MDIG and JAK1 in total cell lysates; (C) Confocal microscopy shows co-localization of MDIG and JAK1 in NCI-H929 and MM1S cells. Primary antibodies: JAK1 (rabbit anti-human) and MDIG (mouse anti-human). Secondary antibodies: Red (goat anti-rabbit) and Green (goat anti-mouse). Sites of co-localization are indicated by arrows. (D) Immunoblotting of MDIG and JAK1 in nuclear extracts (N) and cytosolic fractions (C) in 2 MM cell lines. The volume ratio of final nuclear extracts over cytosolic fractions is 1:4. In this test, cytosolic proteins (30µg) and nuclear protein at identical volume ratio were used to reflect the distribution of target proteins in indicated cellular compartments. Lamin A/C and GAPDH are used as markers for nucleus and cytosol, respectively.

unclear how this crosstalk is established between the oncogenic signal and cytokine signal. It is noteworthy that proteomic study identifies JAK1, a key regulator mediating cytokine-induced signaling, as a significant interaction partner of MDIG (Fig.1.5A and Table 1.1). Based on these observations, co-IP assay was performed using total cell lysates of both NCI-H929 and MM1S cells and confirmed such a physical interaction (Fig.1.5B). The interaction of MDIG and JAK1 was additionally verified by immunofluorescent staining and confocal microscopy. Multiple co-localization sites of MDIG and JAK1 were observed in the extra-nuclear area in both NCI-H929 cells and MM1S cells (Fig.1.5C). MDIG has long been recognized as a nuclear protein, whereas JAK1 is believed to be a cytosolic protein in the proximity of cytokine receptors. It is interesting to know how a nuclear protein can interact with a cytosolic protein. To answer this question, different cellular compartments were separated through fractionation. Surprisingly, in both MM cell lines, a significant portion of MDIG was found in cytosol though the majority of MDIG located in nucleus (Fig.1.5D). Thus, cytosolic localization of MDIG may be accounted for the proximity and physical interaction between MDIG and JAK1. This is also the first observation of MDIG in cytosol of human cell lines without additional manipulation, although we had also noted cytosolic localization of MDIG in MDIG-overexpressed or arsenic-treated A549 cells.

MDIG demethylates and stabilizes JAK1. To investigate the biological function of MDIG-JAK1 interaction, we further studied the role of MDIG on the gene expression and protein stability of the JAK1 protein in MM cells. The co-amplification analysis on MM patients exhibits no significant difference of JAK1 mRNA level between “MDIG high” and “MDIG low” groups (Fig.1.6A). In NCI-H929 cells, genetic silencing of MDIG does not affect mRNA level of JAK1 (Fig.1.6B), while in MM1S cells, MDIG knock-down groups displayed slightly higher JAK1 mRNA expression than the control group (Fig.1.6C). However, on the protein level, silencing MDIG resulted in a considerable decrease of total JAK1 protein (Fig.1.6D). We also

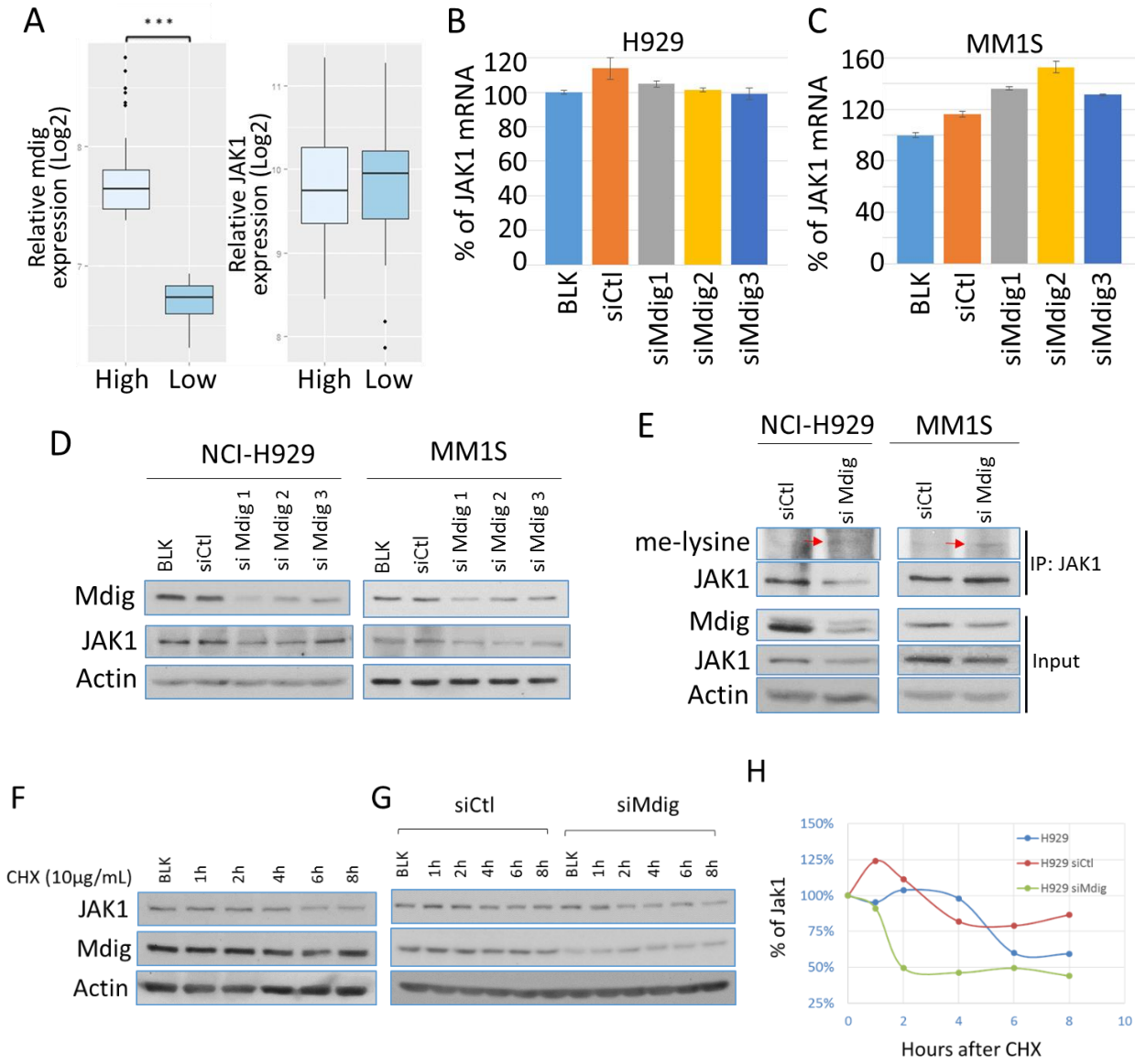

Figure 1.6 MDIG stabilizes JAK 1 through demethylation. (A) Correlation analysis of MDIG and JAK1 mRNA expressions in MM patients. Methods and parameters used are same as described in Figure 1.3 (***p<0.001); (B-C) qRT-PCR shows relative expression levels of JAK1 in NCI-H929 (B) and MM1S (C) cells treated with control siRNA and 3 different siRNAs against MDIG. The values are normalized to blank group (BLK) and displayed as mean ± SD (n = 3, * p<0.05). Raw data are available in Table S1.3 and S1.4; (D) Immunoblotting analysis of JAK1 expression in 2 MM cell lines treated with control and 3 different MDIG siRNAs; (E) Immunoprecipitation (IP) and immunoblotting of JAK1 in 2 MM cell lines treated with control siRNA and siRNA against MDIG. Me-lysine refers to an antibody selectively targets methylated lysine. Bands of methylated lysine residues on JAK1 are indicated by arrows. (F-G) Immunoblotting of cell lysates collected after cycloheximide (CHX) (10μg/mL) treatment at indicated time in non-treated NCI-H929 cells (F) or those pretreated with control siRNA or MDIG siRNA (G). (H) Densitometric analysis of the CHX chase results to determine the half-life of JAK1 protein.

performed cycloheximide (CHX) chase assay in NCI-H929 cells. Without additional treatment, we noted the half-life (T1/2) of JAK1 is over 8h (Figs.1.6F and 1.6H), which is longer than the 3.2 h as suggested by an earlier report. The control siRNA did not significantly affect the T1/2 of JAK1, while selective silencing of MDIG shortened T1/2 of JAK1 to 3.5 h (Fig.1.6G and 1.6H). Collectively, these data suggest that MDIG affects the JAK1 protein level through some posttranslational mechanisms. Given the potential activity of MDIG on lysine demethylation, we hypothesize that MDIG may regulate JAK1's stability by removing the methyl groups from its lysine residue(s). Because there is no report of JAK1 methylation so far and the unavailability of antibodies targeting methylated JAK1, we first immunoprecipitated and collected JAK1 protein from the control and MDIG-silenced MM cells and then probed the samples with an antibody that selectively recognizes methylated lysine. As shown in Figure 1.6E, a notable lysine methylation on JAK1 was detected in both NCI-H929 and MM1S cells when MDIG was genetically silenced. In the cells transfected with a control siRNA, the JAK1 methylation couldn't be detected.

MDIG and C-MYC are required for the hyperactivation of the IL-6 signaling. Synergetic collaborations between C-MYC and IL-6 pathways have been well-documented in MM. Prompted by the implications from proteomics studies above, we next interrogated the possibility of MDIG in mediating the oncogenic crosstalk between C-MYC and IL-6 signaling. Consistent with a previous report, our biochemical analysis demonstrated that genetic silencing of MDIG results in decreased protein levels of GP130, but not IL-6R in both NCI-H929 and MM1S cell lines (Fig.1.7A). Moreover, MDIG silencing further leads to attenuated phosphorylation of major downstream effectors on IL-6 signaling pathway, including STAT3 on both Tyrosine 705 and Serine 727 sites, and AKT on Serine 473 site, but not their total protein levels (Fig.1.7A). On the other hand, inhibition of C-MYC leads to a significant decrease of total protein levels and activity of MDIG and most regulators on IL-6

pathway mentioned above (Fig.1.7B and 1.7C), indicating that C-MYC is an essential transcription factor in MM cells while MDIG specifically cooperates with C-MYC in promoting

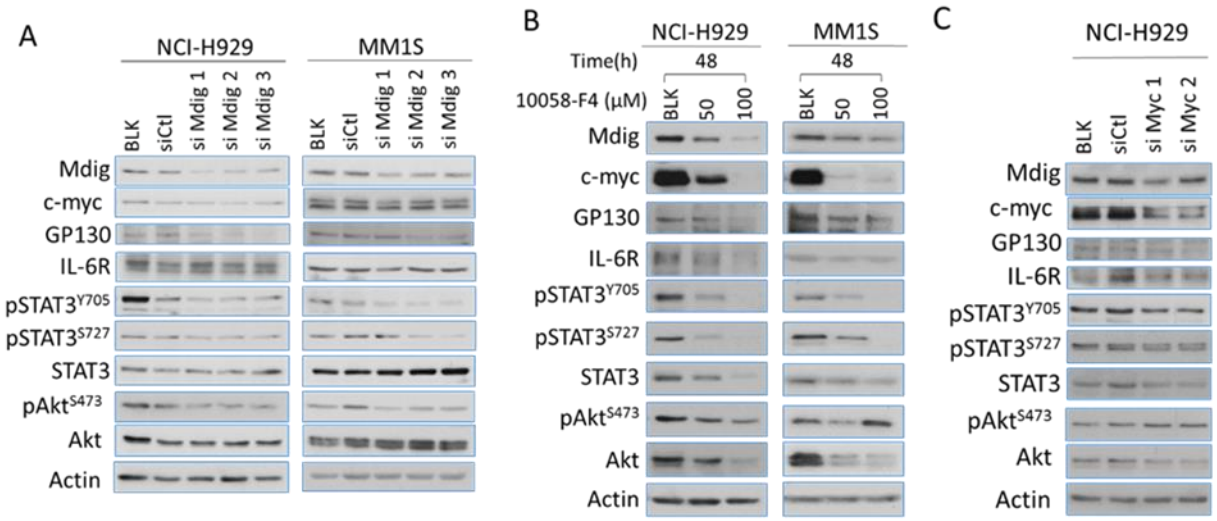

Figure 1.7 Mdig and c-myc modulates IL-6 signaling. (A) Immunoblotting analysis of expression and activity of major regulators involved in IL-6 signaling pathway in human NCI-H929 and MM1S cells treated with control and 3 different mdig siRNAs; (B) Immunoblotting analysis of expression and activity of major regulators involved in IL-6 signaling pathway in human NCI-H929 and MM1S cells treated with c-myc inhibitor, 10058-F4, for 48 h; (C) Immunoblotting analysis of expression and activity of major regulators involved in IL-6 signaling pathway in human NCI-H929 cells treated with control and 2 different c-myc siRNAs.

overexpression of GP130 and, consequently, causes amplification of the IL-6 signaling for cell survival and growth.

Discussion

Considerable progress in understanding the molecular pathogenesis of MM has been achieved in the past years. However, many important questions remain to be answered, such as the risk factors for MM and the extensive crosstalk between various oncogenic mechanisms in MM. Bone marrow is a complex and dynamic microenvironment with stromal cells, osteoclasts, T lymphocytes, cytokines and growth factors, which are critical for disease evolution of MM. In such a profoundly-intertwined regulatory network of malignancy, oncogene C-MYC and cytokine IL-6 have long been viewed as major internal driving forces for MM. Our studies have demonstrated that MDIG is a key mediator in synergizing C-MYC

and IL-6 signaling through direct interaction with C-MYC and JAK1. By both upregulating and sustaining key regulators in IL-6 pathway, MDIG enables MM cells to take advantage of this critical intracellular pathway to achieve abnormal cell proliferation and apoptosis escape. These results explain, at least in part, the mechanisms underlying the observed synergetic collaboration between IL-6 pathway and C-MYC in promoting oncogenesis of the plasma cells.

A study by Moline et al suggested an increased incidence rate and early onset of MM among the first responders exposed to the WTC dust. A follow-up study by Li et al on 55,778 people, including rescue workers, recovery workers, and those who lived or worked near the WTC, also found a higher rate of MM, in addition to thyroid and prostate cancers. The WTC dust released from the collapse of the twin towers after 9/11 attack is a mixture of mineral particles, fibers, metals, and chemicals, many of which are established human carcinogens. Since MDIG was originally identified as a mineral dust-induced gene from coal workers who exposed to mining and coal dust in a daily basis, we sought to determine whether induction of MDIG can be indicative for the association of multiple myeloma and WTC dust. Indeed, we found that WTC dust is highly capable of inducing MDIG expression in bronchial epithelial cells, normal B cells and the MM cells. Although the results reported here can be viewed as circumstantial, they may be considered as “proof of principle” to address the carcinogenic potential of environmental factors on the development of MM.

The findings that MDIG is strongly associated with the disease progression of MM patients suggest that MDIG can be potentially used as a prognostic marker to guide clinical management of the MM patients. A similar role of MDIG had been reported in human gastric carcinoma. Our analysis shows that MDIG mRNA significantly increases as disease progresses. Notably, the increases of MDIG expressions in MM verse MGUS and MM versus SMM are both statistically significant. In addition, high level of MDIG is also significantly associated with poor overall survival of the MM patients. Collectively, these data implicate the

potential of MDIG as a predictor for disease progression and clinical outcomes. Moreover, this study has provided a rationale for targeting MDIG in future anti-MM therapies, especially for early interventions. In the cellular models, we have demonstrated that genetic silencing of MDIG in MM cells leads to constitutive suppression of GP130 (IL-6ST) and pro-survival regulators, STAT3 and AKT, suggesting that MDIG inhibition could be a possible strategy to suppress tumor growth in IL-6-dependent MM subtypes or sensitize them to IL-6-targeted agents. Currently, there is no effective treatment specifically designed for smoldering multiple myeloma (SMM), an asymptomatic transition status between MGUS and active MM. In fact, uncertainties remain on the trade-off between benefits of using routine non-specific therapy and risks of unintended toxicity. According to our findings, MDIG overexpression occurs at early stage of disease and drives oncogenesis of MM. Thus, selective inhibition of MDIG could also be a reasonable option for early clinical intervention or even prevention of MM.

The MDIG protein contains a conserved JmjC domain without classic chromatin- or DNA-binding domains. In accordance with a recent report, our proteomic analysis has unraveled direct interactions of MDIG with a number of chromatin-binding proteins and DNA repair proteins. Given that our current findings have clearly demonstrated a regulatory circuit among C-MYC, MDIG and IL-6 signaling, it is plausible to speculate that MDIG may be assembled into protein complexes along with chromatin- or DNA-binding protein(s), like C-MYC, and be recruited to MM-specific signature genes, including GP130, and exerts its regulatory functions on gene expression. On the other hand, recent studies have discovered that transcription-related regulators can translocate to different cellular compartments and carry out non-canonical functions. For example, Enhancer of Zeste Homolog 2 (EZH2), a well-documented epigenetic silencer for gene transcription, has been shown to directly interact with and methylate STAT3. Similarly, in the present report, we have observed that MDIG binds to and demethylates JAK1 in cytosol, leading to stabilization of the JAK1 protein.

Considering that ubiquitylation is reported as the most common modification on lysine residues of JAK1, and the report that lysine methylation may create a docking site for certain ubiquitin ligases, it is very likely that MDIG may remove the methyl group from the lysine residue(s) on JAK1 and subsequently prevent the action of the ubiquitin ligases on JAK1 protein. On the other hand, MDIG has also demonstrated enzymatic activity that catalyzes histidine hydroxylation of ribosomal proteins in a wide range of organisms, from prokaryotes to humans. Considering that lysine demethylation results from hydroxylation, the MDIG-JAK1 binding may theoretically cause other types of modifications of JAK1 than demethylation in MM cells, for example, hydroxylation. Further studies are required to fully elucidate the molecular basis of MDIG-induced modifications of JAK1 and the precise role of MDIG in maintaining the levels of JAK1 protein and function.

This research has also provided hints for future MDIG and MM studies. For example, our proteomics data show that MDIG interacts with 7 proteins related to DNA damage repair (DDR). A recent study in lung cancer model demonstrates that physical binding between MDIG and some of these DDR-related proteins significantly inhibits the ability of these DDR-related proteins to repair DNA double strand break. If this is the case in MM, MDIG may also contribute to genome instability, which further leads to aberrantly altered karyotypes, a common feature in MM cells.

CHAPTER 2 UNRAVEL NOVEL MECHANISMS OF RESISTANCE TO EGFR TYROSINE KINASE INHIBITORS IN LUNG CANCER

Introduction

Lung cancer is responsible for 1.38 million annual deaths worldwide, making it the leading cause of cancer-related mortality in the USA and throughout the world. Lung cancer can be histologically classified into small cell lung cancer (SCLC) and non-small cell lung cancer (NSCLC) and the latter subtype constitutes 80% of lung cancers. Among all NSCLC patients, overexpression of the epidermal growth factor receptor (EGFR) is found in 40-80% cases while further studies show that about 25% of all NSCLC patients harbor "activating mutations" in the EGFR tyrosine kinase domain, including deletions in exon 19 and L858R in exon 21. Considering the pivotal role of EGFR in transducing signals for cell proliferation, cell-cycle progression and activation of anti-apoptosis, targeting oncogenic EGFR signaling pathway becomes a promising therapeutic strategy against NSCLC.

Gefitinib and erlotinib are two most widely applied first-generation targeted agents inhibiting the activity of EGFR and downstream signaling by competitively blocking the binding of adenosine triphosphate (ATP) to active residues on EGFR tyrosine kinase domain. Though gefitinib has shown dramatic therapeutic effects on patients with certain clinical features, such EGFR tyrosine kinase inhibitor (TKI) -based therapy is still suffering from two major limitations, that is, biased drug responses (primary resistance) and inevitable acquired resistance (secondary resistance).

First of all, predicting gefitinib responses in NSCLC patients has always been challenging partly due to the complexity of EGFR signaling pathway itself and its frequent crosstalk with other intracellular signaling pathways. Responses to gefitinib vary dramatically in NSCLC patients. Clinical evidence has shown that tumors harboring previously mentioned “activating mutations” in EGFR generally respond well to gefitinib treatment but expression

levels of EGFR is not significantly correlated with robust drug response. Theoretically, NSCLC patients with overexpression of wild-type EGFR are also anticipated to benefit from EGFR TKI, but satisfying responses have only been noted in about 10% of these patients. In agreement with the clinical observations, NSCLC cell lines also display a broad range of sensitivity to EGFR TKIs. Such discrepancy between theoretical efficacy and actual statistics indicates there might be some critical mechanisms modulating tumor responses to gefitinib and in-depth researches are needed to fully elucidate them. In the past decade, accumulating evidence has demonstrated that certain key regulators can activate alternative signaling pathways to circumvent the suppressed EGFR after EGFR TKI treatment, such as mutant KRAS, hyperactivated insulin-like growth factor 1 receptor (IGF-1R) and gefitinib-induced STAT3-AKT activation loop. Inspired by these findings, many translational researches and clinical trials testing co-targeting strategies against EGFR and "bypass" regulators have been carried out. For example, it has been reported that AKT inhibitor and gefitinib have shown synergistic anti-tumor effects against NSCLC cell lines. Thus, combinational targeting has gradually become a promising and practical option to enhance the efficacy of targeted agents in cancer treatment. However, intracellular signaling system of cancer cells is a widely interconnected, multidirectional and dynamic network, which makes it very hard to locate the potential "bypass" nodes. In this part, we used integrative methods to approach this problem. We accessed large collections of cancer cell line genomics and drug toxicity profiles and systematically screen gene expressions of 11 gefitinib-sensitive and 5 non-sensitive NSCLC cell lines. Subsequent bioinformatics analysis has identified TGF-β, Wnt, Hedgehog and JAK-STAT pathways as candidate "bypass" pathways. Though these four pathways have been clearly demonstrated to facilitate cell proliferation, apoptosis escape and metastasis in human lung cancer, their potential roles in modulating cellular responses to gefitinib are under-studied.

Considering the active role of STAT3 in EGFR signaling pathway, we picked JAK-STAT pathway for further study. STAT3 belongs to the STAT (Signal transducer and activator of transcription) protein family which is essential for cellular functions. Activation of STAT3 is determined by phosphorylation at tyrosine 705 residue and strengthened by phosphorylation at serine 727 residue. Classically, two categories of pathways are mediating STAT3 tyrosine phosphorylation, one is receptor tyrosine kinase signaling, including EGFR, the other one is cytokine-signaling pathway, including IL-6/ Janus-activated kinases (JAK). Aberrant expression and activity of STAT3 have been observed in both carcinogenesis and development of drug resistance in several cancer types, including NSCLC, suggesting that STAT3 may serve as a bypass regulator to offset EGFR TKI treatment in lung cancer.

Our molecular biology experiments have demonstrated that non-sensitive lung cancer cell lines exhibit highly refractory JAK2-STAT3 signaling axis to gefitinib treatment. Moreover, in these cell lines, gefitinib treatment induces, rather than suppresses STAT3 activation. We have further demonstrated that gefitinib not only promotes the direct interaction between EGFR and STAT3, which is needed for STAT3 activation, but also affects the upstream regulators of STAT3 in a dose-dependent manner. Low dose of gefitinib suppresses SOCS3 only while high dose inhibits both SOCS1 and SOCS3. As a result, activated STAT3 restores activation of AKT that is initially inhibited by gefitinib. AKT is an oncogenic protein kinase that is associated with cell survival and proliferation. Restoration of AKT activation eventually facilitate the lung cancer cells to survive EGFR interruption. Follow-up cell proliferation studies show that simultaneous inhibition of STAT3 sensitizes the cancer cells to gefitinib-induced repression of cell growth. Collectively, our data from this part have indicated that gefitinib-induced STAT3 activation and subsequent AKT recovery may act as a novel mechanism of primary resistance against gefitinib in NSCLC. Accordingly, combinational

targeting of STAT3 and EGFR may enhance the efficacy of EGFR TKI-based therapy in lung cancer patients with EGFR overexpression.

On the other hand, all patients including those who initially respond well to gefitinib will become resistant after 6-9 months' treatment which finally leads to treatment failure. Based on these clinical situations, Jackman and colleagues have introduced the concept of Acquired Resistance to EGFR TKI with the following criteria: 1, previous treatment with a single-agent EGFR TKI; 2, a tumor that harbors an EGFR "activating" mutation or objective clinical benefit from treatment with an EGFR TKI; 3, systemic progression of disease while on continuous treatment with gefitinib or erlotinib within the last 30 days; 4, no intervening systemic therapy between cessation of gefitinib or erlotinib and initiation of new therapy . Researches into this problem have revealed many important resistance mechanisms, such as EGFR T790M secondary mutation resulting in higher ATP binding capacity, aberrant amplification of MET which bypasses the inhibited EGF receptors and in very rare cases, transformation from NSCLC to small cell lung cancer (SCLC). The former two major resistance mechanisms are reported to occur in about 50% and 30% of resistant cases, respectively. However, resistance mechanisms remain unclear in about 20% of all resistant cases. Actually, the situation might be far more complicated than expected given the fact that the resistance mechanisms frequently overlap with others, for example, about 50% of resistant patients with MET amplification also harbor EGFR T790M mutation. Moreover, second generation EGFR TKI (afatinib) designed to overcome the EGFR T790M mutation has failed to show expected therapeutic efficacy. Taken together, these studies suggest that some other unknown mechanisms, such as non-oncogenic or oncogenic dependent drug resistance, existing alone or simultaneously with currently identified alterations of the EGFR signaling, may play an important role in the development of acquired resistance to EGFR TKI. To test this hypothesis, we have established a gefitinib-resistant (GR) NSCLC cell line through 180-day exposure to

gefitinib at maximal tolerable dose (16μM). Compared to Parental cells, GR cells exhibited decreased sensitivity to gefitinib and enhanced anchorage-independent growth and aggressiveness, which is consistent with the clinical manifestation of resistant lung cancers. Then we performed microarray analysis and molecular biology experiments on GR cells to profile the resistant gene expressions and characterize the altered signaling pathways. Our data indicate that multiple resistance mechanisms co-exist in the GR cells. One of them is hyperactivation of STAT3 pathway, characterized by shift of phosphorylation pattern (from tyrosine705 to serine727 residue) and enhanced transcription activity of STAT3. Based on these results, we co-inhibited STAT3 and EGFR in GR cells and this treatment re-sensitizes the GR cells to gefitinib by suppressing several survival-related pathways, including IL6-JAK-STAT3, MAPK, TGF-BETA, ERBB, mTOR and VEGF pathways. Collectively, our study has revealed novel mechanisms of acquired resistance to EGFR TKI in lung cancer, and more importantly, has provided a strong rationale for combinational targeting of STAT3 and EGFR as a potential strategy to overcome acquired resistance.

Material and methods

Cell culture and reagents—The human NSCLC cell lines A549, NCI-H2023 and NCI-H2026 were purchased from the American Type Culture Collection (ATCC) (Manassas, VA) and all the cell lines were maintained in ATCC recommended protocol. Gefitinib-naïve A549 cells were cultured in full growth medium containing 16μM of gefitinib. After 180 days of exposure, the gefitinib-resistant (GR) cell line was established. Parental A549 cells from same original stock cultured in gefitinib-free medium alongside the GR cells during cell line establishment were used as control cell line. STAT3 inhibitor V, Stattic, was purchased from Santa Cruz Biotechnology, Inc. (Santa Cruz, CA).

siRNA transfection—Total of 4×10^5 cells per well were seeded into 6-well plates and incubated until they reached 50% confluence. siRNAs at a final concentration of 50nM were

then forward-transfected using Lipofectamine RNAiMAX™ (Invitrogen) following manufacturer protocol. Cells were cultured for 24 hours for gene silencing followed by sequential treatment of gefitinib. siRNA against STAT3 and control siRNA were purchased from Cell Signaling (Danvers, MA).

Western Blotting—Cells were lysed by 1xRIPA cell lysis buffer (Cell Signaling) supplemented with protease and phosphatase inhibitors cocktail (Roche, Indianapolis, IN) and 1mM PMSF. Collected cell lysates were then homogenized by sonification and insoluble debris was removed through centrifugation of 13,000g at 4 °C for 15 minutes. The concentrations of protein were then determined using Pierce BCA Protein Assay Kit™ (Thermo Scientific, Rockford, IL). The protein samples were prepared using 4×LDS sample buffer (Invitrogen) with dithiothreitol at a final concentration of 200mM and were denatured by boiling at 95°C for 5 minutes before separation by 7.5%, 10% or 12% SDS-PAGE gel, where appropriate. Separated samples were then transferred onto PVDF membrane (Invitrogen) and blocked with 5% non-fat milk diluted in TBST for 1 hour at room temperature. After washing with TBST, the membranes were incubated with indicated primary antibodies for overnight at 4°C and corresponding alkaline phosphatase (AP)-coupled second antibodies for 1hour at room temperature before detecting. CDP-Star™ Reagent (New England Biolabs) was used to visualize the signals on autoradiography films. Primary antibodies against phospho-AKT (Ser473), phospho-AKT (Thr308), total AKT, phospho-STAT3 (Ser727), phospho-STAT3 (Tyr705), total STAT3, phospho-EGFR (Tyr1068), phospho-EGFR (Thr669), total EGFR, phospho-PI3K (Tyr458), PI3K, PTEN, phospho-P38 (Thr180/tyr182), P38, phospho-ERK(1/2) (Thr202/tyr204), ERK, phospho-JNK (Thr183/Tyr185), JNK, phosphor-GAPDH, beta-actin and AP-linked mouse IgG were purchased from Cell Signaling (Danvers, MA). Antibodies against SOCS1 and SOCS3 purchased from Millipore (Temecula, CA) and Abcam (Cambridge, MA), respectively.

Immunofluorescent staining—5×10^4 A549 cells per well were plated into 24-well plates. Cells were allowed to grow and attach for 24hours before time-dependent treatment to 4μM gefitinib for up to 6 hours and fixation with 4% formaldehyde for 15 min at room temperature. After brief washing with PBS, cells were blocked in 1×PBS containing 5% normal goat serum and 0.3% Triton X-100 for 1 hour and EGFR antibody for another hour. Then cells were incubated in Alexa Fluor 488 or FITC-linked goat anti-rabbit IgG (Invitrogen) for 1 hour in dark. One drop of Prolong Gold™ antifade reagent with DAPI (Invitrogen) was added to each well before photography.

Immunoprecipitation—Cells were lysed in non-denaturing lysis buffer containing 137mM NaCl, 20mM Tris-HCl (pH8.0), 10% glycerol, 2mM EDTA and 1% NP-40 supplemented with protease and phosphatase inhibitors cocktail (Roche). After gentle agitation for 30 minutes and purification by centrifugation of 13,000g, the lysates were pre-cleared with rabbit IgG (Santa Cruz) and protein A/G plus beads (Santa Cruz). 800μg of protein for each sample was incubated with indicated antibodies at a dilution ratio of 1:100 at 4°C for overnight. The protein samples were further incubated with 40μL of protein A/G plus beads (Santa Cruz) for 4 hours at 4°C, followed by 3 washes with non-denaturing lysis buffer. The prepared samples were then detected with Western Blot as described above.

Cell proliferation assay—$5x10^3$ A549 cells diluted in 100μL full growth medium were seeded into 96-well plate. After 24 hours, 100μL medium containing indicated concentration of gefitinib with or without STAT3 inhibitor was added to each well and each dose was tested in triplicates. CyQUANT NF Cell Proliferation Assay Kit™ (Invitrogen) was used to stain viable cells. After 30 minutes in dark, the intensity of fluorescence was measured using BioTek Synergy 2 plate reader (BioTek, Winooski, VT).

Soft-agar colony formation assay– $2x10^4$ cells mixed in 0.33% agar were seeded on top of a solidified layer of 0.5% agar in 6-well plates. The cells were fed with full growth

medium every 3 days. After 14 days, all the samples were photographed using Nikon Ti Microscope and the photos were processed using NIS-Elements BR3.2 software. Colonies with a diameter larger than 200μm and area over 30000 μm^2 were considered as qualified colonies. We counted 4 cm^2 area per well and the results were presented as colony number per cm^2.

Migration and invasion assay— Migration and invasion activity of parental cells and GR cells were measured using BD BioCoat™ Matrigel™ Invasion and Migration Chambers following the manufacturer's protocol. All cells were incubated 24 hours for migration test and 48 hours for invasion test before being fixed and stained using Diff-Quik Kit. Cells remaining in the chamber were removed by cotton swabs. The migrated and invasive cells were then photographed and counted using Nikon Ti Microscope and NIS-Elements BR3.2 software.

Microarray and data analysis—Total RNAs of Parental cells, GR cells, GR cells treated with Stattic (GS) were extracted using TRIzol Reagent following manufacture's protocol (Life Technologies, Grand Island, NY, USA) and their integrity was assessed by 18S and 28S ribosomal RNAs. The qualified RNA samples were sent to Phalanx Biotech (San Diego, CA) for further process. RNA quantity and purity were verified, followed by target preparation and hybridization to Human OneArray Plus gene expression microarray (Phalanx Biotech). Standard selection criteria to identify differentially expressed genes (DEGs) are as follows: (1) Log2 value for fold change ≥ 1 and $P < 0.05$, (2) Log2 ratios= NA and the differences of intensity between the two samples >=1000. Gene clustering analysis was performed on selected DEGs after data transformation and mean centering by averagely linkage algorithm.

Gene set enrichment analysis (GSEA) was used to further characterize the differences of the enriched gene sets between Parental cells vs. GR cells, GR cells vs. GS cells. GSEA is a method to identify whether certain gene sets (a collection of mutually related genes) instead of single genes are enriched in an independent rank-ordered profile of genes that are

differentially expressed. In the current analysis, software GSEA2-2.2.2 (Broad Institute) was used and signal-to-noise was selected as genes ranking metric and 1000 was used for number of permutations.

Statistical analysis—Results of quantification of immunoblotting data, colony formation assay, migration and invasion assays were analyzed by Student's t-test and shown as mean±SD. Cell proliferation data was processed using two-way ANOVA and the statistical significance of differences in inhibitory effects between different treatments and samples were determined by Post-hoc tests. For all experiments, $p < 0.05$ is considered as statistically significant.

Results

TGF-β, Wnt, Hedgehog and JAK-STAT pathways are potential "bypass" candidates mediating primary resistance to gefitinib. 16 primary human NSCLC cell lines with EGFR alterations were selected and subject to bioinformatics analysis for primary drug resistance-related pathways. The cell lines were grouped based on their gefitinib sensitivity and major mutation status. Cell lines with IC_{50} under 2μM were defined as sensitive (S group) and those with IC_{50} over 8μM as non-sens itive (N group). Since EGFR activating mutations have been shown to cause potent addiction to EGFR signaling pathways, we further sort the cell lines from S group into "S group with wild-type EGFR" (SW group) and "S group with mutant EGFR" (SM group). Similarly, considering the established role of mutant Kras in counteracting gefitinib, the N group cell lines were also subdivided into "N group with mutant Kras" (NM group) and "N group

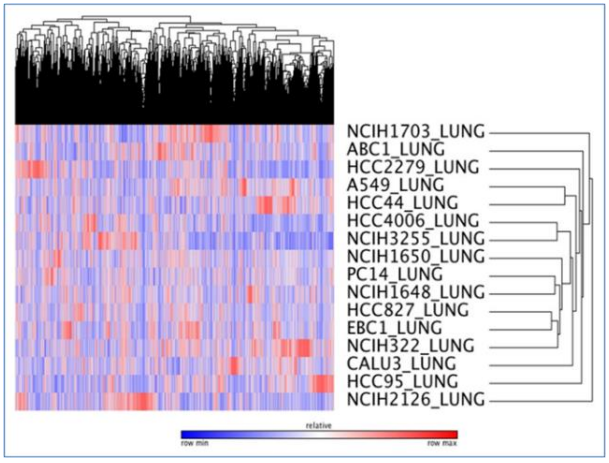

Figure 2.1 Hierarchical clustering of 16 NSCLC cell lines used in the study based on their gene expression profiles.

with wild-type Kras" (NW group). All the groups of NSCLC cell lines are listed in Table 2.1. Then, gene expression data of the designated cell lines were clustered and the differentially expressed genes (DEGs) were identified via Characteristic Direction method. As shown in Figure 2.1, the cell lines sorted into the same groups exhibit similar gene expression profiles. Next, two tests, SW group versus NW group and SW group versus NM group, were performed separately. The identified DEGs were then subject to signaling pathway impact analysis using the Kyoto Encyclopedia of Genes and Genomes (KEGG) database. Then the highlighted

Cell Lines	Histology	IC50(uM)	EGFR CNV	EGFR Expression	EGFR Mutation	Kras Mutation	Group
A549	AD	9.6	0.1163	0.61529	WT	p.G12S	NM
HCC-44	AD	7.9	0.3605	0.87639	WT	p.G12C	NM
ABC-1	AD	8	0.7321	1.0867	WT	WT	NW
EBC-1	SQ	10	0.4354	0.72721	WT	WT	NW
NCI-H1703	AD	8	0.8629	0.60114	WT	WT	NW
HCC-2279	AD	0.03	1.4577	1.4334	exon 19 del	WT	SM
HCC4006	AD	0.02	1.3014	1.1394	exon 19 del	WT	SM
HCC827	AD	0.04	3.2468	3.081	exon 19 del	WT	SM
NCI-H1650	AD	1	1.1195	1.2502	exon 19 del	WT	SM
PC-14	AD	0.0309	1.1248	1.1358	exon 19 del	WT	SM
NCI-H3255	AD	0.015	2.5269	2.6756	L858R	WT	SM
HCC-95	SQ	1.9	0.322	0.65042	WT	WT	SW
NCI-H1648	AD	0.38	0.3608	0.93588	WT	WT	SW
NCI-H2126	LCC	1	0.3287	0.51548	WT	WT	SW
NCI-H322	AD	0.3	-0.0224	1.1254	WT	WT	SW
Calu-3	AD	0.3	0.874	0.19162	WT	WT	SW

Table 2.1 Characteristics of the NSCLC cell lines used in the study including copy number variation and expression level of EGFR, mutation status of EGFR and Kras, gefitinib IC50 and mutation-based classification of gefitinib sensitivity. The CNV and expression level of EGFR are displayed in log2 scale. AD: adenocarcinoma, SQ: squamous-cell carcinoma, LCC: large-cell carcinoma, NM: non-sensitive cells with Kras mutation, NW: non-sensitive cells with wild-type Kras, SM: sensitive cells with EGFR activating mutations, SW: sensitive cells with wild-type EGFR

NM vs. SW	
Rank Order	Candidate Pathways
1	HSA04350 TGF BETA SIGNALING PATHWAY
2	HSA04630 JAK STAT SIGNALING PATHWAY
3	HSA04310 WNT SIGNALING PATHWAY
4	HSA04340 HEDGEHOG SIGNALING PATHWAY

NW vs. SW	
Rank Order	Candidate Pathways
1	HSA04350 TGF BETA SIGNALING PATHWAY
2	HSA04340 HEDGEHOG SIGNALING PATHWAY
3	HSA04310 WNT SIGNALING PATHWAY
4	HSA04630 JAK STAT SIGNALING PATHWAY

Table2.2. Summary of implicated "bypass" pathways involved in mediating gefitinib sensitivity. NM: non-sensitive with Kras mutation, NW: non-sensitive with wild-type Kras, SW: sensitive with wild-type EGFR

signaling pathways were manually filtered based on their biological function. The signaling pathways not related to cell proliferation or apoptosis escape were filtered out and the pathways sharing massive overlapping DEGs with each other were combined into the one with highest significance. In NW group cell lines, TGF-β, Wnt, Hedgehog and JAK-STAT pathways were implicated. Notably, in NM group, the same four pathways were highly implicated with only a minor difference in the rank order, that is, TGF-β, JAK-STAT, Wnt and Hedgehog (Table 2.2), suggesting non-sensitive cell lines, with mutant Kras or not, may share similar alternative downstream pathways to counteract gefitinib treatment. Taken together, these results strongly indicate that TGF-β, Wnt, Hedgehog and JAK-STAT pathways may play a significant role in modulating cellular responses to gefitinib among NSCLC cells.

Sensitive and non-sensitive NSCLC cell lines exhibit distinct response patterns of key protein regulators to gefitinib treatment. Activation of EGFR is closely linked to prosurvival signaling pathways, including AKT and STAT3. Considering STAT3 pertaining to putative "bypass" pathways, we performed time course study to investigate the differences in responses to gefitinib between sensitive and non-sensitive cell lines. 3 NSCLC cell lines were used, including 2 non-sensitive cell lines, A549 and NCI-H2023, and 1 sensitive cell line, NCI-H2126 (Fig.2.2A). As shown in Figure 2.2B and 2.2C, gefitinib is capable of inhibiting the activity of EGFR in all 3 cell lines. Interestingly, in the 2 non-sensitive cell lines the initially inhibited AKT activation was gradually recovered at later time points on both serine473 and threonine308 residues while the AKT activation was substantially inhibited in NCI-H2126 cells.

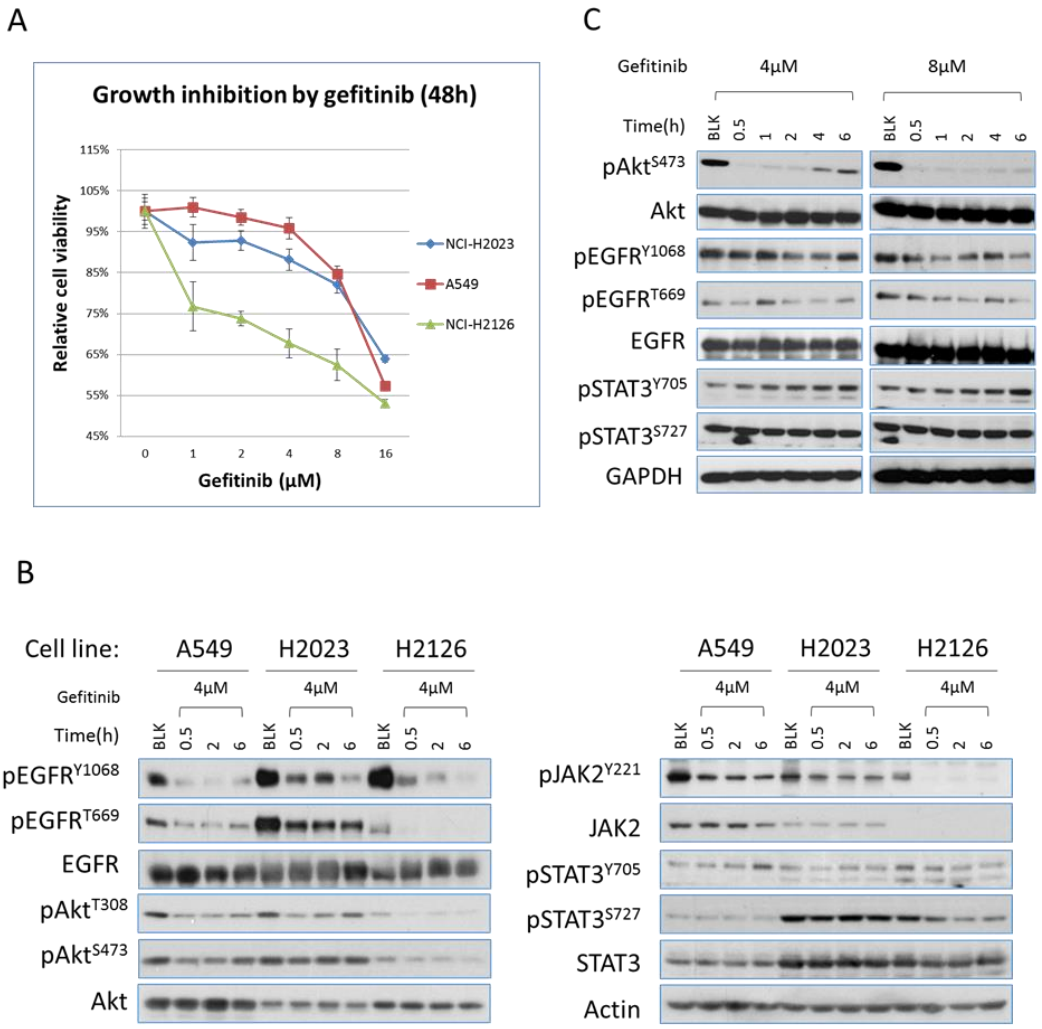

Figure 2.2 Sensitive and non-sensitive NSCLC cell lines show distinct responses to gefitinib treatment. (A) Cell Viability Assay for the percentage of viable cells in A549, NCI-H2023 cells (non-sensitive NSCLC cell lines) and NCI-H2026 cells (sensitive cell line) after 48-hour exposure to gefitinib ranging from 1μM to 16μM. (B) Western blot analysis shows different effects of gefitinib on multiple protein regulators involved in EGFR signaling pathway between A549, NCI-H2023 and NCI-H2126 cells. (C) The expression level and activity of EGFR, AKT and STAT3 in A549 cells treated with gefitinib at 4μM (left panel) and 8μM (right panel) for indicated time periods.

Additionally, the Jak2-STAT3 signaling axis in A549 and NCI-H2023 cells have been demonstrated to be more refractory in response to gefitinib exposure than NCI-H2126 cells, which is in agreement with bioinformatics analysis. Inhibition of EGFR by gefitinib is expected to down-regulate STAT3 activity considering that STAT family proteins, STAT3 in particular, play an essential role in EGFR-mediated cellular functions. However, in both non-sensitive

cell lines, A549 and NCI-H2023, time course test showed that gefitinib treatment, in fact, induces STAT3 activation. When exposed to gefitinib at 4μM, a rapid increase of phosphorylation of STAT3 on tyrosine 705 residues was observed. Such gefitinib-induced cellular responses were confirmed by more detailed follow-up experiments on A549 cells which involved more time points and doses (4μM and 8μM) of gefitinib treatment (Fig.2.2C). Interestingly, we noticed that the trend of gefitinib-induced STAT3 activation was accordant with the recovery pattern of AKT after gefitinib treatment, indicating potential interactions between these two pathways. While in sensitive cell line, NCI-H2126 cells, the activity of STAT3 is time-dependently suppressed on both tyrosine705 and serine727 residues, which is a significant difference between non-sensitive and sensitive cell lines (Fig.2.2B).

AKT recovery is not due to re-activation of the EGFR by gefitinib. EGFR has been viewed as one of the key upstream kinases responsible for growth factor-induced AKT activation. To determine whether the observed recovery of AKT activation is due to failed inhibition of EGFR by gefitinib, we measured the levels of internalization and phosphorylation of EGFR in response to gefitinib. In immunofluorescent staining assay, gefitinib treatment induced a fast and sustained internalization of the EGFR (Fig.2.3A). After treatment of the cells with 4 μM gefitinib, a gradual translocation of the EGFR from cell membrane to intracellular vesicles and finally to the perinuclear area was observed, indicating a constitutive and effective inhibition of the EGFR by gefitinib. To further validate the inhibitory effect of gefitinib on EGFR, we next measured the phosphorylation status of the EGFR in the cells treated with gefitinib. Again, the time course studies demonstrated a rapid recovery of AKT phosphorylation in both serine 473 (S473) and threonine 308 (T308) residues within 6 h following the initial inhibition, especially in the cells treated with 4μM gefitinib (Fig.2.3B). Semi-quantification of the AKT phosphorylation suggested about 40-60% recovery of AKT

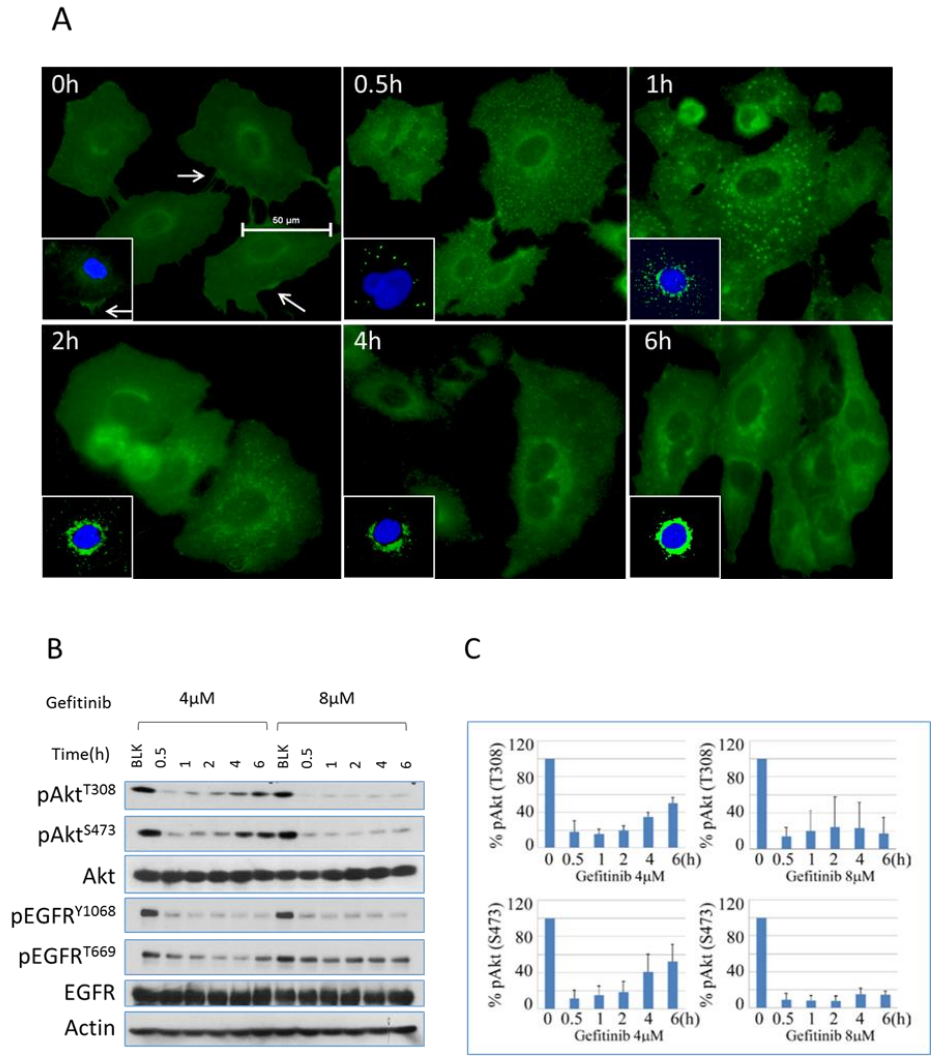

Figure 2.3 Gefitinib inhibits EGFR constitutively and substantially. (A) Immunofluorescence test shows the process of internalization of EGFR at proceeding time points after treatment of gefitinib in A549 cells. (B) Gefitinib treatment induced continuous inhibition of EGFR phosphorylation on tyrosine 1068 (Y1068) and threonine 669 (T669) without recovery at the later time points. (C) Semi-quantification of AKT recovery following gefitinib treatment.

activation at the 4 to 6 h time points of gefitinib treatment (Fig.2.3C). However, there is no similar recovery pattern of EGFR phosphorylation following gefitinib treatment. At both 4 and 8 μM gefitinib treatments, phosphorylation of Y1068 and T669 of EGFR was substantially inhibited from the earlier to later time points (Fig. 2.3B). These data, thus, suggest that the AKT recovery is not due to failed inhibition of EGFR by gefitinib.

Inhibition of STAT3 prevented recovery of AKT activation in gefitinib-treated cells. It has been well-documented that STAT3 signaling pathway contributes to AKT activation in response to a number of extracellular and intracellular signals. More recently, STAT3-AKT activation loop has been uncovered in lung epithelial cells. Based on that rationale, we hypothesized that gefitinib-induced STAT3 activation is responsible for the sequential recovery of AKT phosphorylation. To test that, we co-treated cells with Stattic, a

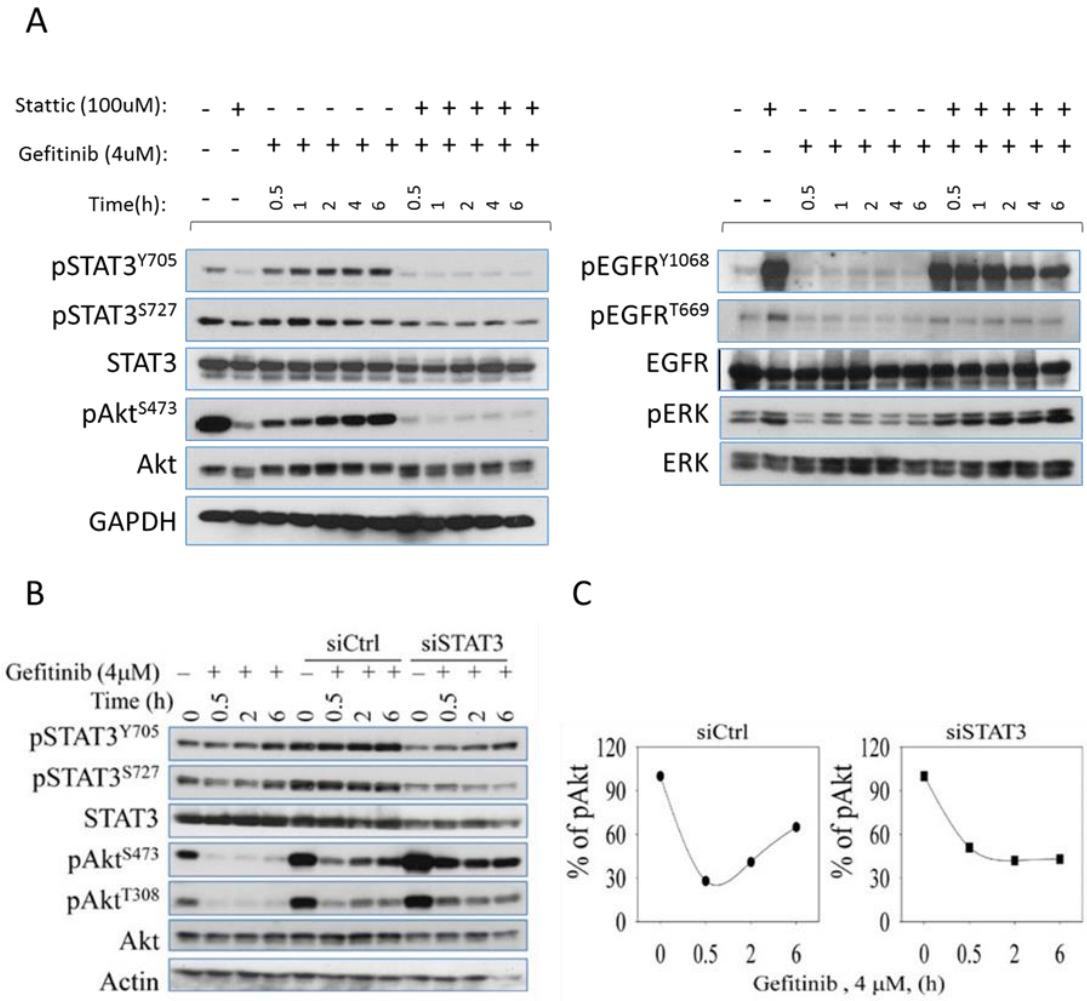

Figure 2.4 Chemical inhibitor and gene silencing of STAT3 suppresses succeeding recovery of AKT activation after gefitinib treatment. (A) Immunoblotting analysis of expressions and activities of EGFR, AKT, STAT3 and ERK under time-dependent treatment with 4μM gefitinib combined with or without 100 μM Stattic (STAT3 inhibitor) for up to 6 hours in A549 cells. (B) Silencing STAT3 by siRNA diminishes gefitinib-induced AKT recovery in A549 cells. (C) Semi-quantification of the AKT S473 phosphorylation in the cells treated with gefitinib and transfected with control siRNA (siCtrl, left panel) or STAT3 siRNA (siSTAT3, right panel).

STAT3 inhibitor, which potently downregulates its phosphorylation without affecting the total amount of STAT3. As shown in the Figure 2.4A, when STAT3 function was inhibited, the recovery pattern of AKT was also eliminated even when EGFR was hyperactivated possibly by the treatment of STAT3 inhibitor, Stattic. In order to exclude the potential off-target effects of the chemical inhibitor, we further employed a siRNA-based gene silencing strategy to confirm the above observation. When the cells were transfected with STAT3 specific siRNA, siSTAT3, the total amount and activity of STAT3 were both reduced and the recovery pattern of AKT was eliminated, though the basal level of AKT phosphorylation was elevated. In contrast, the cells transfected with control siRNA or without transfection showed no inhibitory effects on either STAT3 activation or the AKT recovery (Fig.2.4B and 2.4C).

Gefitinib promotes physical binding of STAT3 to EGFR. In receptor tyrosine kinase-dependent signaling, STAT3 activation is increased by binding to certain STAT3 docking sites on EGFR c-terminal domains. In order to determine the direct physical interaction between STAT3 and EGFR, immuno-precipitation assay was performed. As shown in Figure 2.5A, gefitinib treatment induced potent binding between STAT3 and EGFR when identical amount of total protein was used for pull-down by anti-STAT3 antibody.

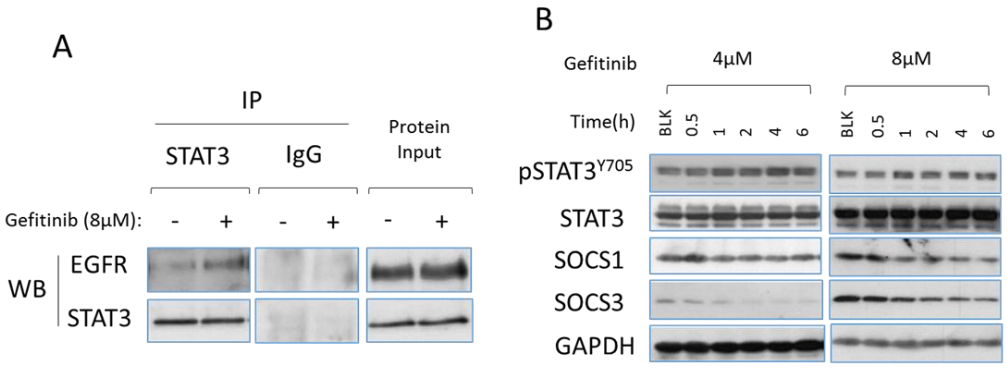

Figure 2.5 Gefitinib promotes EGFR-STAT3 interaction. (A) Immunoprecipitation assay (left pannel) demonstrates direct physical binding of EGFR and STAT3 induced by gefitinib treatment. Cells were treated with 8uM gefitinib for 6 hours. The samples were precipitated with STAT3 antibody and detected using antibodies against EGFR and STAT3. (B) Immunoblotting analysis shows the effect of gefitinib on SOCS1 and SOCS3 in A549 cells.

Another fundamental signaling pathway leading to STAT3 activation is cytokine pathway in which STAT3 is activated by JAK family proteins, which is negatively regulated by the suppressor of cytokine signaling proteins (SOCS), such as SOCS1 and SOCS3. In order to identify the potential role of the regulators in cytokine-activated pathway, we carried out another time course study to determine the levels of the SOCS proteins. Level of SOCS3 is reduced in cells treated with 4uM and 8uM gefitinib, while significant reduction of SOCS1 is observed in 8uM group only (Fig.2.5B), suggesting that gefitinib is able to inhibit SOCS proteins in a manner of dose-dependency, which accounted for an alternative mechanism contributing to gefitinib-induced STAT3 activation.

STAT3 inhibition sensitizes non-sensitive NSCLC cells to gefitinib treatment in vitro. Since gefitinib has been shown to induce STAT3 activation and subsequent AKT recovery (Fig.2.2), we were interested in if combinational suppression of EGFR and STAT3 could overcome the intrinsic insensitivity of certain NSCLC cells. A549 cells were exposed to dose-dependent treatment of gefitinib (2-8μM) in combination with STAT3 inhibitor (5μM) for 24 h and 48 h, respectively, before cell viability was examined and analyzed. As shown in

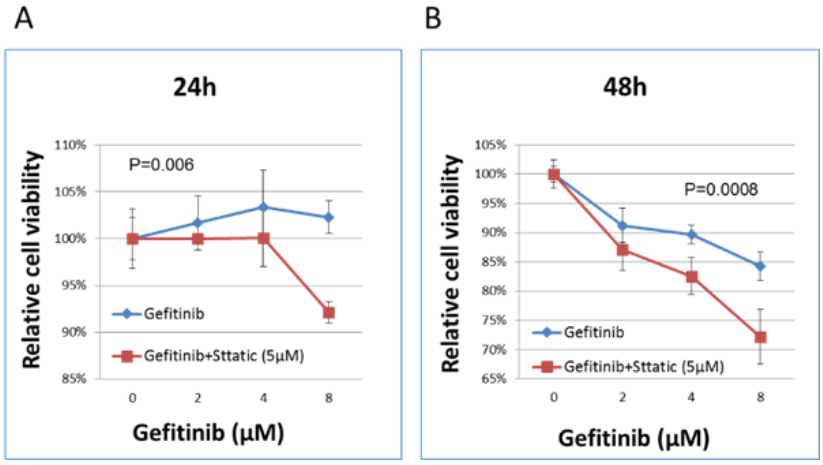

Figure 2.6 STAT3 inhibitor enhances the inhibitory effect of gefitinib on cell growth. Cell Viability Assay Kit was used to stain viable cells. Data show the relative percentage of viable A549 cells after exposed to gefitinib ranging from 2μM to 8μM in the absence or presence of Stattic for 24 hours (A) and 48 hours (B), respectively. (P<0.01 in both tests)

Figure 2.6, combinational STAT3 inhibition significantly fortifies the anti-cell growth effects of gefitinib in A549 cells compared to the group of gefitinib alone.

NSCLC cells with acquired gefitinib resistance (GR) exhibit aggressive phenotype. In order to study the mechanisms of acquired resistance, we have established a

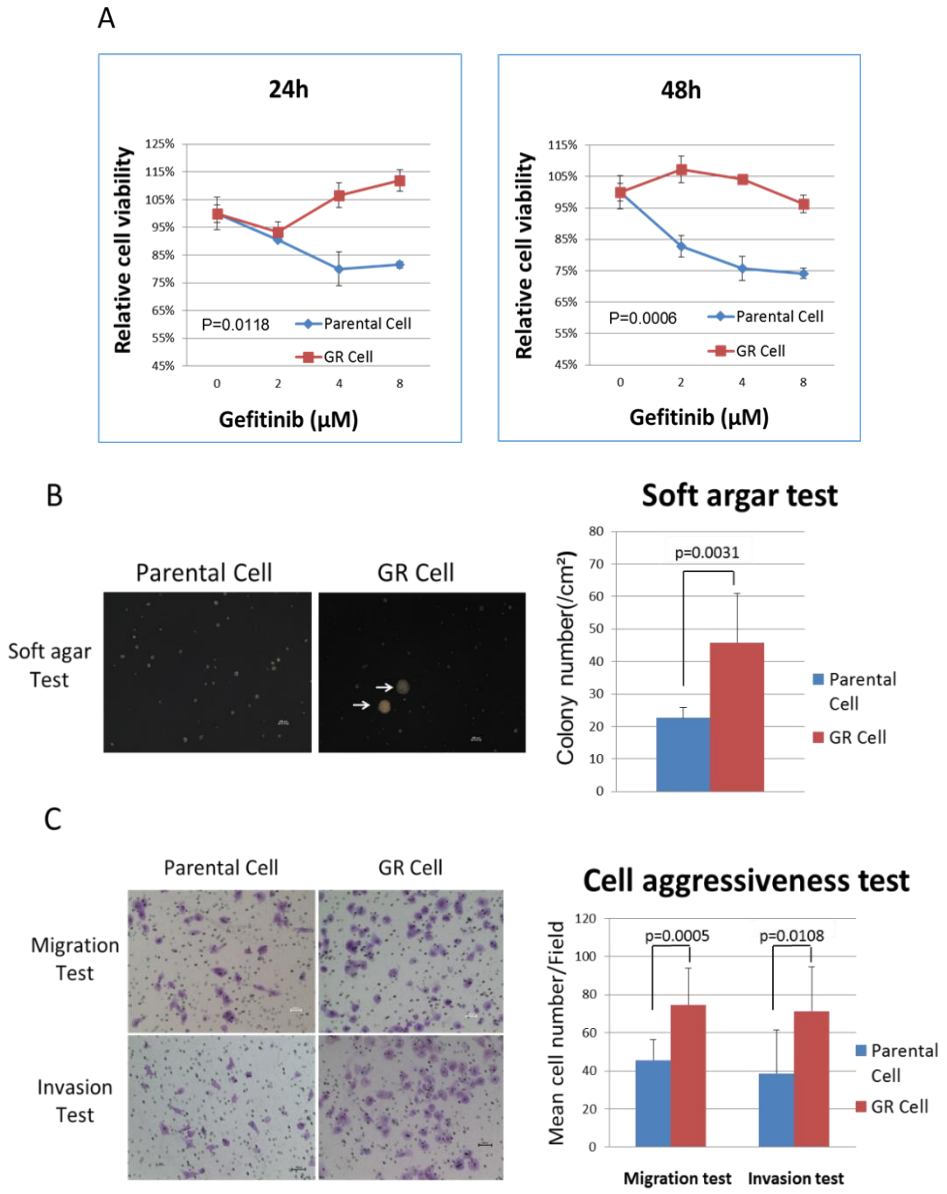

Figure 2.7 Gefitinib resistant cells exhibit enhanced drug resistance and aggressiveness. (A) Cell Viability Assay for the percentage of viable cells in gefitinib resistant (GR) and parental cells when exposed to gefitinib ranging from 2μM to 8μM. (B) Soft agar assay for GR cells and parental cells. Colonies with a diameter larger than 200μm and an area over 30000 μm2 were considered as qualified, as indicated by the white arrows. (C) Cell migration and invasion tests for GR cells and parental cells, summary of results and typical photos are presented. (P<0.05 in all tests)

gefitinib-resistant (GR) cell line derived from A549 cell line (human NSCLC cell line) via long-term drug exposure. GR cells have been demonstrated to be significantly more resistant to gefitinib treatment than Parental cells through dose-dependent treatment to gefitinib for 24h and 48h (Fig.2.7A). It has been reported that about 80% patients with acquired resistance against EGFR TKIs suffer from rapid disease progression and over half of the cases are severe manifestations including intrapulmonary metastasis, intraperitoneal progression and intracranial progression. Through colony formation assay and migration and invasion tests (Fig.2.7B and 2.7C), we have demonstrated that resistant cells exhibit enhanced capability of anchorage-independent growth, migration and invasion, which recapitulated previous clinical observations.

STAT3 hyperactivation and other mechanisms are implicated in GR cells. In order to fully characterize the genes and potential signaling pathways which give rise to acquired resistance, we performed microarray analysis on Parental cells, GR cells and GR cells treated with STAT3 inhibitor. Then we filtered out the DEGs in the whole expression data based on the following selection criteria: (1) Log2 value for fold change ≥ 1 and $P < 0.05$. (2) Log2 ratios= NA and the differences of intensity between the two samples >=1000. 243 identified DEGs were clustered and presented in the heatmap (Fig.2.8A).

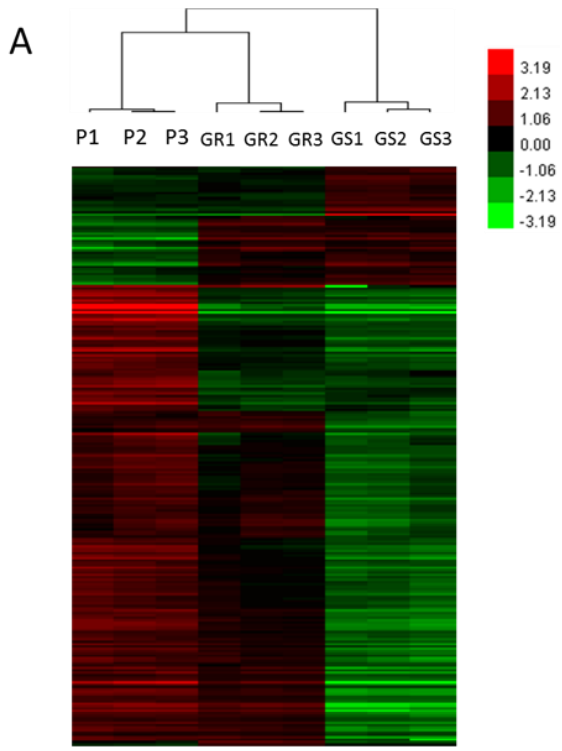

We next performed Gene Set Enrichment Analysis (GSEA) on GR cells versus parental cells to investigate the signaling pathways that

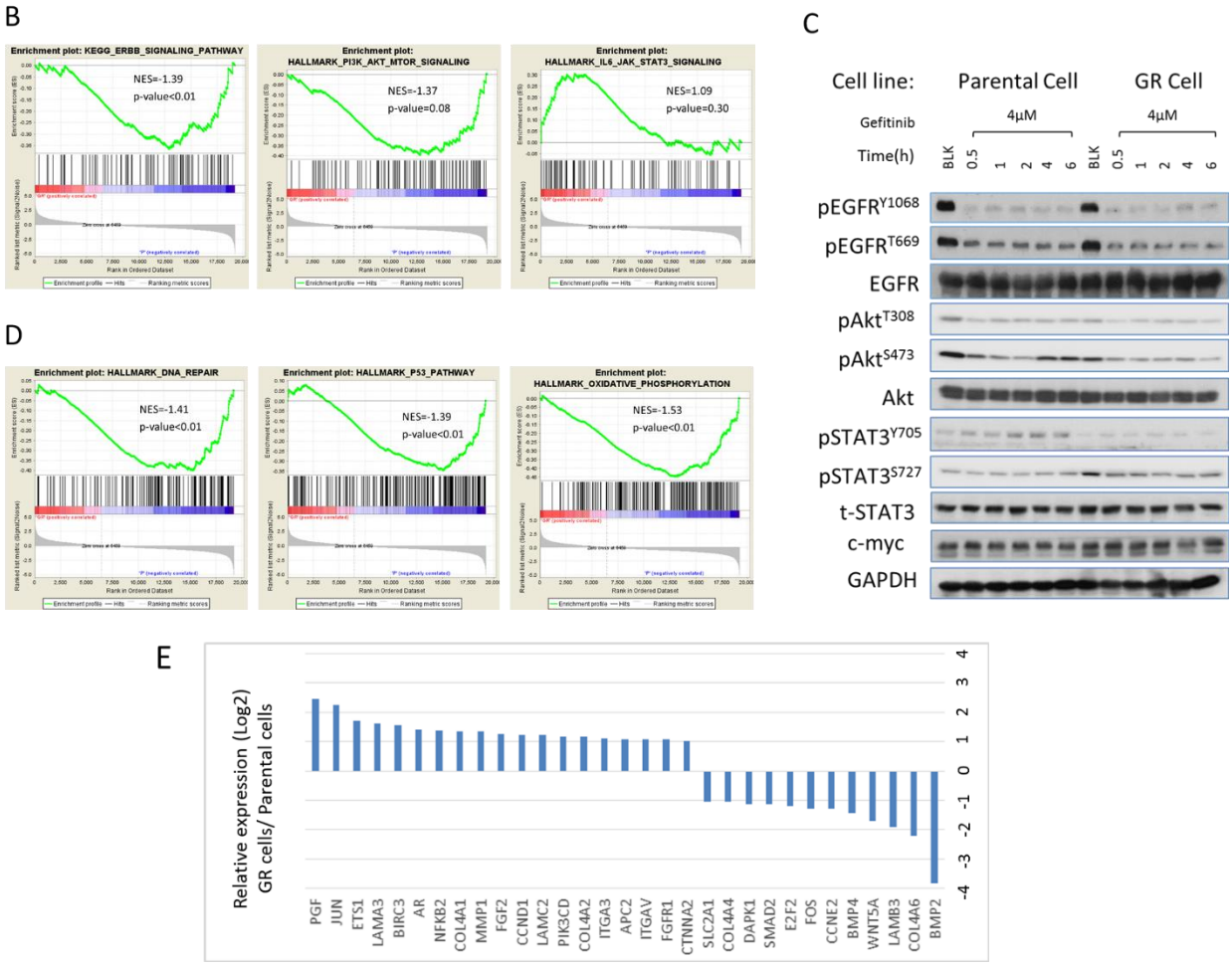

Figure 2.8 GR cells exhibited unique gene expression profiles and hyperactivated STAT3 signaling. (A) Top 243 differentially expressed genes (DEGs) was selected for clustering analysis. Up- and down-regulated genes are represented in red and green colors, respectively. An intensity filter was used to select genes where the difference between the maximum and minimum intensity values exceeds 35,000 among all microarrays. (P: parental cells, GR: GR cells, GS: GR cells treated with Sttatic) (B) GSEA was performed on GR cells vs. parental cells. Plots show the enrichment of transcripts involved in ERBB, PI3K-AKT and JAK-STAT3 signaling pathways. Normalized enrichment score (NES) and p-value are shown in the figure. (C) Immunoblotting analysis showing the differences in major signaling regulators between GR cells and parental cells. (D) Enrichment plots show significantly altered gene sets associated with fundamental cellular functions in GR cells. (E) Expression levels of major malignancy-related DEGs in GR cells and (F) their locations on KEGG cancer pathway map, upregulated and downregulated genes are indicated in red and green, respectively.

are altered in the GR cells. As shown in Figure 2.8B, the transcripts involved in ERBB (EGFR is also known as ERBB1) signaling pathway are significantly downregulated in GR cells after long-term exposure to gefitinib. Interestingly, further analysis on 2 pathways closely related to EGFR signaling pathway exhibit opposite enrichment trends. PI3K-AKT-MTOR pathway

shows a sharp descending curve while majority of genes in IL6-JAK-STAT3 pathway are positively enriched in GR cells. Considering that AKT and STAT3 are both important downstream regulators in EGFR signaling pathway and they frequently interact with each other, such discrepancy may offset the statistical power of GESA on both gene sets (p-values are both larger than 0.05). However, analysis of the leading-edge transcripts from both pathways strongly suggest that STAT3 pathway is hyperactivated while AKT and the whole EGFR pathways are both suppressed in GR cells. Subsequent molecular biology experiments have reinforced the concepts of the bioinformatics analysis (Fig.2.8C). It is noteworthy that the phosphorylation level of STAT3 is significantly enhanced on serine727 (S727) but suppressed on tyrosine705 (Y705) residue in GR cells. This shift of activation site may be explained by the observation that S727 phosphorylation can negatively regulate tyrosine phosphorylation of STAT3. Since previous studies have also demonstrated that S727 phosphorylation is required for maximizing the transcriptional activity of STAT3, the constitutive serine activation in GR cells may reflect a constant upregulation of STAT3 target genes, including C-MYC, which in turn facilitate cell survival and counteract gefitinib-induced responses. In agreement with this notion, we also observed increased level of C-MYC protein, a well-established gene target of STAT3, in GR cells (Fig.2.8C). GSEA also identified that DNA repair, P53 pathway and Oxidative Phosphorylation (OXPHOS) are significantly downregulated in GR cells which may account for other important mechanisms leading to acquired drug resistance (Fig.2.8D).

We next determined the DEGs in GR cells compared to Parental cells and applied signaling pathway impact analysis using KEGG database. The following 8 pathways were highlighted: (1) Complement and coagulation cascades, (2) Focal adhesion, (3) ECM-receptor interaction, (4) Cell adhesion molecules (CAMs), (5) Small cell lung cancer, (6) Leukocyte transendothelial migration, (7) Nitrogen metabolism and (8) Pathways in cancer.

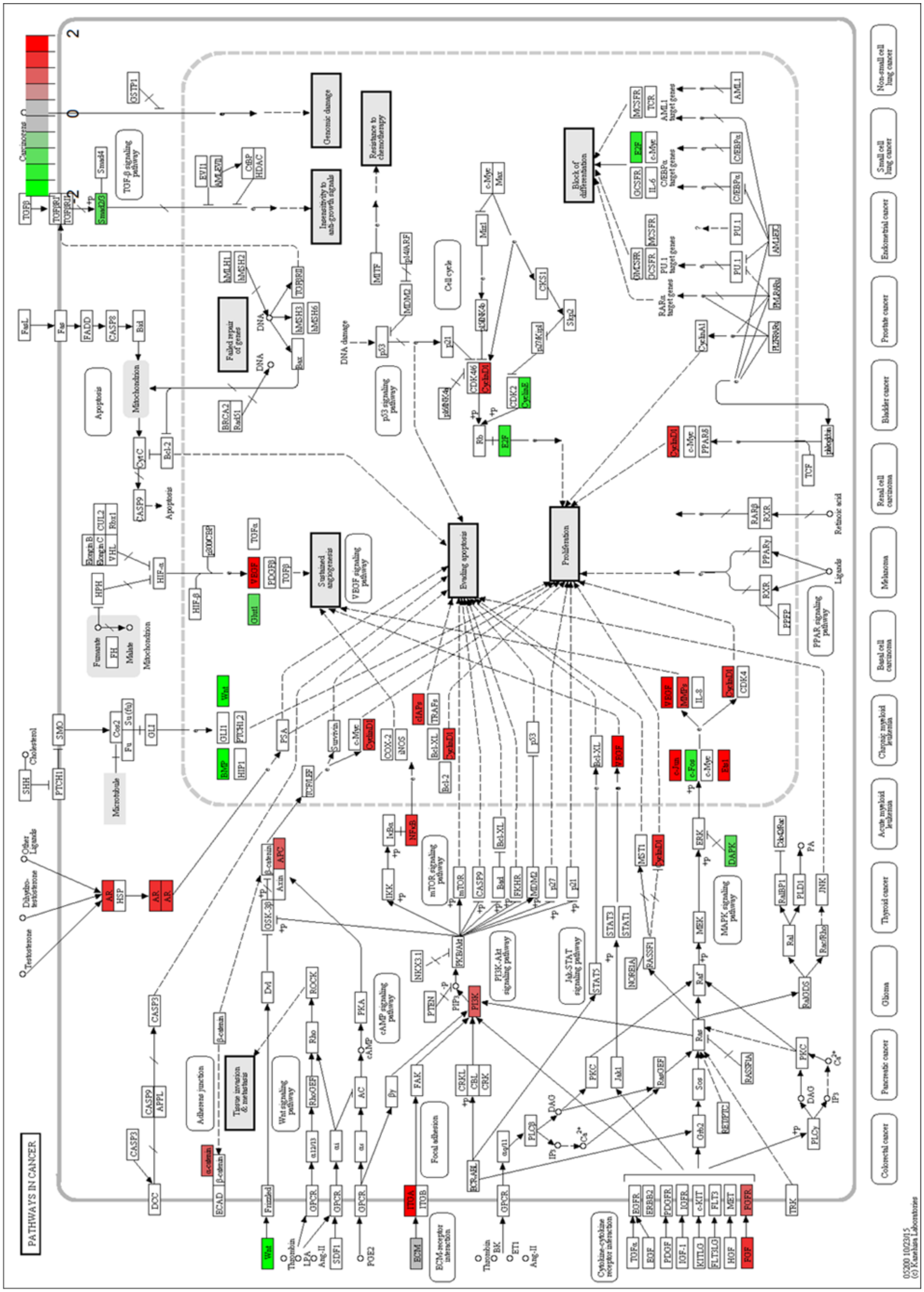

F

The “Pathways in cancer” is shown as representative. Expression levels of the transcripts involved are listed (Fig.2.8E) as well as their locations and functions in the pathway (Fig.2.8F).

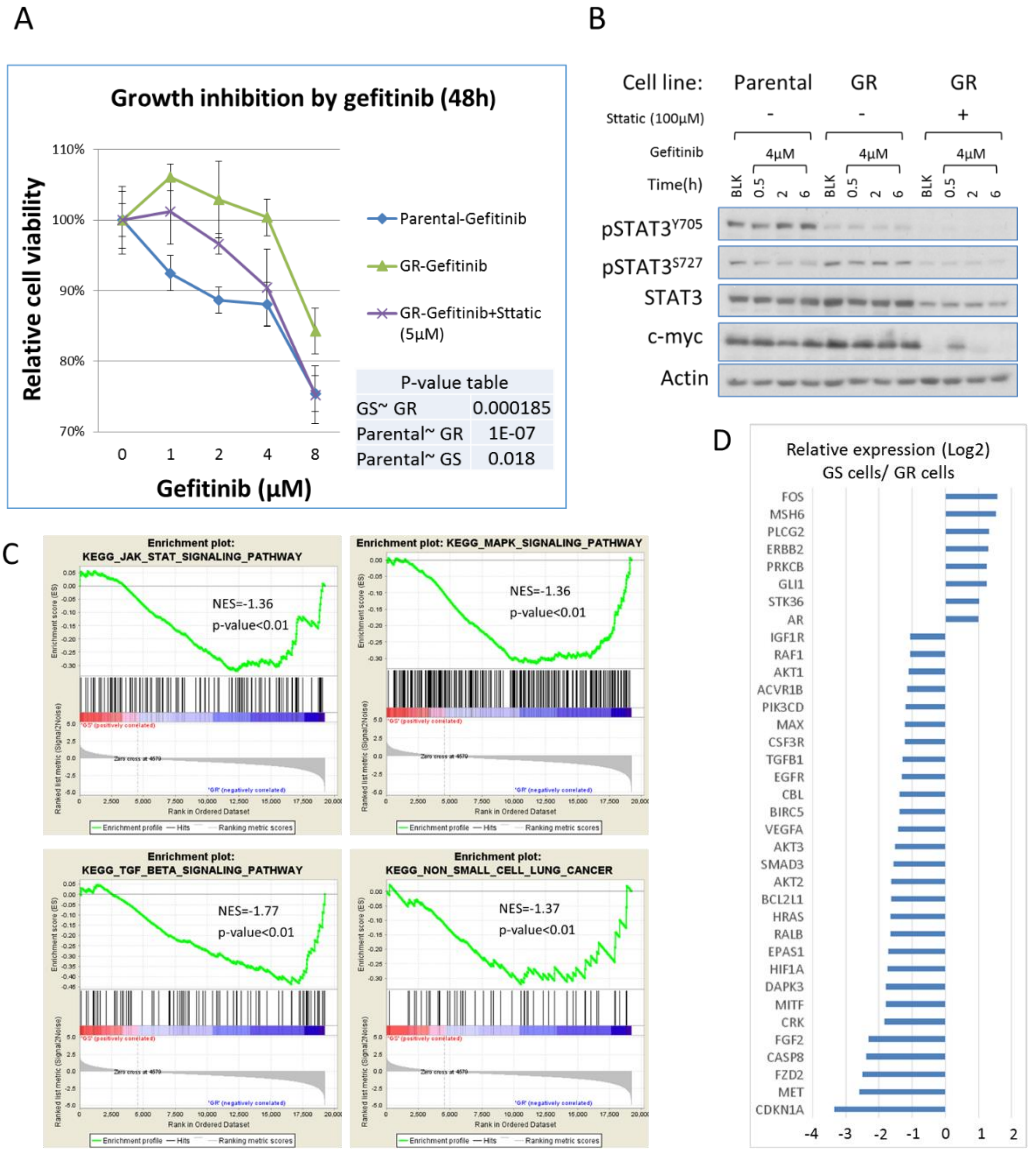

Figure 2.9 STAT3 inhibition overcomes gefitinib resistance by simultaneously suppressing multiple survival-related pathways. (A) Cell viability assay shows the percentage of viable cells of GR and parental cell lines after 48-hour exposure to gefitinib ranging from 2μM to 8μM in the absence or presence of 5μM Stattic. P-value table is shown in the figure. (B) Immunoblotting shows the impact of Stattic and gefitinib co-treatment on STAT3 signaling pathway in GR cells. (C) GSEA was performed on GR cells vs. GS cells. Plots show the enrichment of transcripts involved in JAK-STAT3, MAPK, TGF BETA and typical NSCLC signaling pathways. (D) Expression levels of major malignancy-related DEGs after Stattic treatment. (E) Visualization of the identified DEGs on KEGG cancer pathway map, upregulated and downregulated genes are highlighted in red and green, respectively.

STAT3 inhibition overcomes acquired resistance to gefitinib by downregulating major survival-related pathways. Since STAT3 hyperactivation has been implicated as an important resistance mechanism, we propose STAT3 co-inhibition as a rational method to overcome the acquired drug resistance in the current model. To test that hypothesis, we performed 48-hour cell viability test on Parental cells and GR cells exposed to dose-dependent treatment of gefitinib (2-8μM). Another group of GR cells were treated in combination with STAT3 inhibitor, Stattic (5μM). As shown in Figure 2.9A, combinational STAT3 inhibition significantly assisted the anti-cell growth effects of gefitinib in GR cells, especially at high gefitinib doses like 4μM and 8μM.

Then we moved on to investigate the underlying mechanisms. Our biomedical studies demonstrated that 100μM Stattic treatment is capable of instantly and effectively inhibiting serine phosphorylation of STAT3 and its transcription activity on its target gene, C-MYC, in GR cells (Fig.2.9B). Microarray analysis was performed on STAT3-inhibited GR (GS) cells in parallel with Parental cells and GR cells (Fig.2.8A). Then we conducted GSEA on GS over GR cells to characterize the enrichment of intracellular signaling pathways. As shown in the plots (Fig.2.9C), GSEA demonstrated that major gene sets associated with IL6-JAK-STAT3, MAPK and TGF-BETA pathways were all downregulated following Stattic treatment, which led to significant suppression of genes found in “Non-Small Cell Lung Cancer” pathway. We also carried out pathway impact analysis on the DEGs identified between GS and GR cells. In addition to the 4 pathways determined by GSEA, ErbB signaling pathway, mTOR signaling pathway and VEGF signaling pathway were also found to be affected by STAT3 inhibitor. Again, expressions of major DEGs were summarized (Fig.2.9D) and mapped to the KEGG’s “Pathway in cancers” (Fig.2.9E).

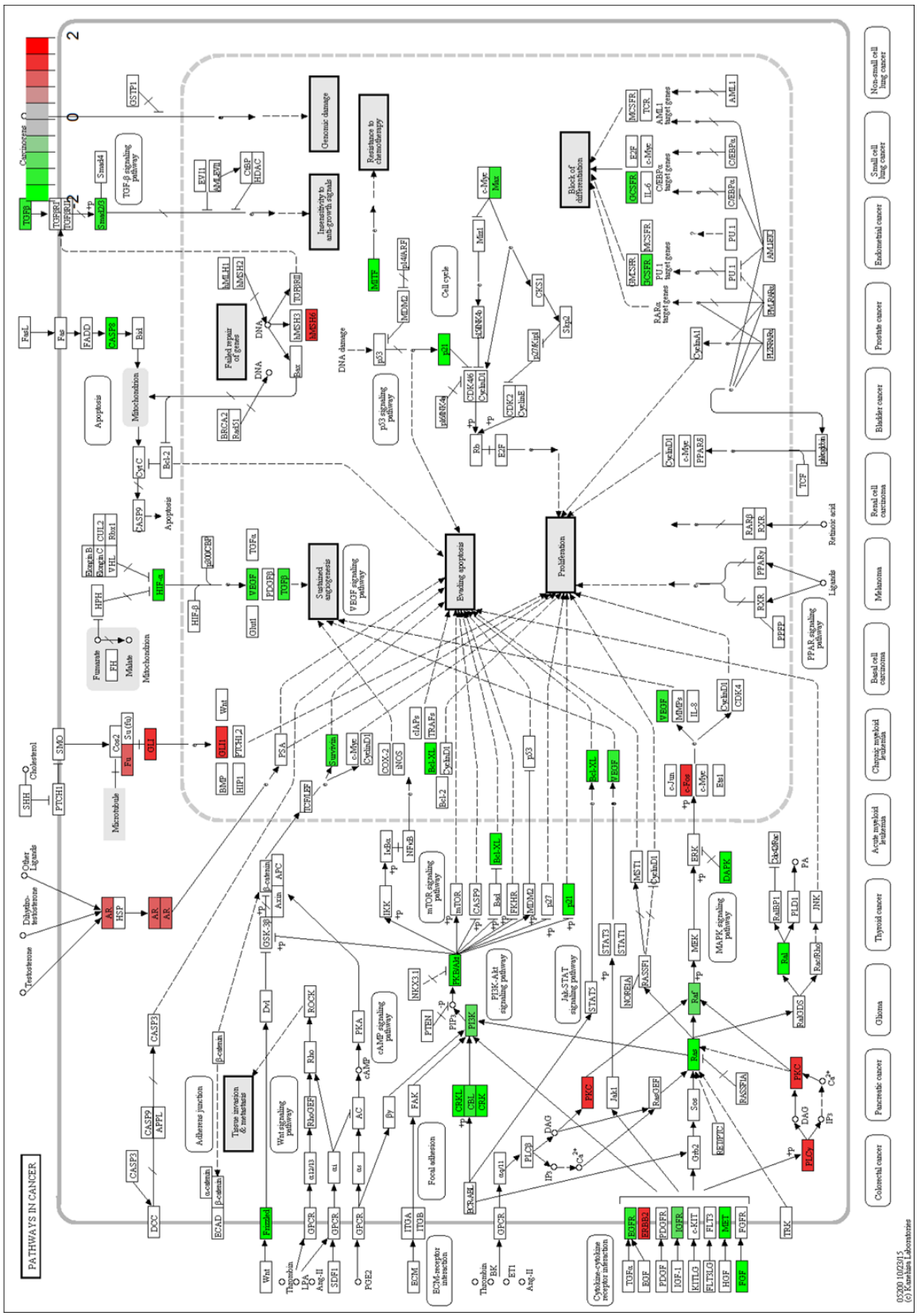

E

Discussion

Drug resistance, both primary and secondary, remains a major obstacle to successful cure of NSCLC via EGFR TKI-based therapies. Biased drug responses caused by primary resistance make it extremely hard to predict efficacy in patients and largely limit the patient population who can benefit from EGFR TKI. Even those patients initially sensitive to EGFR targeting therapy will develop secondary resistance (acquired resistance) and the subsequent relapse and progression of disease finally leads to treatment failure. The observations that several resistance mechanisms frequently overlap with each other lift this problem to a higher level of complexity which urgently requires co-inhibition of multiple targets to replace the current “one gene, one drug ” strategy. Despite some progresses, efforts aiming to selectively co-target some major resistance mechanisms show limited efficacy both in vitro and in vivo, strongly indicating the possibility of some unknown mechanisms which also contribute to resistance against EGFR TKI. In order to successfully carry out the combinational targeting strategy, revealing the hiding resistance mechanisms is undoubtedly the prerequisite, thus, explorations into such mechanisms are of great scientific and clinical significance.

It has long been believed that EGFR TKI, such as gefitinib, function through selectively binding the tyrosine kinase domain on EGFR and suppressing its major downstream pro-survival and anti-apoptosis signaling pathways, including STAT3, AKT and ERK. Our study, however, identifies a unique gefitinib-induced STAT3 activation pattern in non-sensitive NSCLC cell lines, A549 and NCI-H2023, which differs greatly from the classic tyrosine kinase-dependent pathway of STAT3 activation. In addition, based on previously defined STAT3-AKT axis in lung epithelial cells, we have further demonstrated that phosphorylation level of AKT substantially recovers rapidly from initial inhibition within 6 hours after gefitinib treatment and this process is dependent on the synchronous gefitinib-induced STAT3 activation. Considering the pivotal role of STAT3 and AKT in anti-apoptotic machinery, our study

answers, at least partly, why certain types of lung cancer cells do not respond well to gefitinib-induced cell death even if EGFR is overexpressed in these cells. Moreover, this notion has been further substantiated by the cell proliferation assay using combinational inhibition of EGFR and STAT3. Co-targeting of STAT3 can significantly enhance the anti-tumor efficacy of gefitinib, indicating a promising synergistic strategy to enhance efficacy of gefitinib in NSCLC.

Activation of STAT3 can be achieved from receptor tyrosine kinase (RTK) pathway, including EGFR-centered signaling, or cytokine signaling pathway (also known as RTK-independent pathway), like Interleukin-6/JAK/STAT3 pathway. In an effort to explore the mechanisms underlying gefitinib-induced STAT3 activation, we demonstrate that gefitinib not only promotes the direct binding of EGFR and STAT3 but also, surprisingly, affects the receptor tyrosine kinase-independent pathway of STAT3 activation. Multiple tyrosine residues on the C-tails of EGFR, including Y1068, Y1086 and Y1045, have been identified as docking sites where STAT3 uses its SH2 and DNA-binding domains to interact with EGFR and gets activated as a consequence in 293 cells. In agreement with these researches, our study shows that gefitinib treatment is able to directly promote the physical interaction between EGFR and STAT3 and thus regulate its activity in A549 cells. More interestingly, we have also revealed that gefitinib down regulates another important upstream regulator of STAT3, the SOCS family proteins. As shown in Figure 2.5A, gefitinib at 4μM is able to reduce the level of SOCS3, while higher concentration (8μM) is required to more effectively suppress both SOCS1 and SOCS3, suggesting that gefitinib also induces STAT3 activation by altering cytokine signaling. Considering SOCS proteins are also recruited by certain regulatory region of EGFR, extending from Y1114 to E1172, to block STAT3 activation, reduced SOCS proteins by gefitinib may also abrogate the intrinsic inhibitory effects of EGFR on STAT3. In NSCLC cells, differences in mutation status of EGFR, like “activating mutations” and “resistant

mutations", and extent of addiction to EGFR signaling are fundamental factors determining sensitivity to gefitinib. Established evidence has suggested an amplified expression of the wild-type EGFR are more frequent in prevalence yet associated with less sensitivity to gefitinib treatment. The results of this study have revealed novel mechanisms modulating cellular responses to gefitinib, especially in cells with overexpressed wild-type EGFR, which will provide valuable information to optimize future anti-tumor therapy in lung cancer patients.

On the other hand, this study also sheds light on the acquired resistance of gefitinib. Through systemically profiling the global gene expressions and molecular biology experiments, we have demonstrated there are multiple resistance mechanisms occurring in the GR cells simultaneously, which include both novel mechanisms and classic ones as previously reported. In our model, EGFR itself has not become more refractory to gefitinib treatment than the control cell line, moreover, GSEA further indicates that EGFR pathway is significantly suppressed in GR cells after long-term exposure to gefitinib. These results indicate that the mechanisms of acquired resistance in this model are totally different from the most classic and common one, T790M "gate keeper" mutation of EGFR. Accordingly, PI3K-AKT-mTOR pathway also tends to be suppressed in GR cells compared to Parental cells ($p=0.08$).

Interestingly, we noticed that STAT3 is hyperactivated in our model. Similarly, in a previous study, increased phosphorylation of STAT3 on tyrosine 705 (Y705) residue is observed in another gefitinib-resistant lung cancer cell line also derived from A549 cells. Enhanced STAT3 phosphorylation has also been observed in EGFR mAb treatment-resistant cell models of head and neck squamous carcinoma (HNSCC) and bladder cancer. Our model, however, exhibits a unique hyperactivation pattern of STAT3, phosphorylation level is significantly increased on serine727 (S727) but inhibited on Y705 residue in GR cells. Considering that S727 activation is required for maximized transcription activity of STAT3,

this unique shift of phosphorylation sites might cause constant upregulation of STAT3 target genes, for example, C-MYC. Similarly, many major genes associated with STAT3 pathway also tend to be enriched in GR cells, even though EGFR and AKT pathways are both suppressed. We also noticed that gene sets related to DNA repair function, P53 pathway and Oxidative Phosphorylation (OXPHOS) capacity are all significantly downregulated in GR cells. These results suggest that GR cells might be predisposed to accumulating DNA damages and mutations, escape of apoptosis, malignant energy metabolism, which are all hallmarks of cancer pathogenesis and development. Additionally, we have demonstrated that FGF2 and FGFR1 are both significantly upregulated in GR cells, which repeated a previously reported resistance mechanism, FGF2-FGFR1 autocrine bypass loop, in several other gefitinib-resistant NSCLC cell lines.

Rational co-inhibition of STAT3 assisted gefitinib's inhibitory effects on GR cells, especially at relatively high concentrations of gefitinib, like 4μM and 8μM. Our data further demonstrated that effective STAT3 inhibition suppresses several pathways closely related to cell growth and proliferation simultaneously, including MAPK, TGF-beta, EGFR and AKT-mTOR pathways. When interrogating the expression profiles in details, we found that STAT3 inhibition caused significant downregulation of PIK3CD, AKT1, AKT2 and AKT3. This result not only confirms the STAT3-AKT activation loop defined in earlier steps of this study, but also provides answers for the dramatic efficacy of targeting of STAT3 or subsequent AKT/mTOR in overcoming acquired resistance in both *in vitro* and *in vivo* lung cancer models receiving EGFR TKI-based therapy. In addition, Stattic treatment also caused reduced transcription of FGF2 and MET, both of which are key regulators modulating previously-defined alternative pathways in EGFR TKI-resistant lung cancers. Admittedly, it has been demonstrated that the evolutionary paths leading lung cancer cells to resistance are highly variable and heterogeneous, but our data suggest that combinational targeting of STAT3 and

EGFR can be a promising strategy to conquer acquired resistance, at least in certain refractory lung cancers. In the future, more efforts are required to fully elucidate and document the resistance mechanisms, which will make the fundamental step for development of successful combinational therapy with higher selectivity and efficacy against advanced NSCLC.

Appendix A Table S1.1 Full list of significant MDIG pull-downs in H929 cells

Table S1.1 Full list of significant mdig pull-downs in H929 cells

Gene name	ID	Sequence coverage [%]	Mol. weight [kDa]	Sequence length	Enrichment ratio*	# of times in IP	Protein name
MINA	Q8IUF8	41.3	52.8	465	10000.0	3	Bifunctional lysine-specific demethylase and histidyl-hydroxylase MINA
ACTB	P60709	67.5	41.736	375	10000.0	3	Actin, cytoplasmic 1
ACTN4	O43707	64.8	104.85	911	324.0	3	Alpha-actinin-4
SPTBN1	Q01082	63	274.61	2364	53.0	3	Spectrin beta chain, non-erythrocytic 1
PLEC	Q15149-4	49.6	516.19	4547	38.5	3	Isoform 4 of Plectin
AKAP2	Q9Y2D5-6	35.7	120.63	1090	19.0	3	Isoform 4 of A-kinase anchor protein 2
PPP1R18	Q6NYC8	40.6	67.942	613	26.9	3	Phostensin
Q9Y4I1-3	Q9Y4I1-3	50.4	218.61	1880	10000.0	3	Isoform 3 of Unconventional myosin-Va
MYLK	Q15746	34.7	210.71	1914	15.2	3	Myosin light chain kinase, smooth muscle
PPP1R9B	Q96SB3	42.8	89.191	815	355.1	3	Neurabin-2
MYO18A	J3KNX9	46.3	233.14	2054	10.1	3	Unconventional myosin-XVIIIa
HCLS1	P14317	43.2	54.013	486	20.5	3	Hematopoietic lineage cell-specific protein
HADHA	P40939	42.5	82.999	763	157.0	3	Trifunctional enzyme subunit alpha, mitochondrial
FLNA	P21333	37.6	280.74	2647	70.7	3	Filamin-A
XRCC5	P13010	37.4	82.704	732	65.2	3	X-ray repair cross-complementing protein 5
XRCC6	P12956	51.1	69.842	609	997.8	3	X-ray repair cross-complementing protein 6
GNAI2	P04899	40.8	40.45	355	132.5	3	Guanine nucleotide-binding protein G(i) subunit alpha-2
SPECC1L	Q69YQ0	43.9	124.6	1117	833.4	3	Cytospin-A
SVIL	O95425-4	31.9	244.52	2182	33.1	3	Isoform SV4 of Supervillin
H0Y2S9	H0Y2S9	44.7	203.37	1794	10000.0	3	Myosin phosphatase Rho-interacting protein (Fragment)
HNRNPUL1	Q9BUJ2	24.4	95.737	856	21.4	3	Heterogeneous nuclear ribonucleoprotein U-like protein 1
SPECC1	Q5M775	40.2	118.58	1068	10.1	3	Cytospin-B
CAPZA1	P52907	62.6	32.922	286	25.8	3	F-actin-capping protein subunit alpha-1
HIST2H2AA3	Q6FI13	57.7	14.095	130	10000.0	3	Histone H2A type 2-A
SIPA1	Q96FS4	32.1	112.15	1042	11.8	3	Signal-induced proliferation-associated protein 1

EFR3A	H9KV44	31.4	92.94	821	14.6	3	Protein EFR3 homolog A
Q8WWI1-3	Q8WWI1-3	37.4	153.67	1349	10000.0	3	Isoform 3 of LIM domain only protein 7
CTTN	Q14247	38	61.585	550	79.7	3	Src substrate cortactin
IQGAP1	P46940	29.8	189.25	1657	10000.0	3	Ras GTPase-activating-like protein IQGAP1
ARHGEF11	O15085-2	32	172.24	1562	10000.0	3	Isoform 2 of Rho guanine nucleotide exchange factor 11
MX2	P20592	30.9	82.088	715	10000.0	3	Interferon-induced GTP-binding protein Mx2
Q6WCQ1-2	Q6WCQ1-2	59.2	118.1	1038	10000.0	3	Isoform 2 of Myosin phosphatase Rho-interacting protein
DBN1	Q16643-3	27.1	76.299	695	15.2	3	Isoform 3 of Drebrin
DAAM1	Q9Y4D1	22.7	123.47	1078	10000.0	3	Disheveled-associated activator of morphogenesis 1
PPP1R9A	Q9ULJ8-3	16.9	154.05	1374	10000.0	3	Isoform 3 of Neurabin-1
KIF21B	O75037-4	22.6	181.14	1623	10000.0	3	Isoform 4 of Kinesin-like protein KIF21B
EFHD2	Q96C19	55.4	26.697	240	210.4	3	EF-hand domain-containing protein D2
SFPQ	P23246	52.2	76.149	707	13.8	3	Splicing factor, proline- and glutamine-rich
EPB41L3	Q9Y2J2-2	33.5	96.513	865	10000.0	3	Isoform 2 of Band 4.1-like protein 3
TPRN	Q4KMQ1	35.6	75.555	711	31.8	3	Taperin
GNB1	P62873	19.7	37.377	340	10000.0	3	Guanine nucleotide-binding protein G(I)/G(S)/G(T) subunit beta-1
PABPC4	Q13310-3	38.2	72.39	660	10.7	3	Isoform 3 of Polyadenylate-binding protein 4
PRMT5	O14744	13	72.683	637	10000.0	3	Protein arginine N-methyltransferase 5
TMPO	P42166	38	75.491	694	10.9	3	Lamina-associated polypeptide 2, isoform alpha
ACTN1	P12814-3	37.3	105.57	914	10000.0	3	Isoform 3 of Alpha-actinin-1
CD44	P16070	7.4	81.537	742	83.0	3	CD44 antigen
ACTR2	P61160	29.9	44.76	394	229.3	3	Actin-related protein 2
PPP1CA	P62136	29.7	37.512	330	355.3	3	Serine/threonine-protein phosphatase PP1-alpha catalytic subunit
TMOD3	Q9NYL9	44.6	39.594	352	14.2	3	Tropomodulin-3
Q01082-3	Q01082-3	65.2	251.39	2155	10000.0	3	Isoform 2 of Spectrin beta chain, non-erythrocytic 1
CAPZB	B1AK88	33.6	33.781	301	14.3	3	Capping protein (Actin filament) muscle Z-line, beta, isoform CRA_d
RAI14	Q9P0K7-2	26.9	110.42	983	176.6	3	Isoform 2 of Ankycorbin
P06753-2	P06753-2	71	29.032	248	10000.0	3	Isoform 2 of Tropomyosin alpha-3 chain

PTPRG	P23470	12.9	162	1445	10000.0	3	Receptor-type tyrosine-protein phosphatase gamma
ATAD3A	Q9NVI7-2	31.1	66.217	586	10000.0	3	Isoform 2 of ATPase family AAA domain-containing protein 3A
ZDHHC5	Q9C0B5	25.2	77.544	715	10000.0	3	Palmitoyltransferase ZDHHC5
PI4KA	J3KN10	16	236.83	2102	211.9	3	Phosphatidylinositol 4-kinase alpha
CORO1C	Q9ULV4-3	23.5	58.947	527	54.2	3	Isoform 3 of Coronin-1C
DDX1	Q92499	29.3	82.431	740	17.0	3	ATP-dependent RNA helicase DDX1
TUBA1C	F5H5D3	26.8	57.73	519	10000.0	3	Tubulin alpha-1C chain
G3V1L9	G3V1L9	34	197.46	1768	10000.0	3	Tight junction protein 1 (Zona occludens 1), isoform CRA_a
GPC4	O75487	24.6	62.411	556	479.7	3	Glypican-4
FMNL1	O95466-3	14.4	128.33	1158	10000.0	3	Isoform 3 of Formin-like protein 1
EPB41	P11171	15.3	97.016	864	10000.0	3	Protein 4.1
MACF1	H3BQK9	4.5	861.07	7592	282.5	3	Microtubule-actin cross-linking factor 1, isoforms 1/2/3/5
LRCH4	O75427	21.7	73.449	683	11.5	3	Leucine-rich repeat and calponin homology domain-containing protein 4
CNOT1	A5YKK6	14.6	266.94	2376	10000.0	3	CCR4-NOT transcription complex subunit 1
FUS	H3BPE7	10.8	53.496	527	31.3	3	RNA-binding protein FUS
RPL26	P61254	35.2	17.258	145	16.9	3	60S ribosomal protein L26
NT5E	P21589	16.6	63.367	574	10000.0	3	5-nucleotidase
TNKS1BP1	Q9C0C2	17.7	181.79	1729	10000.0	3	182 kDa tankyrase-1-binding protein
GNAI3	P08754	34.2	40.532	354	112.9	3	Guanine nucleotide-binding protein G(k) subunit alpha
SEC31A	D6REX3	16.9	136.22	1251	10000.0	3	Protein transport protein Sec31A
NSF	P46459	14.2	82.593	744	10000.0	3	Vesicle-fusing ATPase
USO1	O60763-2	4.3	109.19	973	203.0	3	Isoform 2 of General vesicular transport factor p115
FARP1	C9JME2	8.6	122.09	1076	10000.0	3	FERM, RhoGEF and pleckstrin domain-containing protein 1
ARHGEF12	Q9NZN5	16.6	173.23	1544	10000.0	3	Rho guanine nucleotide exchange factor 12
ARPC2	O15144	57.3	34.333	300	138.5	3	Actin-related protein 2/3 complex subunit 2
RFTN1	Q14699	21.1	63.145	578	17.0	3	Raftlin
ARPC1B	O15143	14.2	40.949	372	118.7	3	Actin-related protein 2/3 complex subunit 1B
HADHB	P55084	34.8	51.294	474	10000.0	3	Trifunctional enzyme subunit beta, mitochondrial

PRKDC	P78527	6.3	469.08	4128	77.5	3	DNA-dependent protein kinase catalytic subunit
RACGAP1	Q9H0H5	10.6	71.026	632	10.6	3	Rac GTPase-activating protein 1
Q8WWM7	Q8WWM7	31.4	113.37	1075	10000.0	3	Ataxin-2-like protein
PPP1R12C	Q9BZL4	23.8	84.88	782	10000.0	3	Protein phosphatase 1 regulatory subunit 12C
GNAS	Q5JWF2	11.3	111.02	1037	10000.0	3	Guanine nucleotide-binding protein G(s) subunit alpha isoforms XLas
ARHGEF1	M0QZR4	12.5	108.32	968	10000.0	3	Rho guanine nucleotide exchange factor 1
MSN	P26038	15.3	67.819	577	10000.0	3	Moesin
CCDC88C	Q9P219	12.1	228.23	2028	10000.0	3	Protein Daple
HSP90B1	P14625	12	92.468	803	10000.0	3	Endoplasmin
TXNDC5	Q8NBS9	8.8	47.628	432	10000.0	3	Thioredoxin domain-containing protein 5
KHSRP	Q92945	17.4	73.114	711	55.4	3	Far upstream element-binding protein 2
STXBP2	E7EQD5	14.4	67.694	604	32.3	3	Syntaxin-binding protein 2
ALDH16A1	Q8IZ83	6.4	85.126	802	10000.0	3	Aldehyde dehydrogenase family 16 member A1
HSPA1A	P08107	13.6	70.051	641	10000.0	3	Heat shock 70 kDa protein 1A/1B
TTC7A	Q2T9J9	7.8	98.938	882	10000.0	3	TTC7A protein
CNOT3	O75175	10.6	81.871	753	10000.0	3	CCR4-NOT transcription complex subunit 3
DDX10	Q13206	11.3	100.89	875	10000.0	3	Probable ATP-dependent RNA helicase DDX10
LIME1	Q9H400	39	31.288	295	18.1	3	Lck-interacting transmembrane adapter 1
SCRIB	Q14160-3	11.2	177.69	1655	10000.0	3	Isoform 3 of Protein scribble homolog
SNX18	Q96RF0-2	9	69.006	624	10000.0	3	Isoform 2 of Sorting nexin-18
SEMA7A	O75326	9.8	74.823	666	10000.0	3	Semaphorin-7A
AP2B1	P63010-2	11.8	105.69	951	10000.0	3	Isoform 2 of AP-2 complex subunit beta
FAM120A	Q9NZB2-6	14	125.27	1146	21.3	3	Isoform F of Constitutive coactivator of PPAR-gamma-like protein 1
SRSF4	Q08170	14.8	56.678	494	10000.0	3	Serine/arginine-rich splicing factor 4
SHKBP1	Q8TBC3	8.8	76.343	707	114.4	3	SH3KBP1-binding protein 1
CNOT10	Q9H9A5	9.8	82.309	744	10000.0	3	CCR4-NOT transcription complex subunit 10
G3BP1	Q13283	30.7	52.164	466	10.5	3	Ras GTPase-activating protein-binding protein 1
USP10	Q14694-2	16.9	92.596	846	10000.0	3	Isoform 2 of Ubiquitin carboxyl-terminal hydrolase 10
FBXW11	Q9UKB1-3	25.1	60.897	529	10000.0	3	Isoform B of F-box/WD repeat-containing protein 11
MFI2	P08582	7.9	80.214	738	10000.0	3	Melanotransferrin

SKT	Q5T5P2	9.6	214.11	1943	10000.0	3	Sickle tail protein homolog
GSN	P06396	11.3	85.696	782	14.4	3	Gelsolin
KIAA0528	F5H2A1	6.5	116.3	1053	10000.0	3	C2 domain-containing protein 5
IGF2BP3	O00425	18.5	63.704	579	10000.0	3	Insulin-like growth factor 2 mRNA-binding protein 3
SIPA1L1	O43166	11.6	200.03	1804	10000.0	3	Signal-induced proliferation-associated 1-like protein 1
AMOTL1	Q8IY63	15.8	106.57	956	15.9	3	Angiomotin-like protein 1
GARS	P41250	9.7	83.165	739	10000.0	3	Glycine--tRNA ligase
IMMT	Q16891	14.8	83.677	758	11.0	3	Mitochondrial inner membrane protein
RECK	O95980	3.3	106.46	971	10000.0	3	Reversion-inducing cysteine-rich protein with Kazal motifs
NCKIPSD	Q9NZQ3	10.8	78.959	722	10000.0	3	NCK-interacting protein with SH3 domain
RIOK1	Q9BRS2	12.3	65.582	568	10000.0	3	Serine/threonine-protein kinase RIO1
PRKD2	M0QZW1	9.2	97.77	888	16.9	3	Serine/threonine-protein kinase D
A8MXP9	A8MXP9	15.2	99.966	895	10000.0	3	Matrin-3
SUN2	Q9UH99	9.8	80.31	717	10000.0	3	SUN domain-containing protein 2
FKBP15	Q5T1M5	12.6	133.63	1219	25.5	3	FK506-binding protein 15
HIST1H1C	P16403	27.2	21.364	213	10000.0	3	Histone H1.2
SF1	Q15637	15	68.329	639	10000.0	3	Splicing factor 1
PPFIBP2	Q8ND30	9	98.543	876	10000.0	3	Liprin-beta-2
MYO5B	Q9ULV0	13	213.67	1848	10000.0	3	Unconventional myosin-Vb
SHCBP1	Q8NEM2	7	75.69	672	10000.0	3	SHC SH2 domain-binding protein 1
RPN1	P04843	8.7	68.569	607	10000.0	3	Dolichyl-diphosphooligosaccharide--protein glycosyltransferase subunit 1
RPA1	P27694	4.7	68.137	616	10000.0	3	Replication protein A 70 kDa DNA-binding subunit
LMTK2	Q8IWU2	8.7	164.9	1503	18.0	3	Serine/threonine-protein kinase LMTK2
LRRC47	Q8N1G4	11	63.472	583	10.9	3	Leucine-rich repeat-containing protein 47
NUMA1	Q14980	6.9	238.26	2115	15.7	3	Nuclear mitotic apparatus protein 1
MYO1E	Q12965	7.3	127.06	1108	10000.0	3	Unconventional myosin-Ie
PFKP	Q01813	8	85.595	784	10000.0	3	6-phosphofructokinase type C
MTHFD1	F5H2F4	3.5	110.61	1020	22.6	3	C-1-tetrahydrofolate synthase, cytoplasmic
ITCH	Q96J02	5.2	102.8	903	10000.0	3	E3 ubiquitin-protein ligase Itchy homolog
Q9H4G0-2	Q9H4G0-2	7.3	87.644	779	10000.0	3	Isoform 2 of Band 4.1-like protein 1

DLST	P36957	9.9	48.755	453	10000.0	3	Dihydrolipoamide S-Succinyltransferase (E2 Component Of 2-Oxo-Glutarate Complex)
RIF1	Q5UIP0	7.4	274.46	2472	10000.0	3	Telomere-associated protein RIF1
SRGAP2	O75044	8.8	120.88	1071	83.5	3	SLIT-ROBO Rho GTPase-activating protein 2
MAGEA4	P43358	16.4	34.899	317	10000.0	3	Melanoma-associated antigen 4
EPB41L2	O43491	13.4	112.59	1005	10000.0	3	Band 4.1-like protein 2
SIPA1L3	O60292	8.4	194.61	1781	10000.0	3	Signal-induced proliferation-associated 1-like protein 3
CEP170	Q5SW79	13	175.29	1584	18.2	3	Centrosomal protein of 170 kDa
SDC1	P18827	16.1	32.461	310	10000.0	3	Syndecan-1
HSPA4	P34932	8.2	94.33	840	10000.0	3	Heat shock 70 kDa protein 4
CPSF6	Q16630-2	10.4	63.47	588	13.5	3	Isoform 2 of Cleavage and polyadenylation specificity factor subunit 6
VPS35	Q96QK1	7.2	91.706	796	10000.0	3	Vacuolar protein sorting-associated protein 35
CDKN2AIP	Q9NXV6	17.9	61.124	580	12.0	3	CDKN2A-interacting protein
DLG1	Q12959-2	7.6	103.32	926	10000.0	3	Isoform 2 of Disks large homolog 1
AKNA	Q7Z591	6.7	155.14	1439	10000.0	3	AT-hook-containing transcription factor
EPRS	P07814	10	170.59	1512	11.3	3	Bifunctional glutamate/proline--tRNA ligase
ALDH1L2	Q3SY69	5.9	101.74	923	10000.0	3	Mitochondrial 10-formyltetrahydrofolate dehydrogenase
CUL3	Q13618	7.2	88.929	768	35.3	3	Cullin-3
SPTBN2	O15020	9.4	271.32	2390	10000.0	3	Spectrin beta chain, non-erythrocytic 2
AHNAK	Q09666	5.2	629.09	5890	10000.0	3	Neuroblast differentiation-associated protein AHNAK
PKM2	P14618	19	57.936	531	10000.0	3	Pyruvate kinase PKM
DIDO1	Q9BTC0	12.3	243.87	2240	10000.0	3	Death-inducer obliterator 1
THEMIS2	Q5TEJ8	3.6	72.048	643	10000.0	3	Protein THEMIS2
Q5JVM0	Q5JVM0	48.9	20.601	174	10000.0	3	Unconventional myosin-VI (Fragment)
SEC16A	J3KNL6	7.4	251.89	2357	10000.0	3	Protein transport protein Sec16A
KHDRBS1	Q07666	7.2	48.227	443	21.1	3	KH domain-containing, RNA-binding, signal transduction-associated protein 1
CCDC102A	Q96A19	10.4	62.595	550	10000.0	3	Coiled-coil domain-containing protein 102A
KPNB1	Q14974	6.6	97.169	876	10000.0	3	Importin subunit beta-1
SLTM	Q9NWH9	6.7	117.15	1034	16.3	3	SAFB-like transcription modulator
SLC3A2	P08195-4	5.1	71.122	661	10000.0	3	Isoform 4 of 4F2 cell-surface antigen heavy chain

MTA2	O94776	7.3	75.022	668	10000.0	3	Metastasis-associated protein MTA2
EPS15L1	Q9UBC2-2	6	99.605	910	10000.0	3	Isoform 2 of Epidermal growth factor receptor substrate 15-like 1
ERBB2IP	Q96RT1-8	5.3	159.02	1419	10000.0	3	Isoform 8 of Protein LAP2
LARP4B	Q92615	5.6	80.551	738	10000.0	3	La-related protein 4B
SEC23B	Q15437	2.9	86.478	767	28.3	3	Protein transport protein Sec23B
ZNF217	O75362	5.9	115.27	1048	52.2	3	Zinc finger protein 217
VCP	P55072	7.2	89.321	806	10000.0	3	Transitional endoplasmic reticulum ATPase
SSH1	Q8WYL5	9.7	115.51	1049	10000.0	3	Protein phosphatase Slingshot homolog 1
C2CD2L	O14523-2	5	76.178	707	10000.0	3	Isoform 2 of C2 domain-containing protein 2-like
EIF3CL	B5ME19	10.8	105.47	914	10000.0	3	Eukaryotic translation initiation factor 3 subunit C-like protein
EIF4G1	Q04637-9	7.7	176.23	1606	10000.0	3	Isoform 9 of Eukaryotic translation initiation factor 4 gamma 1
MYO1B	O43795	4	131.98	1136	10000.0	3	Unconventional myosin-Ib
SRRT	Q9BXP5	2.4	100.67	876	12.7	3	Serrate RNA effector molecule homolog
FAM129A	Q9BZQ8	4.1	103.13	928	10000.0	3	Protein Niban
EDC4	Q6P2E9	11.8	151.66	1401	10000.0	3	Enhancer of mRNA-decapping protein 4
YTHDF2	Q9Y5A9	10.5	62.333	579	10000.0	3	YTH domain-containing family protein 2
NOS1AP	O75052	9.9	56.149	506	10000.0	3	Carboxyl-terminal PDZ ligand of neuronal nitric oxide synthase protein
RAD50	Q92878-2	4.7	154.59	1318	13.5	3	Isoform 2 of DNA repair protein RAD50
FARP2	O94887	5.8	119.89	1054	10000.0	3	FERM, RhoGEF and pleckstrin domain-containing protein 2
SRPR	P08240	8.8	69.81	638	45.1	3	Signal recognition particle receptor subunit alpha
PDIA4	P13667	7.1	72.932	645	10000.0	3	Protein disulfide-isomerase A4
GPC1	H7C410	7	66.4	598	10000.0	3	Glypican-1 (Fragment)
MAP4	E7EVA0	3.5	245.44	2297	10000.0	3	Microtubule-associated protein
NCBP1	Q09161	5.7	91.838	790	10000.0	3	Nuclear cap-binding protein subunit 1
PRRC2A	P48634	8.1	228.86	2157	10000.0	3	Protein PRRC2A
EXOC4	Q96A65	5.6	110.5	974	10000.0	3	Exocyst complex component 4
ATP2A2	P16615	3.9	114.76	1042	10000.0	3	Sarcoplasmic/endoplasmic reticulum calcium ATPase 2
EZR	P15311	11.6	69.412	586	10000.0	3	Ezrin
SSH2	F5H527	6.9	161.15	1450	10000.0	3	Protein phosphatase Slingshot homolog 2

JAK1	P23458	3.6	133.28	1154	10000.0	3	Tyrosine-protein kinase JAK1
OAS2	P29728	3.2	82.43	719	10000.0	3	2-5-oligoadenylate synthase 2
ITGB7	P26010	3.8	86.902	798	10000.0	3	Integrin beta-7
SYNM	O15061	7	172.77	1565	10000.0	3	Synemin
KANK1	Q14678	3	147.29	1352	10000.0	3	KN motif and ankyrin repeat domain-containing protein 1
RANBP2	P49792	4.3	358.2	3224	10000.0	3	E3 SUMO-protein ligase RanBP2
HCFC1	A6NEM2	2.5	213.47	2080	10000.0	3	HCF N-terminal chain 5
DSG2	Q14126	8.1	122.29	1118	10000.0	3	Desmoglein-2
GSPT2	P15170-3	4.7	68.699	637	10000.0	3	G1 To S Phase Transition Protein 2
ITPKB	P27987	3.5	102.38	946	10000.0	3	Inositol-trisphosphate 3-kinase B
IARS	P41252	5.5	144.5	1262	10000.0	3	Isoleucine--tRNA ligase, cytoplasmic
MAP1B	P46821	5	270.63	2468	10000.0	3	Microtubule-associated protein 1B
KIF13B	Q9NQT8	3.9	202.79	1826	10000.0	3	Kinesin-like protein KIF13B
JMY	Q8N9B5	5	111.44	988	10000.0	3	Junction-mediating and -regulatory protein
CACNA2D1	P54289	4.4	124.57	1103	10000.0	3	Voltage-dependent calcium channel subunit alpha-2/delta-1
KLC1	E7EVH7	7.5	83.694	732	10000.0	3	Kinesin light chain 1
CAD	P27708	1.8	242.98	2225	10000.0	3	CAD protein
P14923	P14923	11.1	81.744	745	10000.0	3	Junction plakoglobin
ZNF295	Q9ULJ3	3.6	118.87	1066	10000.0	3	Zinc finger and BTB domain-containing protein 21
TAF15	Q92804	16.7	61.829	592	10000.0	3	TATA-binding protein-associated factor 2N
PRRC2B	Q5JSZ5	3.2	242.96	2229	10000.0	3	Protein PRRC2B
WRN	Q14191	3.1	162.46	1432	10000.0	3	Werner syndrome ATP-dependent helicase
KIAA1671	Q9BY89	2.3	196.71	1806	10000.0	3	Uncharacterized protein KIAA1671
KIAA1211	Q6ZU35	4.9	136.76	1233	10000.0	3	Uncharacterized protein KIAA1211
ASCC3	Q8N3C0	2.7	251.46	2202	10000.0	3	Activating signal cointegrator 1 complex subunit 3
ITPR3	Q14573	1.5	304.1	2671	10000.0	3	Inositol 1,4,5-trisphosphate receptor type 3

*: 10000.0 indicates that the sample were identified 3

Appendix B Table S1.2 Full list of significant C-MYC pull-downs in H929 cells

Table S1.2 Full list of significant c-myc pull-downs in H929 cells

Gene name	ID	Sequence coverage [%]	Mol. weight [kDa]	Sequence length	Enrichment ratio*	# of times in real IP	Protein name
ACTB	P60709	67.5	41.7	375	10000.0	3	Actin, cytoplasmic 1
SPTBN1	Q01082	63	274.6	2364	15.5	3	Spectrin beta chain, non-erythrocytic 1
PABPC1	P11940	48.6	70.7	636	13.1	3	Polyadenylate-binding protein 1
SFPQ	P23246	52.2	76.1	707	172.7	3	Splicing factor, proline- and glutamine-rich
Q9Y4I1-3	Q9Y4I1-3	50.4	218.6	1880	10000.0	3	Isoform 3 of Unconventional myosin-Va
ACTN4	O43707	64.8	104.9	911	25.6	3	Alpha-actinin-4
THRAP3	Q9Y2W1	40	108.7	955	12.4	3	Thyroid hormone receptor-associated protein 3
BCLAF1	Q9NYF8	39.3	106.1	920	12.6	3	Bcl-2-associated transcription factor 1
HIST2H2AA3	Q6FI13	57.7	14.1	130	10000.0	3	Histone H2A type 2-A
FLNA	P21333	37.6	280.7	2647	31.7	3	Filamin-A
CAPRIN1	Q14444	29.1	78.4	709	10.1	3	Caprin-1
Q8WWM7	Q8WWM7	31.4	113.4	1075	10000.0	3	Ataxin-2-like protein
PABPC4	Q13310-3	38.2	72.4	660	25.3	3	Isoform 3 of Polyadenylate-binding protein 4
CAPZA1	P52907	62.6	32.9	286	17.1	3	F-actin-capping protein subunit alpha-1
NONO	Q15233	57.7	54.2	471	67.8	3	Non-POU domain-containing octamer-binding protein
DDX1	Q92499	29.3	82.4	740	54.1	3	ATP-dependent RNA helicase DDX1
TOP2A	P11388-4	20.8	182.7	1612	14.7	3	Isoform 4 of DNA topoisomerase 2-alpha
FXR2	P51116	40	74.2	673	10.6	3	Fragile X mental retardation syndrome-related protein 2
SVIL	O95425-4	31.9	244.5	2182	10.7	3	Isoform SV4 of Supervillin
H0Y2S9	H0Y2S9	44.7	203.4	1794	10000.0	3	Myosin phosphatase Rho-interacting protein (Fragment)
RBM14	Q96PK6	24.5	69.5	669	13.5	3	RNA-binding protein 14
NUFIP2	Q7Z417	27.9	76.1	695	29.0	3	Nuclear fragile X mental retardation-interacting protein 2
TMOD3	Q9NYL9	44.6	39.6	352	18.6	3	Tropomodulin-3
TUBA1C	F5H5D3	26.8	57.7	519	10000.0	3	Tubulin alpha-1C chain
UBAP2L	Q14157-5	23.6	116.6	1104	13.2	3	Isoform 5 of Ubiquitin-associated protein 2-like
PPP1R9B	Q96SB3	42.8	89.2	815	32.7	3	Neurabin-2

SPECC1L	Q69YQ0	43.9	124.6	1117	149.6	3	Cytospin-A
GNAI2	P04899	40.8	40.5	355	21.9	3	Guanine nucleotide-binding protein G(i) subunit alpha-2
P06753-2	P06753-2	71	29.0	248	10000.0	3	Isoform 2 of Tropomyosin alpha-3 chain
USP10	Q14694-2	16.9	92.6	846	10000.0	3	Isoform 2 of Ubiquitin carboxyl-terminal hydrolase 10
FUS	H3BPE7	10.8	53.5	527	58.3	3	RNA-binding protein FUS
HNRNPA2B1	P22626	45	37.4	353	65.2	3	Heterogeneous nuclear ribonucleoproteins A2/B1
G3BP1	Q13283	30.7	52.2	466	48.9	3	Ras GTPase-activating protein-binding protein 1
Q6WCQ1-2	Q6WCQ1-2	59.2	118.1	1038	10000.0	3	Isoform 2 of Myosin phosphatase Rho-interacting protein
HNRNPA1	P09651	40.1	38.7	372	25.4	3	Heterogeneous nuclear ribonucleoprotein A1
PRRC2C	Q9Y520-7	11.5	317.1	2898	20.8	3	Isoform 7 of Protein PRRC2C
HADHA	P40939	42.5	83.0	763	11.3	3	Trifunctional enzyme subunit alpha, mitochondrial
Q8WWI1-3	Q8WWI1-3	37.4	153.7	1349	10000.0	3	Isoform 3 of LIM domain only protein 7
SRSF4	Q08170	14.8	56.7	494	10000.0	3	Serine/arginine-rich splicing factor 4
TPRN	Q4KMQ1	35.6	75.6	711	10.7	3	Taperin
G3V1L9	G3V1L9	34	197.5	1768	10000.0	3	Tight junction protein 1 (Zona occludens 1), isoform CRA_a
C22orf28	Q9Y3I0	30.7	55.2	505	17.3	3	tRNA-splicing ligase RtcB homolog
TRA2B	P62995	32.3	33.7	288	41.6	3	Transformer-2 protein homolog beta
FAM120A	Q9NZB2-6	14	125.3	1146	36.3	3	Isoform F of Constitutive coactivator of PPAR-gamma-like protein 1
TSGA10	Q9BZW7	4.2	81.4	698	10000.0	3	Testis-specific gene 10 protein
XRCC6	P12956	51.1	69.8	609	40.2	3	X-ray repair cross-complementing protein 6
CTTN	Q14247	38	61.6	550	10.6	3	Src substrate cortactin
ACTR2	P61160	29.9	44.8	394	73.4	3	Actin-related protein 2
IGF2BP3	O00425	18.5	63.7	579	10000.0	3	Insulin-like growth factor 2 mRNA-binding protein 3
RAI14	Q9P0K7-2	26.9	110.4	983	59.5	3	Isoform 2 of Ankycorbin
RPL26	P61254	35.2	17.3	145	10.3	3	60S ribosomal protein L26
PPP1CA	P62136	29.7	37.5	330	103.4	3	Serine/threonine-protein phosphatase PP1-alpha catalytic subunit
HNRNPA3	P51991	31.2	39.6	378	78.6	3	Heterogeneous nuclear ribonucleoprotein A3
PI4KA	J3KN10	16	236.8	2102	70.3	3	Phosphatidylinositol 4-kinase alpha
FBXW11	Q9UKB1-3	25.1	60.9	529	10000.0	3	Isoform B of F-box/WD repeat-containing protein 11

DHX30	Q7L2E3-2	13.9	136.1	1222	14.6	3	Isoform 2 of Putative ATP-dependent RNA helicase DHX30
EDC4	Q6P2E9	11.8	151.7	1401	10000.0	3	Enhancer of mRNA-decapping protein 4
PA2G4	Q9UQ80	28.7	43.8	394	23.4	3	Proliferation-associated protein 2G4
EFHD2	Q96C19	55.4	26.7	240	27.8	3	EF-hand domain-containing protein D2
RBMX	P38159	30.9	42.3	391	20.9	3	RNA-binding motif protein, X chromosome
MACF1	H3BQK9	4.5	861.1	7592	111.4	3	Microtubule-actin cross-linking factor 1, isoforms 1/2/3/5
TWF2	Q6IBS0	46.7	39.5	349	10000.0	3	Twinfilin-2
A8MXP9	A8MXP9	15.2	100.0	895	10000.0	3	Matrin-3
HNRNPC	P07910	26.1	33.7	306	77.1	3	Heterogeneous nuclear ribonucleoproteins C1/C2
GNAI3	P08754	34.2	40.5	354	40.0	3	Guanine nucleotide-binding protein G(k) subunit alpha
EIF4G1	Q04637-9	7.7	176.2	1606	10000.0	3	Isoform 9 of Eukaryotic translation initiation factor 4 gamma 1
GNB1	P62873	19.7	37.4	340	10000.0	3	Guanine nucleotide-binding protein G(I)/G(S)/G(T) subunit beta-1
Q14103	Q14103	21.7	38.4	355	10000.0	3	Heterogeneous nuclear ribonucleoprotein D0
HNRNPAB	Q99729-3	26.3	30.6	285	10000.0	3	Isoform 3 of Heterogeneous nuclear ribonucleoprotein A/B
MX2	P20592	30.9	82.1	715	10000.0	3	Interferon-induced GTP-binding protein Mx2
HIST1H1C	P16403	27.2	21.4	213	10000.0	3	Histone H1.2
IQGAP1	P46940	29.8	189.3	1657	10000.0	3	Ras GTPase-activating-like protein IQGAP1
RPSAP58	A6NE09	22	32.9	295	10000.0	3	40S ribosomal protein SA
PRRC2A	P48634	8.1	228.9	2157	10000.0	3	Protein PRRC2A
TWF1	Q12792	29.1	40.3	350	45.2	3	Twinfilin-1
CPSF6	Q16630-2	10.4	63.5	588	16.6	3	Isoform 2 of Cleavage and polyadenylation specificity factor subunit 6
SF1	Q15637	15	68.3	639	10000.0	3	Splicing factor 1
PCBP1	Q15365	19.4	37.5	356	71.0	3	Poly(rC)-binding protein 1
AP2B1	P63010-2	11.8	105.7	951	10000.0	3	Isoform 2 of AP-2 complex subunit beta
ANXA2	P07355-2	31.7	40.4	357	10000.0	3	Isoform 2 of Annexin A2
SRSF1	J3KTL2	33.2	28.3	253	16.3	3	Serine/arginine-rich-splicing factor 1
ILF2	Q12905	21	43.1	390	11.6	3	Interleukin enhancer-binding factor 2
KHSRP	Q92945	17.4	73.1	711	20.2	3	Far upstream element-binding protein 2
PRKDC	P78527	6.3	469.1	4128	21.2	3	DNA-dependent protein kinase catalytic subunit

IFITM3	Q01628	12.8	14.6	133	174.5	3	Interferon-induced transmembrane protein 3
P23396	P23396	56.8	26.7	243	10000.0	3	40S ribosomal protein S3
CASC3	O15234	11.2	76.3	703	10000.0	3	Protein CASC3
NSF	P46459	14.2	82.6	744	10000.0	3	Vesicle-fusing ATPase
ACTN1	P12814-3	37.3	105.6	914	10000.0	3	Isoform 3 of Alpha-actinin-1
DAAM1	Q9Y4D1	22.7	123.5	1078	10000.0	3	Disheveled-associated activator of morphogenesis 1
TAF15	Q92804	16.7	61.8	592	10000.0	3	TATA-binding protein-associated factor 2N
TRA2A	Q13595	34.8	32.7	282	64.0	3	Transformer-2 protein homolog alpha
ELAVL1	B4DVB8	25.8	39.0	353	49.9	3	ELAV-like protein 1
PPP1R9A	Q9ULJ8-3	16.9	154.1	1374	10000.0	3	Isoform 3 of Neurabin-1
EIF4A3	P38919	23.8	46.9	411	16.7	3	Eukaryotic initiation factor 4A-III
RPL10	P27635	23.4	24.6	214	10000.0	3	60S ribosomal protein L10
HSPA1A	P08107	13.6	70.1	641	10000.0	3	Heat shock 70 kDa protein 1A/1B
YTHDF3	Q7Z739	11.8	63.9	585	10000.0	3	YTH domain-containing family protein 3
ATAD3A	Q9NVI7-2	31.1	66.2	586	10000.0	3	Isoform 2 of ATPase family AAA domain-containing protein 3A
PPP1CB	P62140	21.1	37.2	327	15.7	3	Serine/threonine-protein phosphatase PP1-beta catalytic subunit
ARPC1B	O15143	14.2	40.9	372	22.3	3	Actin-related protein 2/3 complex subunit 1B
HSP90B1	P14625	12	92.5	803	10000.0	3	Endoplasmin
PUM2	Q8TB72-3	3.9	114.0	1064	10000.0	3	Isoform 3 of Pumilio homolog 2
SRSF2	Q01130	27.1	25.5	221	19.3	3	Serine/arginine-rich splicing factor 2
PKM2	P14618	19	57.9	531	10000.0	3	Pyruvate kinase PKM
NT5E	P21589	16.6	63.4	574	10000.0	3	5-nucleotidase
TUBGCP2	Q9BSJ2-4	6.5	105.6	930	10000.0	3	Isoform 3 of Gamma-tubulin complex component 2
CAPZA2	P47755	47.6	32.9	286	11.0	3	F-actin-capping protein subunit alpha-2
KIF21B	O75037-4	22.6	181.1	1623	10000.0	3	Isoform 4 of Kinesin-like protein KIF21B
ARPC4	P59998-3	54	21.6	187	26.6	3	Isoform 3 of Actin-related protein 2/3 complex subunit 4
EIF3CL	B5ME19	10.8	105.5	914	10000.0	3	Eukaryotic translation initiation factor 3 subunit C-like protein
HNRNPL	P14866	22.9	64.1	589	21.8	3	Heterogeneous nuclear ribonucleoprotein L
YTHDF2	Q9Y5A9	10.5	62.3	579	10000.0	3	YTH domain-containing family protein 2
FMNL1	O95466-3	14.4	128.3	1158	10000.0	3	Isoform 3 of Formin-like protein 1

KHDRBS1	Q07666	7.2	48.2	443	16.3	3	KH domain-containing, RNA-binding, signal transduction-associated protein 1
DDX10	Q13206	11.3	100.9	875	10000.0	3	Probable ATP-dependent RNA helicase DDX10
GPC4	O75487	24.6	62.4	556	36.6	3	Glypican-4
PSPC1	Q8WXF1	18.9	58.7	523	10000.0	3	Paraspeckle component 1
PTPRG	P23470	12.9	162.0	1445	10000.0	3	Receptor-type tyrosine-protein phosphatase gamma
HADHB	P55084	34.8	51.3	474	10000.0	3	Trifunctional enzyme subunit beta, mitochondrial
MSN	P26038	15.3	67.8	577	10000.0	3	Moesin
USO1	O60763-2	4.3	109.2	973	22.6	3	Isoform 2 of General vesicular transport factor p115
TDRD3	Q9H7E2-3	8.2	83.1	744	10000.0	3	Isoform 3 of Tudor domain-containing protein 3
NCBP1	Q09161	5.7	91.8	790	10000.0	3	Nuclear cap-binding protein subunit 1
EPB41L3	Q9Y2J2-2	33.5	96.5	865	10000.0	3	Isoform 2 of Band 4.1-like protein 3
TUBGCP3	Q96CW5	4.9	103.6	907	10000.0	3	Gamma-tubulin complex component 3
ARF3	P61204	35.4	20.6	181	10000.0	3	ADP-ribosylation factor 3
YTHDF1	Q9BYJ9	18.2	60.9	559	10000.0	3	YTH domain-containing family protein 1
TXNDC5	Q8NBS9	8.8	47.6	432	10000.0	3	Thioredoxin domain-containing protein 5
PFKP	Q01813	8	85.6	784	10000.0	3	6-phosphofructokinase type C
SRSF7	Q16629	18.1	27.4	238	17.1	3	Serine/arginine-rich splicing factor 7
MYO1E	Q12965	7.3	127.1	1108	10000.0	3	Unconventional myosin-Ie
ITCH	Q96J02	5.2	102.8	903	10000.0	3	E3 ubiquitin-protein ligase Itchy homolog
HSPA4	P34932	8.2	94.3	840	10000.0	3	Heat shock 70 kDa protein 4
GNAS	Q5JWF2	11.3	111.0	1037	10000.0	3	Guanine nucleotide-binding protein G(s) subunit alpha isoforms XLas
ARPC2	O15144	57.3	34.3	300	12.4	3	Actin-related protein 2/3 complex subunit 2
SRGAP2	O75044	8.8	120.9	1071	28.0	3	SLIT-ROBO Rho GTPase-activating protein 2
MTA2	O94776	7.3	75.0	668	10000.0	3	Metastasis-associated protein MTA2
RELA	Q2TAM5	4.2	42.9	377	10000.0	3	RELA protein
SIPA1L1	O43166	11.6	200.0	1804	10000.0	3	Signal-induced proliferation-associated 1-like protein 1
NCKIPSD	Q9NZQ3	10.8	79.0	722	10000.0	3	NCK-interacting protein with SH3 domain
PTMA	P06454	34.2	12.2	111	21.0	3	Prothymosin alpha
EPB41	P11171	15.3	97.0	864	10000.0	3	Protein 4.1
VPS35	Q96QK1	7.2	91.7	796	10000.0	3	Vacuolar protein sorting-associated protein 35

ARHGEF11	O15085-2	32	172.2	1562	10000.0	3	Isoform 2 of Rho guanine nucleotide exchange factor 11
TUBG1	P23258	15.7	51.2	451	10000.0	3	Tubulin gamma-1 chain
DLST	P36957	9.9	48.8	453	10000.0	3	Dihydrolipoamide S-Succinyltransferase (E2 Component Of 2-Oxo-Glutarate Complex)
TTC7A	Q2T9J9	7.8	98.9	882	10000.0	3	TTC7A protein
ZNF217	O75362	5.9	115.3	1048	24.2	3	Zinc finger protein 217
EIF3B	P55884-2	2.7	99.0	873	10000.0	3	Isoform 2 of Eukaryotic translation initiation factor 3 subunit B
RBBP4	Q09028	14.8	47.7	425	10000.0	3	Histone-binding protein RBBP4
ZDHHC5	Q9C0B5	25.2	77.5	715	10000.0	3	Palmitoyltransferase ZDHHC5
RPS5	M0R0R2	12.9	25.3	225	10000.0	3	40S ribosomal protein S5
SEMA7A	O75326	9.8	74.8	666	10000.0	3	Semaphorin-7A
MYO1B	O43795	4	132.0	1136	10000.0	3	Unconventional myosin-Ib
SIPA1L3	O60292	8.4	194.6	1781	10000.0	3	Signal-induced proliferation-associated 1-like protein 3
CUL3	Q13618	7.2	88.9	768	11.7	3	Cullin-3
SEC16A	J3KNL6	7.4	251.9	2357	10000.0	3	Protein transport protein Sec16A
KCTD10	Q9H3F6	23.6	35.4	313	373.9	3	BTB/POZ domain-containing adapter for CUL3-mediated RhoA degradation protein 3
PURA	Q00577	11.2	34.9	322	12.8	3	Transcriptional activator protein Pur-alpha
SMC3	Q9UQE7	6.6	141.5	1217	10000.0	3	Structural maintenance of chromosomes protein 3
MBNL1	Q9NR56	5.7	41.8	388	10000.0	3	Muscleblind-like protein 1
P51608-2	P51608-2	9.8	53.3	498	10000.0	3	Isoform B of Methyl-CpG-binding protein 2
KPNB1	Q14974	6.6	97.2	876	10000.0	3	Importin subunit beta-1
ARHGEF1	M0QZR4	12.5	108.3	968	10000.0	3	Rho guanine nucleotide exchange factor 1
BUB3	O43684	14.3	37.2	328	54.3	3	Mitotic checkpoint protein BUB3
EIF3EIP	B0QY89	7.2	70.9	607	10000.0	3	Eukaryotic translation initiation factor 3 subunit L
CCDC102A	Q96A19	10.4	62.6	550	10000.0	3	Coiled-coil domain-containing protein 102A
EIF3A	Q14152	4.3	166.6	1382	10000.0	3	Eukaryotic translation initiation factor 3 subunit A
RPN1	P04843	8.7	68.6	607	10000.0	3	Dolichyl-diphosphooligosaccharide--protein glycosyltransferase subunit 1
ORF1	Q9UN81	17.8	40.1	338	37.6	3	LINE-1 retrotransposable element ORF1 protein
SRPR	P08240	8.8	69.8	638	18.7	3	Signal recognition particle receptor subunit alpha
DSG1	Q02413	3.3	113.8	1049	10.8	3	Desmoglein-1

RANGAP1	P46060	9	63.5	587	10000.0	3	Ran GTPase-activating protein 1
AHCY	P23526	14.4	47.7	432	21.3	3	Adenosylhomocysteinase
PGAM5	Q96HS1	16.6	32.0	289	12.4	3	Serine/threonine-protein phosphatase PGAM5, mitochondrial
PAICS	P22234-2	13.4	48.0	432	10000.0	3	Isoform 2 of Multifunctional protein ADE2
AKNA	Q7Z591	6.7	155.1	1439	10000.0	3	AT-hook-containing transcription factor
FARP1	C9JME2	8.6	122.1	1076	10000.0	3	FERM, RhoGEF and pleckstrin domain-containing protein 1
UAP1	Q16222	7.5	58.8	522	10000.0	3	UDP-N-acetylhexosamine pyrophosphorylase
PDLIM2	Q96JY6-5	17.8	62.7	602	10000.0	3	Isoform 5 of PDZ and LIM domain protein 2
NACA	E9PAV3	1.4	205.4	2078	22.1	3	Nascent polypeptide-associated complex subunit alpha
U2AF1	Q01081	10.4	27.9	240	10000.0	3	Splicing factor U2AF 35 kDa subunit
TNRC6B	Q9UPQ9	2	194.0	1833	10000.0	3	Trinucleotide repeat-containing gene 6B protein
PRRC2B	Q5JSZ5	3.2	243.0	2229	10000.0	3	Protein PRRC2B
YTHDC1	Q96MU7-2	9.3	82.7	709	10000.0	3	Isoform 2 of YTH domain-containing protein 1
PPP2R2A	P63151-2	8.3	53.0	457	10000.0	3	Serine/threonine-protein phosphatase 2A 55 kDa regulatory subunit B, isoform alpha
TARDBP	Q13148	12.3	44.7	414	56.5	3	TAR DNA-binding protein 43
SRSF10	O75494	17.9	31.3	262	10000.0	3	Serine/arginine-rich splicing factor 10
RNPS1	Q15287	20.3	34.2	305	10000.0	3	RNA-binding protein with serine-rich domain 1
H1FX	Q92522	23.5	22.5	213	11.5	3	Histone H1x
CCT6A	P40227	7	58.0	531	10000.0	3	T-complex protein 1 subunit zeta
YWHAZ	E7EX29	17.1	28.0	246	10000.0	3	14-3-3 protein zeta/delta (Fragment)
PRMT1	H7C2I1	10.8	42.5	371	10000.0	3	Protein arginine N-methyltransferase 1
DDX39B	F8VQ10	8.1	50.7	443	10000.0	3	Spliceosome RNA helicase DDX39B
LSR	Q86X29	5.7	71.4	649	10000.0	3	Lipolysis-stimulated lipoprotein receptor
EIF3F	B3KSH1	7.8	39.1	372	10000.0	3	Eukaryotic translation initiation factor 3 subunit F
GNA13	Q14344	25.7	44.0	377	10000.0	3	Guanine nucleotide-binding protein subunit alpha-13
FUBP3	Q96I24	8.7	61.6	572	10000.0	3	Far upstream element-binding protein 3
RFC4	P35249	10.7	39.7	363	10000.0	3	Replication factor C subunit 4
EMD	P50402	8.7	29.0	254	10000.0	3	Emerin
MINA	Q8IUF8	41.3	52.8	465	10000.0	3	Bifunctional lysine-specific demethylase and histidyl-hydroxylase MINA
CNOT2	Q9NZN8	18.5	59.7	540	10000.0	3	CCR4-NOT transcription complex subunit 2

REFERENCES

Aggarwal, B. B., A. B. Kunnumakkara, K. B. Harikumar, S. R. Gupta, S. T. Tharakan, C. Koca, S. Dey and B. Sung. "Signal Transducer and Activator of Transcription-3, Inflammation, and Cancer: How Intimate Is the Relationship?" *Ann N Y Acad Sci* 1171, (2009): 59-76.

Al-Lazikani, B., U. Banerji and P. Workman. "Combinatorial Drug Therapy for Cancer in the Post-Genomic Era." *Nat Biotechnol* 30, no. 7 (2012): 679-92.

Araki, T., H. Yashima, K. Shimizu, T. Aomori, T. Hashita, K. Kaira, T. Nakamura and K. Yamamoto. "Review of the Treatment of Non-Small Cell Lung Cancer with Gefitinib." *Clin Med Insights Oncol* 6, (2012): 407-21.

Bae, N. C., M. H. Chae, M. H. Lee, K. M. Kim, E. B. Lee, C. H. Kim, T. I. Park, S. B. Han, S. Jheon, T. H. Jung and J. Y. Park. "Egfr, Erbb2, and Kras Mutations in Korean Non-Small Cell Lung Cancer Patients." *Cancer Genet Cytogenet* 173, no. 2 (2007): 107-13.

Berg, M. and K. Soreide. "Egfr and Downstream Genetic Alterations in Kras/Braf and Pi3k/AKT Pathways in Colorectal Cancer: Implications for Targeted Therapy." *Discov Med* 14, no. 76 (2012): 207-14.

Bettelli, E., Y. Carrier, W. Gao, T. Korn, T. B. Strom, M. Oukka, H. L. Weiner and V. K. Kuchroo. "Reciprocal Developmental Pathways for the Generation of Pathogenic Effector Th17 and Regulatory T Cells." *Nature* 441, no. 7090 (2006): 235-8.

Bianchi, G. and N. C. Munshi. "Pathogenesis Beyond the Cancer Clone(S) in Multiple Myeloma." *Blood* 125, no. 20 (2015): 3049-3058.

Blagosklonny, M. V. "Oncogenic Resistance to Growth-Limiting Conditions." *Nat Rev Cancer* 2, no. 3 (2002): 221-5.

Blagosklonny, M. V. "Why Therapeutic Response May Not Prolong the Life of a Cancer Patient: Selection for Oncogenic Resistance." *Cell Cycle* 4, no. 12 (2005): 1693-8.

Bommert, K., R. C. Bargou and T. Stuhmer. "Signalling and Survival Pathways in Multiple Myeloma." *Eur J Cancer* 42, no. 11 (2006): 1574-80.

Bowman, T., R. Garcia, J. Turkson and R. Jove. "Stats in Oncogenesis." *Oncogene* 19, no. 21 (2000): 2474-88.

Bromberg, J. F., M. H. Wrzeszczynska, G. Devgan, Y. Zhao, R. G. Pestell, C. Albanese and J. E. Darnell, Jr. "Stat3 as an Oncogene." *Cell* 98, no. 3 (1999): 295-303.

Brown, R., S. Yang, C. Weatherburn, J. Gibson, P. J. Ho, H. Suen, D. Hart and D. Joshua. "Phospho-Flow Detection of Constitutive and Cytokine-Induced Pstat3/5, PAKT and Perk Expression Highlights Novel Prognostic Biomarkers for Patients with Multiple Myeloma." *Leukemia* 29, no. 2 (2015): 483-90.

Calo, V., M. Migliavacca, V. Bazan, M. Macaluso, M. Buscemi, N. Gebbia and A. Russo. "Stat Proteins: From Normal Control of Cellular Events to Tumorigenesis." *J Cell Physiol* 197, no. 2 (2003): 157-68.

Catlett-Falcone, R., T. H. Landowski, M. M. Oshiro, J. Turkson, A. Levitzki, R. Savino, G. Ciliberto, L. Moscinski, J. L. Fernandez-Luna, G. Nunez, W. S. Dalton and R. Jove. "Constitutive Activation of Stat3 Signaling Confers Resistance to Apoptosis in Human U266 Myeloma Cells." *Immunity* 10, no. 1 (1999): 105-15.

Chapman, M. A., M. S. Lawrence, J. J. Keats, K. Cibulskis, C. Sougnez, A. C. Schinzel, C. L. Harview, J. P. Brunet, G. J. Ahmann, M. Adli, K. C. Anderson, K. G. Ardlie, D. Auclair, A. Baker, P. L. Bergsagel, B. E. Bernstein, Y. Drier, R. Fonseca, S. B. Gabriel, C. C. Hofmeister, S. Jagannath, A. J. Jakubowiak, A. Krishnan, J. Levy, T. Liefeld, S. Lonial, S. Mahan, B. Mfuko, S. Monti, L. M. Perkins, R. Onofrio, T. J. Pugh, S. V. Rajkumar, A. H. Ramos, D. S. Siegel, A. Sivachenko, A. K. Stewart, S.

Trudel, R. Vij, D. Voet, W. Winckler, T. Zimmerman, J. Carpten, J. Trent, W. C. Hahn, L. A. Garraway, M. Meyerson, E. S. Lander, G. Getz and T. R. Golub. "Initial Genome Sequencing and Analysis of Multiple Myeloma." *Nature* 471, no. 7339 (2011): 467-72.

Chauhan, D., Z. Tian, B. Nicholson, K. G. Kumar, B. Zhou, R. Carrasco, J. L. McDermott, C. A. Leach, M. Fulcinniti, M. P. Kodrasov, J. Weinstock, W. D. Kingsbury, T. Hideshima, P. K. Shah, S. Minvielle, M. Altun, B. M. Kessler, R. Orlowski, P. Richardson, N. Munshi and K. C. Anderson. "A Small Molecule Inhibitor of Ubiquitin-Specific Protease-7 Induces Apoptosis in Multiple Myeloma Cells and Overcomes Bortezomib Resistance." *Cancer Cell* 22, no. 3 (2012): 345-58.

Chen, B., J. Liu, Q. Chang, K. Beezhold, Y. Lu and F. Chen. "Jnk and Stat3 Signaling Pathways Converge on AKT-Mediated Phosphorylation of Ezh2 in Bronchial Epithelial Cells Induced by Arsenic." *Cell Cycle* 12, no. 1 (2013): 112-21.

Chen, B., M. Yu, Q. Chang, Y. Lu, C. Thakur, D. Ma, Z. Yi and F. Chen. "MDIG De-Represses H19 Large Intergenic Non-Coding Rna (Lincrna) by Down-Regulating H3k9me3 and Heterochromatin." *Oncotarget* 4, no. 9 (2013): 1427-37.

Chiu, H. C., D. L. Chou, C. T. Huang, W. H. Lin, T. W. Lien, K. J. Yen and J. T. Hsu. "Suppression of Stat3 Activity Sensitizes Gefitinib-Resistant Non Small Cell Lung Cancer Cells." *Biochem Pharmacol* 81, no. 11 (2011): 1263-70.

Chng, W. J., G. F. Huang, T. H. Chung, S. B. Ng, N. Gonzalez-Paz, T. Troska-Price, G. Mulligan, M. Chesi, P. L. Bergsagel and R. Fonseca. "Clinical and Biological Implications of Myc Activation: A Common Difference between Mgus and Newly Diagnosed Multiple Myeloma." *Leukemia* 25, no. 6 (2011): 1026-35.

Chng, W. J., S. Kumar, S. Vanwier, G. Ahmann, T. Price-Troska, K. Henderson, T. H. Chung, S. Kim, G. Mulligan, B. Bryant, J. Carpten, M. Gertz, S. V. Rajkumar, M. Lacy, A. Dispenzieri, R. Kyle, P. Greipp, P. L. Bergsagel and R. Fonseca. "Molecular Dissection of Hyperdiploid Multiple Myeloma by Gene Expression Profiling." *Cancer Res* 67, no. 7 (2007): 2982-9.

Chong, C. R. and P. A. Janne. "The Quest to Overcome Resistance to Egfr-Targeted Therapies in Cancer." *Nat Med* 19, no. 11 (2013): 1389-400.

Chowdhury, R., R. Sekirnik, N. C. Brissett, T. Krojer, C. H. Ho, S. S. Ng, I. J. Clifton, W. Ge, N. J. Kershaw, G. C. Fox, J. R. Muniz, M. Vollmar, C. Phillips, E. S. Pilka, K. L. Kavanagh, F. von Delft, U. Oppermann, M. A. McDonough, A. J. Doherty and C. J. Schofield. "Ribosomal Oxygenases Are Structurally Conserved from Prokaryotes to Humans." *Nature* 510, no. 7505 (2014): 422-6.

Chung, J., E. Uchida, T. C. Grammer and J. Blenis. "Stat3 Serine Phosphorylation by Erk-Dependent and -Independent Pathways Negatively Modulates Its Tyrosine Phosphorylation." *Mol Cell Biol* 17, no. 11 (1997): 6508-16.

Cottini, F., T. Hideshima, R. Suzuki, Y. T. Tai, G. Bianchini, P. G. Richardson, K. C. Anderson and G. Tonon. "Synthetic Lethal Approaches Exploiting DNA Damage in Aggressive Myeloma." *Cancer Discov*, (2015).

Cottini, F., T. Hideshima, C. Xu, M. Sattler, M. Dori, L. Agnelli, E. ten Hacken, M. T. Bertilaccio, E. Antonini, A. Neri, M. Ponzoni, M. Marcatti, P. G. Richardson, R. Carrasco, A. C. Kimmelman, K. K. Wong, F. Caligaris-Cappio, G. Blandino, W. M. Kuehl, K. C. Anderson and G. Tonon. "Rescue of Hippo Coactivator Yap1 Triggers DNA Damage-Induced Apoptosis in Hematological Cancers." *Nat Med* 20, no. 6 (2014): 599-606.

Dechow, T., S. Steidle, K. S. Gotze, M. Rudelius, K. Behnke, K. Pechloff, S. Kratzat, L. Bullinger, F. Fend, V. Soberon, N. Mitova, Z. Li, M. Thaler, J. Bauer, E. Pietschmann, C. Albers, R. Grundler, M. Schmidt-Supprian, J. Ruland, C. Peschel, J. Duyster, S. Rose-John, F. Bassermann and U. Keller. "Gp130 Activation Induces Myeloma and Collaborates with Myc." *J Clin Invest* 124, no. 12 (2014): 5263-74.

Dispenzieri, A., A. K. Stewart, A. Chanan-Khan, S. V. Rajkumar, R. A. Kyle, R. Fonseca, P. Kapoor, P. L. Bergsagel, A. McCurdy, M. A. Gertz, M. Q. Lacy, J. A. Lust, S. J. Russell, S. R. Zeldenrust, C. Reeder, V. Roy, F. Buadi, D. Dingli, S. R. Hayman, N. Leung, Y. Lin, J. Mikhael and S. K. Kumar. "Smoldering Multiple Myeloma Requiring Treatment: Time for a New Definition?" *Blood* 122, no. 26 (2013): 4172-81.

Eilbracht, J., S. Kneissel, A. Hofmann and M. S. Schmidt-Zachmann. "Protein No52--a Constitutive Nucleolar Component Sharing High Sequence Homologies to Protein No66." *Eur J Cell Biol* 84, no. 2-3 (2005): 279-94.

Eilers, M. and R. N. Eisenman. "Myc's Broad Reach." *Genes Dev* 22, no. 20 (2008): 2755-66.

Engelman, J. A., K. Zejnullahu, T. Mitsudomi, Y. Song, C. Hyland, J. O. Park, N. Lindeman, C. M. Gale, X. Zhao, J. Christensen, T. Kosaka, A. J. Holmes, A. M. Rogers, F. Cappuzzo, T. Mok, C. Lee, B. E. Johnson, L. C. Cantley and P. A. Janne. "Met Amplification Leads to Gefitinib Resistance in Lung Cancer by Activating Erbb3 Signaling." *Science* 316, no. 5827 (2007): 1039-43.

Ercan, D., C. Xu, M. Yanagita, C. S. Monast, C. A. Pratilas, J. Montero, M. Butaney, T. Shimamura, L. Sholl, E. V. Ivanova, M. Tadi, A. Rogers, C. Repellin, M. Capelletti, O. Maertens, E. M. Goetz, A. Letai, L. A. Garraway, M. J. Lazzara, N. Rosen, N. S. Gray, K. K. Wong and P. A. Janne. "Reactivation of Erk Signaling Causes Resistance to Egfr Kinase Inhibitors." *Cancer Discov* 2, no. 10 (2012): 934-47.

Eskens, F. A., C. H. Mom, A. S. Planting, J. A. Gietema, A. Amelsberg, H. Huisman, L. van Doorn, H. Burger, P. Stopfer, J. Verweij and E. G. de Vries. "A Phase I Dose Escalation Study of Bibw 2992, an Irreversible Dual Inhibitor of Epidermal Growth Factor Receptor 1 (Egfr) and 2 (Her2) Tyrosine Kinase in a 2-Week on, 2-Week Off Schedule in Patients with Advanced Solid Tumours." *Br J Cancer* 98, no. 1 (2008): 80-5.

Ferlay, J., H. R. Shin, F. Bray, D. Forman, C. Mathers and D. M. Parkin. "Estimates of Worldwide Burden of Cancer in 2008: Globocan 2008." *Int J Cancer* 127, no. 12 (2010): 2893-917.

Ferlay, J., E. Steliarova-Foucher, J. Lortet-Tieulent, S. Rosso, J. W. Coebergh, H. Comber, D. Forman and F. Bray. "Cancer Incidence and Mortality Patterns in Europe: Estimates for 40 Countries in 2012." *Eur J Cancer* 49, no. 6 (2013): 1374-403.

Fukuoka, M., S. Yano, G. Giaccone, T. Tamura, K. Nakagawa, J. Y. Douillard, Y. Nishiwaki, J. Vansteenkiste, S. Kudoh, D. Rischin, R. Eek, T. Horai, K. Noda, I. Takata, E. Smit, S. Averbuch, A. Macleod, A. Feyereislova, R. P. Dong and J. Baselga. "Multi-Institutional Randomized Phase Ii Trial of Gefitinib for Previously Treated Patients with Advanced Non-Small-Cell Lung Cancer (the Ideal 1 Trial) [Corrected]." *J Clin Oncol* 21, no. 12 (2003): 2237-46.

Garcia Campelo, M. R., G. Alonso Curbera, G. Aparicio Gallego, E. Grande Pulido and L. M. Anton Aparicio. "Stem Cell and Lung Cancer Development: Blaming the Wnt, Hh and Notch Signalling Pathway." *Clin Transl Oncol* 13, no. 2 (2011): 77-83.

Grant, S., L. Qiao and P. Dent. "Roles of Erbb Family Receptor Tyrosine Kinases, and Downstream Signaling Pathways, in the Control of Cell Growth and Survival." *Front Biosci* 7, (2002): d376-89.

Hamamoto, R., V. Saloura and Y. Nakamura. "Critical Roles of Non-Histone Protein Lysine Methylation in Human Tumorigenesis." *Nat Rev Cancer* 15, no. 2 (2015): 110-24.

Han, S. W., T. Y. Kim, Y. K. Jeon, P. G. Hwang, S. A. Im, K. H. Lee, J. H. Kim, D. W. Kim, D. S. Heo, N. K. Kim, D. H. Chung and Y. J. Bang. "Optimization of Patient Selection for Gefitinib in Non-Small Cell Lung Cancer by Combined Analysis of Epidermal Growth Factor Receptor Mutation, K-Ras Mutation, and AKT Phosphorylation." *Clin Cancer Res* 12, no. 8 (2006): 2538-44.

Hanamura, I., Y. Huang, F. Zhan, B. Barlogie and J. Shaughnessy. "Prognostic Value of Cyclin D2 Mrna Expression in Newly Diagnosed Multiple Myeloma Treated with High-Dose Chemotherapy and Tandem Autologous Stem Cell Transplantations." *Leukemia* 20, no. 7 (2006): 1288-90.

Hata, A. N., M. J. Niederst, H. L. Archibald, M. Gomez-Caraballo, F. M. Siddiqui, H. E. Mulvey, Y. E. Maruvka, F. Ji, H. E. Bhang, V. Krishnamurthy Radhakrishna, G. Siravegna, H. Hu, S. Raoof, E. Lockerman, A. Kalsy, D. Lee, C. L. Keating, D. A. Ruddy, L. J. Damon, A. S. Crystal, C. Costa, Z. Piotrowska, A. Bardelli, A. J. Iafrate, R. I. Sadreyev, F. Stegmeier, G. Getz, L. V. Sequist, A. C. Faber and J. A. Engelman. "Tumor Cells Can Follow Distinct Evolutionary Paths to Become Resistant to Epidermal Growth Factor Receptor Inhibition." *Nat Med* 22, no. 3 (2016): 262-9.

Haura, E. B., E. Sommers, L. Song, A. Chiappori and A. Becker. "A Pilot Study of Preoperative Gefitinib for Early-Stage Lung Cancer to Assess Intratumor Drug Concentration and Pathways Mediating Primary Resistance." *J Thorac Oncol* 5, no. 11 (2010): 1806-14.

Hemmers, S. and K. A. Mowen. "T(H)2 Bias: Mina Tips the Balance." *Nat Immunol* 10, no. 8 (2009): 806-8.

Hideshima, T., C. Mitsiades, G. Tonon, P. G. Richardson and K. C. Anderson. "Understanding Multiple Myeloma Pathogenesis in the Bone Marrow to Identify New Therapeutic Targets." *Nat Rev Cancer* 7, no. 8 (2007): 585-98.

Hideshima, T., N. Nakamura, D. Chauhan and K. C. Anderson. "Biologic Sequelae of Interleukin-6 Induced Pi3-K/AKT Signaling in Multiple Myeloma." *Oncogene* 20, no. 42 (2001): 5991-6000.

Hirsch, F. R., M. Varella-Garcia, P. A. Bunn, Jr., M. V. Di Maria, R. Veve, R. M. Bremmes, A. E. Baron, C. Zeng and W. A. Franklin. "Epidermal Growth Factor Receptor in Non-Small-Cell Lung Carcinomas: Correlation between Gene Copy Number and Protein Expression and Impact on Prognosis." *J Clin Oncol* 21, no. 20 (2003): 3798-807.

Holien, T., T. K. Vatsveen, H. Hella, A. Waage and A. Sundan. "Addiction to C-MYC in Multiple Myeloma." *Blood* 120, no. 12 (2012): 2450-3.

Ishikawa, H., N. Tsuyama, S. Liu, S. Abroun, F. J. Li, K. Otsuyama, X. Zheng, Z. Ma, Y. Maki, M. S. Iqbal, M. Obata and M. M. Kawano. "Accelerated Proliferation of Myeloma Cells by Interleukin-6 Cooperating with Fibroblast Growth Factor Receptor 3-Mediated Signals." *Oncogene* 24, no. 41 (2005): 6328-32.

Ishizaki, H., H. Yano, M. Tsuneoka, S. Ogasawara, J. Akiba, N. Nishida, S. Kojiro, S. Fukahori, F. Moriya, K. Matsuoka and M. Kojiro. "Overexpression of the Myc Target Gene Mina53 in Advanced Renal Cell Carcinoma." *Pathol Int* 57, no. 10 (2007): 672-80.

Jackman, D., W. Pao, G. J. Riely, J. A. Engelman, M. G. Kris, P. A. Janne, T. Lynch, B. E. Johnson and V. A. Miller. "Clinical Definition of Acquired Resistance to Epidermal

Growth Factor Receptor Tyrosine Kinase Inhibitors in Non-Small-Cell Lung Cancer." *J Clin Oncol* 28, no. 2 (2010): 357-60.

Jeon, H. S. and J. Jen. "Tgf-Beta Signaling and the Role of Inhibitory Smads in Non-Small Cell Lung Cancer." *J Thorac Oncol* 5, no. 4 (2010): 417-9.

John, T., G. Liu and M. S. Tsao. "Overview of Molecular Testing in Non-Small-Cell Lung Cancer: Mutational Analysis, Gene Copy Number, Protein Expression and Other Biomarkers of Egfr for the Prediction of Response to Tyrosine Kinase Inhibitors." *Oncogene* 28 Suppl 1, (2009): S14-23.

Jorissen, R. N., F. Walker, N. Pouliot, T. P. Garrett, C. W. Ward and A. W. Burgess. "Epidermal Growth Factor Receptor: Mechanisms of Activation and Signalling." *Exp Cell Res* 284, no. 1 (2003): 31-53.

Jung, M. J., J. K. Rho, Y. M. Kim, J. E. Jung, Y. B. Jin, Y. G. Ko, J. S. Lee, S. J. Lee, J. C. Lee and M. J. Park. "Upregulation of Cxcr4 Is Functionally Crucial for Maintenance of Stemness in Drug-Resistant Non-Small Cell Lung Cancer Cells." *Oncogene* 32, no. 2 (2013): 209-21.

Katakami, N., S. Atagi, K. Goto, T. Hida, T. Horai, A. Inoue, Y. Ichinose, K. Koboyashi, K. Takeda, K. Kiura, K. Nishio, Y. Seki, R. Ebisawa, M. Shahidi and N. Yamamoto. "Lux-Lung 4: A Phase Ii Trial of Afatinib in Patients with Advanced Non-Small-Cell Lung Cancer Who Progressed During Prior Treatment with Erlotinib, Gefitinib, or Both." *J Clin Oncol* 31, no. 27 (2013): 3335-41.

Katanasaka, Y., Y. Kodera, M. Yunokawa, Y. Kitamura, T. Tamura and F. Koizumi. "Synergistic Anti-Tumor Effects of a Novel Phosphatidyl Inositol-3 Kinase/Mammalian Target of Rapamycin Dual Inhibitor Bgt226 and Gefitinib in Non-Small Cell Lung Cancer Cell Lines." *Cancer Lett*, (2014).

Kelley, M. R., D. Logsdon and M. L. Fishel. "Targeting DNA Repair Pathways for Cancer Treatment: What's New?" *Future Oncol* 10, no. 7 (2014): 1215-37.

Kijima, T., H. Niwa, R. A. Steinman, S. D. Drenning, W. E. Gooding, A. L. Wentzel, S. Xi and J. R. Grandis. "Stat3 Activation Abrogates Growth Factor Dependence and Contributes to Head and Neck Squamous Cell Carcinoma Tumor Growth in Vivo." *Cell Growth Differ* 13, no. 8 (2002): 355-62.

Kim, E., M. Kim, D. H. Woo, Y. Shin, J. Shin, N. Chang, Y. T. Oh, H. Kim, J. Rheey, I. Nakano, C. Lee, K. M. Joo, J. N. Rich, D. H. Nam and J. Lee. "Phosphorylation of Ezh2 Activates Stat3 Signaling Via Stat3 Methylation and Promotes Tumorigenicity of Glioblastoma Stem-Like Cells." *Cancer Cell* 23, no. 6 (2013): 839-52.

Kiuchi, N., K. Nakajima, M. Ichiba, T. Fukada, M. Narimatsu, K. Mizuno, M. Hibi and T. Hirano. "Stat3 Is Required for the Gp130-Mediated Full Activation of the C-MYC Gene." *J Exp Med* 189, no. 1 (1999): 63-73.

Korde, N., S. Y. Kristinsson and O. Landgren. "Monoclonal Gammopathy of Undetermined Significance (Mgus) and Smoldering Multiple Myeloma (Smm): Novel Biological Insights and Development of Early Treatment Strategies." *Blood* 117, no. 21 (2011): 5573-81.

Korn, T., E. Bettelli, W. Gao, A. Awasthi, A. Jager, T. B. Strom, M. Oukka and V. K. Kuchroo. "Il-21 Initiates an Alternative Pathway to Induce Proinflammatory T(H)17 Cells." *Nature* 448, no. 7152 (2007): 484-7.

Kosaka, T., Y. Yatabe, H. Endoh, H. Kuwano, T. Takahashi and T. Mitsudomi. "Mutations of the Epidermal Growth Factor Receptor Gene in Lung Cancer: Biological and Clinical Implications." *Cancer Res* 64, no. 24 (2004): 8919-23.

Kris, M. G., R. B. Natale, R. S. Herbst, T. J. Lynch, Jr., D. Prager, C. P. Belani, J. H. Schiller, K. Kelly, H. Spiridonidis, A. Sandler, K. S. Albain, D. Cella, M. K. Wolf, S. D.

Averbuch, J. J. Ochs and A. C. Kay. "Efficacy of Gefitinib, an Inhibitor of the Epidermal Growth Factor Receptor Tyrosine Kinase, in Symptomatic Patients with Non-Small Cell Lung Cancer: A Randomized Trial." *JAMA* 290, no. 16 (2003): 2149-58.

Lee, J. M., J. S. Lee, H. Kim, K. Kim, H. Park, J. Y. Kim, S. H. Lee, I. S. Kim, J. Kim, M. Lee, C. H. Chung, S. B. Seo, J. B. Yoon, E. Ko, D. Y. Noh, K. I. Kim, K. K. Kim and S. H. Baek. "Ezh2 Generates a Methyl Degron That Is Recognized by the Dcaf1/Ddb1/Cul4 E3 Ubiquitin Ligase Complex." *Mol Cell* 48, no. 4 (2012): 572-86.

Li, D., T. Shimamura, H. Ji, L. Chen, H. J. Haringsma, K. McNamara, M. C. Liang, S. A. Perera, S. Zaghlul, C. L. Borgman, S. Kubo, M. Takahashi, Y. Sun, L. R. Chirieac, R. F. Padera, N. I. Lindeman, P. A. Janne, R. K. Thomas, M. L. Meyerson, M. J. Eck, J. A. Engelman, G. I. Shapiro and K. K. Wong. "Bronchial and Peripheral Murine Lung Carcinomas Induced by T790m-L858r Mutant Egfr Respond to Hki-272 and Rapamycin Combination Therapy." *Cancer Cell* 12, no. 1 (2007): 81-93.

Li, H., G. Schmid-Bindert, D. Wang, Y. Zhao, X. Yang, B. Su and C. Zhou. "Blocking the Pi3k/AKT and Mek/Erk Signaling Pathways Can Overcome Gefitinib-Resistance in Non-Small Cell Lung Cancer Cell Lines." *Adv Med Sci* 56, no. 2 (2011): 275-84.

Li, J., J. E. Cone, A. R. Kahn, R. M. Brackbill, M. R. Farfel, C. M. Greene, J. L. Hadler, L. T. Stayner and S. D. Stellman. "Association between World Trade Center Exposure and Excess Cancer Risk." *JAMA* 308, no. 23 (2012): 2479-88.

Lioy, P. J., C. P. Weisel, J. R. Millette, S. Eisenreich, D. Vallero, J. Offenberg, B. Buckley, B. Turpin, M. Zhong, M. D. Cohen, C. Prophete, I. Yang, R. Stiles, G. Chee, W. Johnson, R. Porcja, S. Alimokhtari, R. C. Hale, C. Weschler and L. C. Chen. "Characterization of the Dust/Smoke Aerosol That Settled East of the World Trade

Center (Wtc) in Lower Manhattan after the Collapse of the Wtc 11 September 2001." *Environ Health Perspect* 110, no. 7 (2002): 703-14.

Lippmann, M., M. D. Cohen and L. C. Chen. "Health Effects of World Trade Center (Wtc) Dust: An Unprecedented Disaster's Inadequate Risk Management." *Crit Rev Toxicol* 45, no. 6 (2015): 492-530.

Liu, J., B. Chen, Y. Lu, Y. Guan and F. Chen. "Jnk-Dependent Stat3 Phosphorylation Contributes to AKT Activation in Response to Arsenic Exposure." *Toxicol Sci* 129, no. 2 (2012): 363-71.

Loffler, D., K. Brocke-Heidrich, G. Pfeifer, C. Stocsits, J. Hackermuller, A. K. Kretzschmar, R. Burger, M. Gramatzki, C. Blumert, K. Bauer, H. Cvijic, A. K. Ullmann, P. F. Stadler and F. Horn. "Interleukin-6 Dependent Survival of Multiple Myeloma Cells Involves the Stat3-Mediated Induction of Microrna-21 through a Highly Conserved Enhancer." *Blood* 110, no. 4 (2007): 1330-3.

Lu, Y., Q. Chang, Y. Zhang, K. Beezhold, Y. Rojanasakul, H. Zhao, V. Castranova, X. Shi and F. Chen. "Lung Cancer-Associated Jmjc Domain Protein MDIG Suppresses Formation of Tri-Methyl Lysine 9 of Histone H3." *Cell Cycle* 8, no. 13 (2009): 2101-9.

Lynch, T. J., D. W. Bell, R. Sordella, S. Gurubhagavatula, R. A. Okimoto, B. W. Brannigan, P. L. Harris, S. M. Haserlat, J. G. Supko, F. G. Haluska, D. N. Louis, D. C. Christiani, J. Settleman and D. A. Haber. "Activating Mutations in the Epidermal Growth Factor Receptor Underlying Responsiveness of Non-Small-Cell Lung Cancer to Gefitinib." *N Engl J Med* 350, no. 21 (2004): 2129-39.

Moline, J. M., R. Herbert, L. Crowley, K. Troy, E. Hodgman, G. Shukla, I. Udasin, B. Luft, S. Wallenstein, P. Landrigan and D. A. Savitz. "Multiple Myeloma in World Trade Center Responders: A Case Series." *J Occup Environ Med* 51, no. 8 (2009): 896-902.

Morgan, G. J., B. A. Walker and F. E. Davies. "The Genetic Architecture of Multiple Myeloma." *Nat Rev Cancer* 12, no. 5 (2012): 335-48.

Morris, L. G. and T. A. Chan. "Resistance to Egfr Inhibitors: Molecular Determinants and the Enigma of Head and Neck Cancer." *Oncotarget* 2, no. 12 (2011): 894-5.

Niederst, M. J. and J. A. Engelman. "Bypass Mechanisms of Resistance to Receptor Tyrosine Kinase Inhibition in Lung Cancer." *Sci Signal* 6, no. 294 (2013): re6.

Ohashi, K., L. V. Sequist, M. E. Arcila, T. Moran, J. Chmielecki, Y. L. Lin, Y. Pan, L. Wang, E. de Stanchina, K. Shien, K. Aoe, S. Toyooka, K. Kiura, L. Fernandez-Cuesta, P. Fidias, J. C. Yang, V. A. Miller, G. J. Riely, M. G. Kris, J. A. Engelman, C. L. Vnencak-Jones, D. Dias-Santagata, M. Ladanyi and W. Pao. "Lung Cancers with Acquired Resistance to Egfr Inhibitors Occasionally Harbor Braf Gene Mutations but Lack Mutations in Kras, Nras, or Mek1." *Proc Natl Acad Sci U S A* 109, no. 31 (2012): E2127-33.

Onitsuka, T., H. Uramoto, N. Nose, M. Takenoyama, T. Hanagiri, K. Sugio and K. Yasumoto. "Acquired Resistance to Gefitinib: The Contribution of Mechanisms Other Than the T790m, Met, and Hgf Status." *Lung Cancer* 68, no. 2 (2010): 198-203.

Ono, M., A. Hirata, T. Kometani, M. Miyagawa, S. Ueda, H. Kinoshita, T. Fujii and M. Kuwano. "Sensitivity to Gefitinib (Iressa, Zd1839) in Non-Small Cell Lung Cancer Cell Lines Correlates with Dependence on the Epidermal Growth Factor (Egf) Receptor/Extracellular Signal-Regulated Kinase 1/2 and Egf Receptor/AKT Pathway for Proliferation." *Mol Cancer Ther* 3, no. 4 (2004): 465-72.

Paez, J. G., P. A. Janne, J. C. Lee, S. Tracy, H. Greulich, S. Gabriel, P. Herman, F. J. Kaye, N. Lindeman, T. J. Boggon, K. Naoki, H. Sasaki, Y. Fujii, M. J. Eck, W. R. Sellers, B. E. Johnson and M. Meyerson. "Egfr Mutations in Lung Cancer:

Correlation with Clinical Response to Gefitinib Therapy." *Science* 304, no. 5676 (2004): 1497-500.

Pallis, A. G. and K. N. Syrigos. "Epidermal Growth Factor Receptor Tyrosine Kinase Inhibitors in the Treatment of Nsclc." *Lung Cancer* 80, no. 2 (2013): 120-30.

Pao, W., V. Miller, M. Zakowski, J. Doherty, K. Politi, I. Sarkaria, B. Singh, R. Heelan, V. Rusch, L. Fulton, E. Mardis, D. Kupfer, R. Wilson, M. Kris and H. Varmus. "Egf Receptor Gene Mutations Are Common in Lung Cancers from "Never Smokers" and Are Associated with Sensitivity of Tumors to Gefitinib and Erlotinib." *Proc Natl Acad Sci U S A* 101, no. 36 (2004): 13306-11.

Pao, W., T. Y. Wang, G. J. Riely, V. A. Miller, Q. Pan, M. Ladanyi, M. F. Zakowski, R. T. Heelan, M. G. Kris and H. E. Varmus. "Kras Mutations and Primary Resistance of Lung Adenocarcinomas to Gefitinib or Erlotinib." *PLoS Med* 2, no. 1 (2005): e17.

Papadimitrakopoulou, V. and A. A. Adjei. "The AKT/Mtor and Mitogen-Activated Protein Kinase Pathways in Lung Cancer Therapy." *J Thorac Oncol* 1, no. 7 (2006): 749-51.

Pelengaris, S., M. Khan and G. Evan. "C-MYC: More Than Just a Matter of Life and Death." *Nat Rev Cancer* 2, no. 10 (2002): 764-76.

Rajkumar, S. V., O. Landgren and M. V. Mateos. "Smoldering Multiple Myeloma." *Blood* 125, no. 20 (2015): 3069-75.

Rojanasakul, Y. "Linking Jnk-Stat3-AKT Signaling Axis to Ezh2 Phosphorylation: A Novel Pathway of Carcinogenesis." *Cell Cycle* 12, no. 2 (2013): 202-3.

Rutsch, S., V. T. Neppalli, D. M. Shin, W. DuBois, H. C. Morse, 3rd, H. Goldschmidt and S. Janz. "Il-6 and Myc Collaborate in Plasma Cell Tumor Formation in Mice." *Blood* 115, no. 9 (2010): 1746-54.

Sakaguchi, M., M. Oka, T. Iwasaki, Y. Fukami and C. Nishigori. "Role and Regulation of Stat3 Phosphorylation at Ser727 in Melanocytes and Melanoma Cells." *J Invest Dermatol* 132, no. 7 (2012): 1877-85.

Sen, M., S. Joyce, M. Panahandeh, C. Li, S. M. Thomas, J. Maxwell, L. Wang, W. E. Gooding, D. E. Johnson and J. R. Grandis. "Targeting Stat3 Abrogates Egfr Inhibitor Resistance in Cancer." *Clin Cancer Res* 18, no. 18 (2012): 4986-96.

Shepherd, F. A., J. Rodrigues Pereira, T. Ciuleanu, E. H. Tan, V. Hirsh, S. Thongprasert, D. Campos, S. Maoleekoonpiroj, M. Smylie, R. Martins, M. van Kooten, M. Dediu, B. Findlay, D. Tu, D. Johnston, A. Bezjak, G. Clark, P. Santabarbara, L. Seymour and Group National Cancer Institute of Canada Clinical Trials. "Erlotinib in Previously Treated Non-Small-Cell Lung Cancer." *N Engl J Med* 353, no. 2 (2005): 123-32.

Siegel, R., J. Ma, Z. Zou and A. Jemal. "Cancer Statistics, 2014." *CA Cancer J Clin* 64, no. 1 (2014): 9-29.

Siewert, E., W. Muller-Esterl, R. Starr, P. C. Heinrich and F. Schaper. "Different Protein Turnover of Interleukin-6-Type Cytokine Signalling Components." *Eur J Biochem* 265, no. 1 (1999): 251-7.

Solaini, G., G. Sgarbi and A. Baracca. "Oxidative Phosphorylation in Cancer Cells." *Biochim Biophys Acta* 1807, no. 6 (2011): 534-42.

Sordella, R., D. W. Bell, D. A. Haber and J. Settleman. "Gefitinib-Sensitizing Egfr Mutations in Lung Cancer Activate Anti-Apoptotic Pathways." *Science* 305, no. 5687 (2004): 1163-7.

Sos, M. L., H. B. Rode, S. Heynck, M. Peifer, F. Fischer, S. Kluter, V. G. Pawar, C. Reuter, J. M. Heuckmann, J. Weiss, L. Ruddigkeit, M. Rabiller, M. Koker, J. R. Simard, M. Getlik, Y. Yuza, T. H. Chen, H. Greulich, R. K. Thomas and D. Rauh. "Chemogenomic Profiling Provides Insights into the Limited Activity of Irreversible

Egfr Inhibitors in Tumor Cells Expressing the T790m Egfr Resistance Mutation." *Cancer Res* 70, no. 3 (2010): 868-74.

Stewart, D. J. "Wnt Signaling Pathway in Non-Small Cell Lung Cancer." *J Natl Cancer Inst* 106, no. 1 (2014): djt356.

Taja-Chayeb, L., M. Candelaria, R. Brom, C. Trejo-Becerril, F. Meza and A. Duenas-Gonzalez. "Response to Gefitinib in Bronchioloalveolar Carcinoma in the Absence of Egfr Mutation." *Lung Cancer* 50, no. 2 (2005): 259-63.

Teye, K., N. Arima, Y. Nakamura, K. Sakamoto, E. Sueoka, H. Kimura and M. Tsuneoka. "Expression of Myc Target Gene Mina53 in Subtypes of Human Lymphoma." *Oncol Rep* 18, no. 4 (2007): 841-8.

Teye, K., M. Tsuneoka, N. Arima, Y. Koda, Y. Nakamura, Y. Ueta, K. Shirouzu and H. Kimura. "Increased Expression of a Myc Target Gene Mina53 in Human Colon Cancer." *Am J Pathol* 164, no. 1 (2004): 205-16.

Thakur, C., Y. Lu, J. Sun, M. Yu, B. Chen and F. Chen. "Increased Expression of MDIG Predicts Poorer Survival of the Breast Cancer Patients." *Gene* 535, no. 2 (2014): 218-24.

Thakur, C., M. Wolfarth, J. Sun, Y. Zhang, Y. Lu, L. Battelli, D. W. Porter and F. Chen. "Oncoprotein MDIG Contributes to Silica-Induced Pulmonary Fibrosis by Altering Balance between Th17 and Treg T Cells." *Oncotarget* 6, no. 6 (2015): 3722-36.

Tsuneoka, M., H. Fujita, N. Arima, K. Teye, T. Okamura, H. Inutsuka, Y. Koda, K. Shirouzu and H. Kimura. "Mina53 as a Potential Prognostic Factor for Esophageal Squamous Cell Carcinoma." *Clin Cancer Res* 10, no. 21 (2004): 7347-56.

Tsuneoka, M., Y. Koda, M. Soejima, K. Teye and H. Kimura. "A Novel Myc Target Gene, Mina53, That Is Involved in Cell Proliferation." *J Biol Chem* 277, no. 38 (2002): 35450-9.

Vogt, P. K. and J. R. Hart. "Pi3k and Stat3: A New Alliance." *Cancer Discov* 1, no. 6 (2011): 481-6.

Wagner, S. A., P. Beli, B. T. Weinert, M. L. Nielsen, J. Cox, M. Mann and C. Choudhary. "A Proteome-Wide, Quantitative Survey of in Vivo Ubiquitylation Sites Reveals Widespread Regulatory Roles." *Mol Cell Proteomics* 10, no. 10 (2011): M111 013284.

Wakahara, R., H. Kunimoto, K. Tanino, H. Kojima, A. Inoue, H. Shintaku and K. Nakajima. "Phospho-Ser727 of Stat3 Regulates Stat3 Activity by Enhancing Dephosphorylation of Phospho-Tyr705 Largely through Tc45." *Genes Cells* 17, no. 2 (2012): 132-45.

Walker, B. A., C. P. Wardell, L. Chiecchio, E. M. Smith, K. D. Boyd, A. Neri, F. E. Davies, F. M. Ross and G. J. Morgan. "Aberrant Global Methylation Patterns Affect the Molecular Pathogenesis and Prognosis of Multiple Myeloma." *Blood* 117, no. 2 (2011): 553-62.

Wang, B., X. Zhang, L. Lin, X. Hao, X. Zhang, J. Li and Y. Shi. "[Progressive Patterns of Gifitinib Treating Advanced Non-Small Cell Lung Cancer after Obtained Resistance]." *Zhongguo Fei Ai Za Zhi* 16, no. 10 (2013): 510-3.

Wang, W., Y. Lu, P. M. Stemmer, X. Zhang, Y. Bi, Z. Yi and F. Chen. "The Proteomic Investigation Reveals Interaction of MDIG Protein with the Machinery of DNA Double-Strand Break Repair." *Oncotarget* 6, no. 29 (2015): 28269-81.

Ware, K. E., T. K. Hinz, E. Kleczko, K. R. Singleton, L. A. Marek, B. A. Helfrich, C. T. Cummings, D. K. Graham, D. Astling, A. C. Tan and L. E. Heasley. "A Mechanism of

Resistance to Gefitinib Mediated by Cellular Reprogramming and the Acquisition of an Fgf2-Fgfr1 Autocrine Growth Loop." *Oncogenesis* 2, (2013): e39.

Wen, Z., Z. Zhong and J. E. Darnell, Jr. "Maximal Activation of Transcription by Stat1 and Stat3 Requires Both Tyrosine and Serine Phosphorylation." *Cell* 82, no. 2 (1995): 241-50.

Wu, K., Q. Chang, Y. Lu, P. Qiu, B. Chen, C. Thakur, J. Sun, L. Li, A. Kowluru and F. Chen. "Gefitinib Resistance Resulted from Stat3-Mediated AKT Activation in Lung Cancer Cells." *Oncotarget* 4, no. 12 (2013): 2430-8.

Xia, L., L. Wang, A. S. Chung, S. S. Ivanov, M. Y. Ling, A. M. Dragoi, A. Platt, T. M. Gilmer, X. Y. Fu and Y. E. Chin. "Identification of Both Positive and Negative Domains within the Epidermal Growth Factor Receptor Cooh-Terminal Region for Signal Transducer and Activator of Transcription (Stat) Activation." *J Biol Chem* 277, no. 34 (2002): 30716-23.

Xing, J., K. Wang, P. W. Liu, Q. Miao and X. Y. Chen. "Mina53, a Novel Molecular Marker for the Diagnosis and Prognosis of Gastric Adenocarcinoma." *Oncol Rep* 31, no. 2 (2014): 634-40.

Yosef, N., A. K. Shalek, J. T. Gaublomme, H. Jin, Y. Lee, A. Awasthi, C. Wu, K. Karwacz, S. Xiao, M. Jorgolli, D. Gennert, R. Satija, A. Shakya, D. Y. Lu, J. J. Trombetta, M. R. Pillai, P. J. Ratcliffe, M. L. Coleman, M. Bix, D. Tantin, H. Park, V. K. Kuchroo and A. Regev. "Dynamic Regulatory Network Controlling Th17 Cell Differentiation." *Nature* 496, no. 7446 (2013): 461-8.

Yu, H. A., M. E. Arcila, N. Rekhtman, C. S. Sima, M. F. Zakowski, W. Pao, M. G. Kris, V. A. Miller, M. Ladanyi and G. J. Riely. "Analysis of Tumor Specimens at the Time of Acquired Resistance to Egfr-Tki Therapy in 155 Patients with Egfr-Mutant Lung Cancers." *Clin Cancer Res* 19, no. 8 (2013): 2240-7.

Yu, H., D. Pardoll and R. Jove. "Stats in Cancer Inflammation and Immunity: A Leading Role for Stat3." *Nat Rev Cancer* 9, no. 11 (2009): 798-809.

Yu, M., J. Sun, C. Thakur, B. Chen, Y. Lu, H. Zhao and F. Chen. "Paradoxical Roles of Mineral Dust Induced Gene on Cell Proliferation and Migration/Invasion." *PLoS One* 9, no. 2 (2014): e87998.

Zhang, Q., C. M. Hu, Y. S. Yuan, C. H. He, Q. Zhao and N. Z. Liu. "Expression of Mina53 and Its Significance in Gastric Carcinoma." *Int J Biol Markers* 23, no. 2 (2008): 83-8.

Zhang, Y., Y. Lu, B. Z. Yuan, V. Castranova, X. Shi, J. L. Stauffer, L. M. Demers and F. Chen. "The Human Mineral Dust-Induced Gene, MDIG, Is a Cell Growth Regulating Gene Associated with Lung Cancer." *Oncogene* 24, no. 31 (2005): 4873-82.

ABSTRACT

EXPLORATION OF CANCER PROLIFERATIVE SIGNALING IN CHEMOTHERAPY DRUG RESISTANCE AND MDIG-INDUCED TUMORIGENESIS

by

KAI WU

August 2016

Advisor: Dr. Fei Chen

Major: Pharmaceutical Sciences

Degree: Doctor of Philosophy

Aberrant intracellular signaling pathway is one of the major driving forces of malignancy through multiple stages of human cancers. Our study demonstrates that in cancer cells, the signaling pathways are profoundly and actively intertwined with each other so they can synergistically affect cell biology, including promoting development of malignancy and compensating the loss of proliferation or survival signals in responses to anti-tumor drug. Moreover, cancer cells can also adopt "non-canonical" mechanisms to modulate the activities of key protein regulators so the whole signaling pathway is strengthened.

In the first project, we performed integrative studies to investigate the oncogenic role of a WTC (World Trade Center) dust-induced regulator, MDIG, in multiple myeloma (MM). MM is a malignancy of plasma cells located within bone-marrow compartment and several post 9/11 health surveillance programs and epidemiological studies suggested an increased incidence rate of multiple myeloma (MM) among the individuals who intensively exposed to WTC dust. However, the potential connections between WTC dust and MM remain to be elucidated. Expressions of MDIG were investigated in bronchial epithelial cells, B cells, MM cell lines and in the bone marrow specimens from the MM patients. We found that WTC dust is potent in inducing MDIG protein and/or mRNA in bronchial epithelial cells, B cells and MM

cell lines. An increased MDIG expression in MM bone marrow was observed, which is associated with the disease progression and prognosis of the MM patients. Using integrative genomics and proteomics approaches, we further demonstrated that in MM cell lines, MDIG directly interacts with C-MYC and JAK1, which contributes to hyperactivation of the JAK-STAT3 signaling important for the pathogenesis of MM. Genetic silencing of MDIG reduced activity of the major downstream effectors in the JAK-STAT3 pathway. Our results indicate that WTC dust induced-MDIG overexpression bridges C-MYC pathway and STAT3 pathway in MM, which is essential for the tumorigenesis of MM.

In the second project, we focused on the underlying mechanisms of both primary and secondary resistance to Epidermal Growth Factor Receptor Tyrosine Kinase Inhibitor (EGFR TKI), including gefitinib, in Non-small cell lung cancer (NSCLC), which are two major obstacles compromising the clinical success of targeted therapy. In the part studying primary resistance, we observed that JAK2-STAT3 signaling axis in non-sensitive lung cancer cell lines is highly refractory to gefitinib treatment. Follow-up experiments further revealed a unique STAT3-dependent AKT restoration pattern in non-sensitive lung cancer cells, which impairs the efficacy of gefitinib. Mechanistically, gefitinib increased physical binding between EGFR and STAT3, which de-repressed STAT3 from SOCS3, an upstream suppressor of STAT3. Such a de-repression of STAT3 in turn fostered AKT activation. Genetic or pharmacological inhibition of STAT3 abrogated AKT activation and combined gefitinib with STAT3 inhibition synergistically reduced the growth of the tumor cells. In order to study the mechanisms of secondary resistance (acquired resistance), we established a gefitinib-resistant lung cancer (GR) cell line. Through profiling the gene expression pattern and investigating the alterations of intracellular signaling pathways, we discovered multiple resistance mechanisms in GR cells, including a unique hyperactivation pattern of STAT3. A rational co-inhibition of STAT3 and EGFR simultaneously suppressed several survival-related

pathways in GR cells. As a result, such combinational targeting re-sensitized the GR cells to gefitinib treatment. Taken together, our studies have unraveled novel mechanisms of resistance to EGFR TKI in lung cancer and have provided important information for rationale-based combinational targeting strategies to overcome drug resistance.

AUTOBIOGRAPHICAL STATEMENT

Education

2011—2016 School of Pharmacy (EACPHS), Wayne State University, Detroit, MI.

PhD in Pharmaceutical Sciences (Mentor: Dr. Fei Chen)

2006—2011 Southern Medical University (former First Military University), Guangzhou, Guangdong Province, China

Bachelor of Medicine

Research Publications

(1) Kai Wu, Yongju Lu, Xiangmin Zhang, Zhengping Yi, Fei Chen. “MDIG orchestrates oncogenic crosstalk between C-MYC and IL-6 pathways and predicts disease progression of multiple myeloma patients” Submitted to Oncogene, (2016)

(2) Wu, K., Q. Chang, Y. Lu, P. Qiu, B. Chen, C. Thakur, J. Sun, L. Li, A. Kowluru and F. Chen. "Gefitinib Resistance Resulted from Stat3-Mediated AKT Activation in Lung Cancer Cells." Oncotarget 4, no. 12 (2013): 2430-8

(3) Li, L., P. Qiu, B. Chen, Y. Lu, K. Wu, C. Thakur, Q. Chang, J. Sun and F. Chen. "Reactive Oxygen Species Contribute to Arsenic-Induced Ezh2 Phosphorylation in Human Bronchial Epithelial Cells and Lung Cancer Cells." Toxicol Appl Pharmacol 276, no. 3 (2014): 165-70.